Jihočeská univerzita
v Českých Budějovicích
University of South Bohemia
in České Budějovice

Author
Joan Elorm Abla Ahiable

Submission
Applied Experimental Biophysics, Linz

Thesis Supervisor
Assoc. Univ.-Prof. Dr. Andreas Ebner

Month Year
October 2016

Reusable Avidin Based Anti-Absorptive Gold Functionalization for Biosensing QCM Measurements & Flat Erythrocyte Ghost Preparation for AFM Investigation

Master's Thesis

in the Master's Program

JMP Biological Chemistry

UNIVERSITY OF SOUTH BOHEMIA IN CESKE BUDEJOVICE
Branišovská 1645
370 05 České Budějovice
Czech Republic
www.jcu.cz

Ahiable JEA, 2016. Reusable Avidin Based Anti-Absorptive Gold Functionalization for Biosensing QCM Measurements & Flat Erythrocyte Ghost Preparation for AFM Investigation (Master´s thesis in English) – 79 p., Applied Experimental Biophysics, Institute of Biophysics, Johannes Kepler University, Linz, Austria.

SWORN DECLARATION

I hereby declare that I have worked on my master's thesis independently and used only the sources listed in the bibliography.

I hereby declare that, in accordance with Article 47b of Act No. 111/1998 in the valid wording, I agree with the publication of my master thesis, in full form to be kept in the Faculty of Science archive, in electronic form in publicly accessible part of the STAG database operated by the University of South Bohemia in České Budějovice accessible through its web pages.
Further, I agree to the electronic publication of the comments of my supervisor and thesis opponents and the record of the proceedings and results of the thesis defence in accordance with aforementioned Act No. 111/1998. I also agree to the comparison of the text of my thesis with the Theses.cz thesis database operated by the National Registry of University Theses and a plagerism detection system.

Place and Date: _____ Signature: _____

DEDICATION

This master's thesis is dedicated to my husband, Eric Edem Ahiable, and my mothers Olivia Panzl and Benedicta Alornyo for their immense love and support.

ABSTRACT

The Quartz Crystal Microbalance (QCM) is an excellent label-free acoustic affinity sensor for determining mass adsorption at ng/cm² range [1]. Biomolecular interaction analysis with high sensitivity and specificity using QCM is possible due to a biochemical functionalization of the quartz. In the course of measurement, it is ideal to regenerate the quartz surface within the flow cell so as to allow immediate reuse of the chip for further analysis. During this study, a re-usable surface where biotinylated bait molecules could be bound to the surface in a one-step reaction was developed, and the binding of prey molecules to the bait molecules could be traced. For this, the sensor surface was functionalized with biotin-PEG_8-thiol linker (mixed with hydroxyl/methoxy-PEG_6-thiol) and different avidin based molecules were bound via the high affinity interaction between avidin and biotin. A comparison of the regenerations of avidin, streptavidin and an avidin mutant M96H, as well as with different regeneration conditions was carried out. In contrast to an analogous SPR study [2], it was discovered that not only could M96H be removed by SDS (0.25%) and citric acid (2.5%), but also by 8 M Guanidine-hydrochloride (GuHCl) at pH 1.5 as well as by regeneration-solution-x. (RSX). Very incomplete chip regeneration was seen with wild-type avidin and streptavidin, where it was shown that the unremovable fraction of streptavidin and avidin corresponded to those molecules, which were bound to two adjacent biotin groups on the chip surface.

Red Blood Cells (RBC), also known as **erythrocytes (ERY)** are the transporters of oxygen in the body and they develop from the bone marrow stem cells. Besides, these cells are the most common type of blood cells in the human mammals [3, 4]. One of the most complex blood group classification known in humans is the Rh blood group and so far 49 Rh antigens are known [5]. As part of a protein complex in the ERY membrane, these Rh antigens are exclusively expressed in cells of the erythroid line, thus only in ERYs [5]. In the realm of this project, the focus was laid on investigating the RhD by applying Atomic Force Microscopy (AFM). Firstly, flat ERY ghosts were prepared by flashing out all organelles in the ERY and fixing back the two membranes. Subsequently, the antibody, BRAD5 was attached to the cantilever tip via a flexible acetal-polyethylene glycol (PEG)-NSH [6] cross linker and measurements revealing interaction forces were carried out on the ERYs. Visualization, identification and quantification of the RhD receptors on the flat ERY ghost could be determined with simultaneous topography and recognition (TREC) mapping.

ACKNOWLEDGEMENTS

My foremost and sincere appreciation goes to my supervisor, Assoc. Univ.-Prof. Dr. Andreas Ebner for his help, patience and the time spent supervising and ensuring the excellent completion of this thesis. His leadership, contributions and encouragements have brought me this far. Also my sincere appreciation goes to the head of the department, Univ.-Prof. Dr. Peter Hinterdorfer for his cordial assistant throughout my research.

I would like to pay respects to the following individuals: Dr.in Constanze Lamprecht for constructive discussions and diverse assistance during this project; Dr. Michael Leitner, Dipl.-Ing. Lukas Traxler, Aleksej Lakic, DI. Boris Buchroithner, Barbara Hartl, Manuel Kasper BSc and Martina Mittermayr MSc for their supports. My gratitude equally goes to a. Univ.-Prof. Dr. Hermann Gruber for providing mutant avidin M96H and biotin linkers for QCM experiments and for helpful discussions as well, likewise to Dieter Blaas, PhD for supplying human rhinovirus and 8F5 antibody. Thank you to Dr. Sc. Tomislav Vuletic for his support during my QCM-D measurements in Croatia.

Moreover, I render much gratitude to my program coordinators Univ.-Prof. Mag. Dr. Nobert Müller (Johannes Kepler University Linz, Austria) and Prof. RNDr. Libor Grubhoffer, CSc. (University of South Bohemia in České Budějovice, Czech) for making this JMP Biological Chemistry a remarkable one. They were ever ready in assisting in all means possible, resulting in a sound discipline.

I owe this success largely to my family, that has been my backbone. Eric Edem Ahiable, my dearest husband, I very much appreciate your immense love and support, and I love you into eternity. On the same note, I express a heart full of gratitude to my parents and sisters: Olivia Panzl, Hannes Panzl, Benedicta Alornyo, Laura Fafa Panzl and Tamara-Kafui Panzl, not forgetting Sedem Sabina Hlordzi. Thank you all for being there for me. I love you all!

In addition, I would like to extend my profound gratefulness to the Austrian Agency for International Cooperation in Education & Research (OeAD) for supporting this work.

Finally, I say a special thank you to the almighty God for His wonderful provisions.

TABLE OF CONTENTS

LIST OF ABBREVIATIONS AND ACRONYMS

AC	alternating current
AFM	atomic force microscopy
APTES	aminopropyl-triethoxysilane
BVD	butterworth-van-dyke
C	capacitance
D	dissipation
DMSO	dimethyl sulfoxide
DNA	deoxyribonucleic acid
EGS	ethyleneglycol-bis(succimidyl-succinate)
EGTA	ethylene glycol-bis(2-aminoethylether)-N,N,N′,N′- tetra-acetic acid
ERY	erythrocytes
FCD	force distance curve
FPW	flexural-plate-wave
FS	force spectroscopy
GuHCl	guanidine-hydrochloride
HDN	hemolytic disease of the newborn
HRV	human rhinovirus
HTR	hemolytic transfusion reaction
Ig	immunoglobulin
KCl	potassium chloride
KH_2PO_4	potassium dihydrogen phosphate
L	inductance
mQH_2O	milli-Q water
Na_2HPO_4	sodium hydrogen phosphate
NaCl	sodium chloride
$NaCNBH_3$	sodium cyanoborohydride
NaOH	sodium hydroxide
NHS	N-hydroxysuccinimide
NHS-LC-Biotin	succinimidyl-6-(biotinamido)hexanoate
PBS	phosphate buffered saline
PEG	poly(ethylene glycol)
Q	quality factor
QCM	quartz crystal microbalance
QCM-D	quartz crystal microbalance with dissipation monitoring

QCM-IA	quartz crystal microbalance with impedance analyzer
QUI	graphical user interface
R	resistance
RBC	red blood cells
RES	reticuloendothelia system
Rh	rhesus
RSX	regeneration-solution-x
RT	room temperature
SAM	self-assembled monolayer
SAW	surface-acoustic-wave
SDS	sodium dodecyl sulfate
SH-APM	shear-horizontal-acoustic-plate-mode
SiN_3	silicon nitride
SPM	scanning probe microscopy
SPR	surface plasmon resonance
TEA	triethylamine
TREC	topography and recognition
TSM	thickness-shear-mode

1. Introduction

1.1. Introduction to Quartz Crystal Microbalance (QCM) and the avidin-biotin test system

1.1.1. A chronicle of QCM cite scientific paper with numbers

Quartz resonance is found in varieties of electronic devices such as computers and watches to give accurate time base and reference systems or signal generators [1]. Not until just before World War II, quartz resonance became of commercial interest, due to a high demand of communication devices, which required more than 30 million resonators [1]. After the linear relationship between frequency response and deposited mass [1, 7] was discovered as illustrated by Sauerbrey in 1959 [8], quartz crystals gained importance as analytical devices. If a strong association between the ideal layer of the foreign mass and resonator is present, only then is this proportionality true, hence the justification for calling this device “quartz-crystal microbalance” (QCM) [1]. The QCM technique attained significance in devices for detecting thicknesses in air and vacuum in the 1960s and 1970s, and up to the present time it is used to observe thicknesses of layers in laboratories [1]. Thanks to the discovery of circuitry by Nomura and Okuhara in 1982 [9], the appropriate oscillator circuits that allowed the shear-wave resonator to function in liquid became possible [1].

Thus, QCM is an excellent real-time and label-free acoustic affinity sensor for determining mass adsorption at ng/cm² range [1]. The piezoelectric quartz disc of the QCM (Figure 1) can either be coated with gold on both sides or with gold on one side and other electrode materials of interest like aluminum, silicon, silver, titanium, nickel, copper and chromium etc. [10] on the other side. These coats are linked with a strip of gold to permit the application of high frequency AC-voltage. An acoustic oscillation is induced in the piezoelectric quartz crystal when the electric field between the upper and the lower gold area oscillates. Any additional deposition of mass on the quartz crystal causes an increase in its thickness, resulting in a decrease in the resonance frequency. With biochemically functionalized quartz, QCM can be employed in analyzing biomolecular interaction with high sensitivity and specificity.

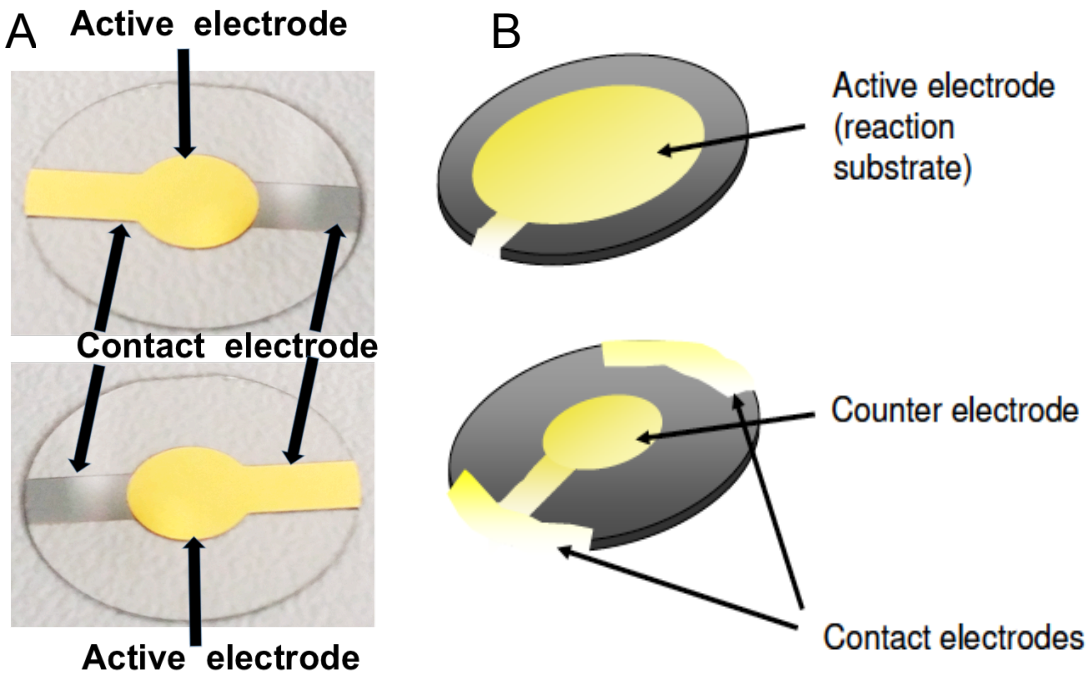

Figure 1: Typical piezoelectric quartz disc coated with gold electrodes on both sides. In (A) and (B) the electrodes are contacted by two counter-electrodes for QCM measurements and they are compatible with QCM with impedance analyzer, abbreviated QCM-IA. Only the quartz disc in (B) is compatible with quartz crystal microbalance with dissipation monitoring, abbreviated QCM-D.

1.1.2. Physical background

A frequency range of 14 orders of magnitude, which extends from 10^{-2} Hz, known as seismic wave, to 10^{12} Hz, also known as thermoelastic excited phonons, is covered by acoustic waves [1]. When periodic perturbation (known as stress) is applied to a solid it results in elastic deformations (also called strain) and this travels through the solid as a wave. The structure of the crystal hence determines the phase velocity and the type of wave, either transversal or longitudinal [1]. Employing the definition of strain, the equation of motion and the constitutive equations, the wave equation that describes the acoustic wave in solids can be derived [11]:

$$\nabla c : \nabla_s u = \rho \frac{\partial^2 u}{\partial t^2} \qquad (1)$$

u denotes the displacement of the particle, *p* the density of the material, and *t* the time. The elasticity modulus of the solid is described by matrix *c*.

1.1.2.1. Piezoelectric excited acoustic waves in solids

Piezoelectricity (Figure 2) was first discovered by the Curie brothers in 1880, when they realized that different kinds of crystals when subjected to mechanical pressure, by pulling, torsion or pressure, could generate positive and negative electrical charges [1, 12, 13]. Contrarily, the converse piezoelectric effect (Figure 2) is the phenomenon by which a mechanical deformation arises from an

external field [1, 14].The precondition for the phenomenon of piezoelectricity to occur in crystals is an inversion center. Comparing other crystals, even though a large number of them exhibit piezoelectricity, only quartz crystals possess the peculiar combination of electrical, mechanical, thermal and chemical properties [1].

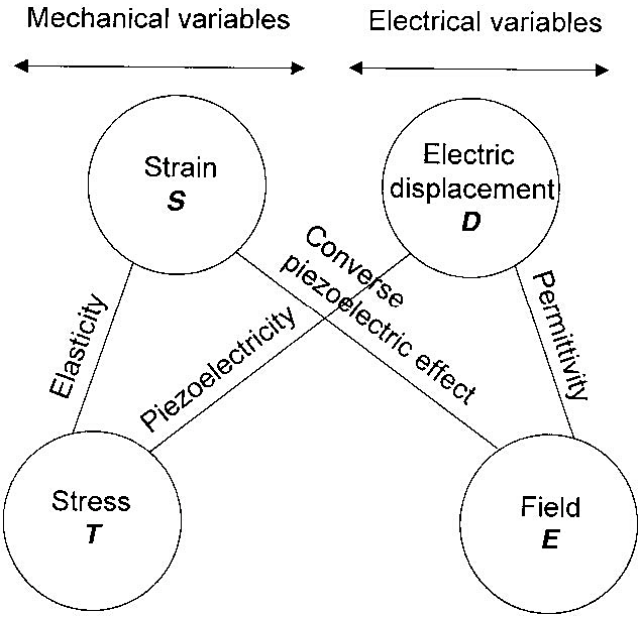

Figure 2: The interaction between mechanical and electrical variables. The generation of electrical displacement due to an applied mechanical stress results in the direct piezoelectric effect. The converse piezoelectric effect, on the other hand is determined in a strain in the crystal as a result of an applied electrical field. The elasticity of the solid determines the correlation between stress and strain. Taken from (Janshoff, Gala, & Steinem, 2000) and (Ballantine, et al., 1997).

1.1.2.2. Piezoelectric Resonator

There are four common kinds of acoustic resonators, namely thickness-shear-mode (TSM), flexural-plate-wave (FPW), surface-acoustic-wave (SAW) and shear-horizontal-acoustic-plate-mode (SH-APM) resonators (Figure 3). These differences come about as a result of the kind of cut-angle taken from a mother crystal with eigenfrequencies ranging from 5 x 10^2 to 3 x 10^8 [1]. Generally, the TMS resonators are also referred to as the QCM.

Quartz-crystals can have either BT-cut or AT-cut (Figure 4), with an angle of 49° to the z-axis for the former and 35.25° for the latter [1]. AT-cut is however, the ideal cut for QCM crystals due to the following reasons:

a. The AT-cut crystals are more appropriate for several electronic devices, since they present a high stability in frequency with $\Delta f/f$ being ca. 10^{-8} [1, 15, 16]

b. Such crystals exhibit temperature stability, because between 0°C and 50°C they have a temperature coefficient of almost zero, a condition that best suits QCM sensors [17].

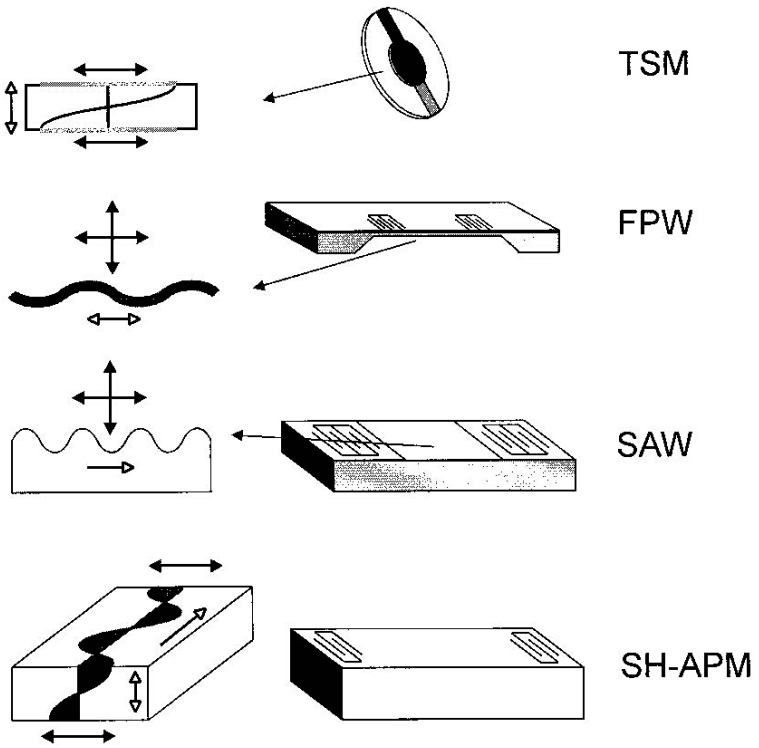

Figure 3: Diagrammatic representation of the four common kinds of acoustic resonators, including their wave propagation modes. TSM stands for thickness-shear-mode, FPW for flexural-plate-wave, SAW for surface-acoustic-wave and SH-APM for shear-horizontal-acoustic-plate-mode. The black arrow demonstrates the particle displacement and the open arrow the direction of the wave propagation. Taken from (Janshoff, Gala, & Steinem, 2000).

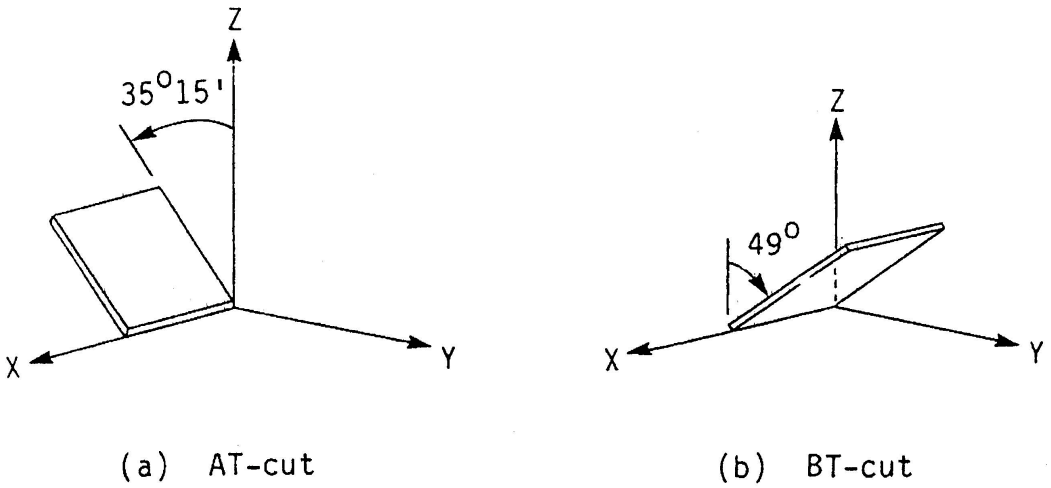

Figure 4: Schematic sketches of AT-cut with a 35° to the z-axis and BT-cut with 49° to the z-axis. Taken from (O'Sullivan & Guilbault, 1999).

Expressing the wave equation in cylindrical coordinates is an appropriate means of illustrating the travelling of acoustic waves in a circular, lossless and stress-free AT-cut crystal with thickness d_q. (Figure 5). The propagation direction of the acoustic wave is perpendicular to the AT-cut crystal surface [18]. In a piezoelectric TSM resonator the propagation velocity of the acoustic wave is expressed as:

$$\boldsymbol{v_\rho} = \sqrt{\mu_q / \boldsymbol{\rho_q}} \tag{2}$$

with v_p being the propagation velocity, μ_q the shear modulus and $\boldsymbol{\rho_q}$ the density of the quartz.

Equally, simplification of the eigenfrequency (Equation (3)) is achieved with the constructive interference [1] where $\boldsymbol{d_q} = \frac{\boldsymbol{n\lambda}}{\boldsymbol{2}}$ (with λ indicating wavelength):

$$f = \frac{nK_R}{d_q} \tag{3}$$

f stands for eigenfrequency, n for overtones, K_R stands for the frequency constant of AT-cut crystal with $K_R = 1664\ m\ s^{-1}$ and d_q for thickness of quartz.

Only odd overtones can be excited from the wave equation´s solution. Moreover, energy trapping is regarded as insufficient on low harmonics [18]. A conclusion drawn from Equation (3) shows that the resonance frequency of an AT-cut quartz is indirectly proportional to the thickness of the crystal. Usually the fundamental resonance frequency used for most quartz crystals in QCM measurements ranges from 5 MHz to 30 MHz, which corresponds to a plate thickness of 330 µm to 55 µm respectively [1].

Several material-specific parameters are provided by TSM resonators. It is important to comprehend the transformation between mechanical and electrical parameters so as to completely utilize the capability of acoustic resonators [1]. Mechanical models can be converted into equivalent electrical circuits, this completely describes the oscillation in the presence of an adsorbent. In 1965, Mason proposed a general one-dimensional acoustic wideband model [20], which presents the foundation for the theoretical explanation of complex composite resonators that exist in life science. In specific instances like low load, the Mason model can be transformed near resonance into an equivalent circuit with lumped elements, which is called Butterworth-van-Dyke (BVD) circuit [1]. This BVD is further modified with an additional complex impedance to represent typical load conditions such as thin rigid films, viscous liquids and viscoelastic polymers. The component of the discrete impedance elements of the modified BVD-equivalent circuit (Figure 5) are:

1. the capacitance, C_q, which embodies the mechanical elasticity of the quartz;

2. the inductance, L_q, which represents the initial mass;
3. the motional resistance, R_q, which determines energy losses or dissipation occurring from internal friction, viscous effects, and damping caused by the crystal holder;
4. the static capacitance, C_o, which while the motional components dominate near resonance, determines the admittance away from resonance, and
5. the complex impedance, Z_m^1 , represents the load on the surface [1].

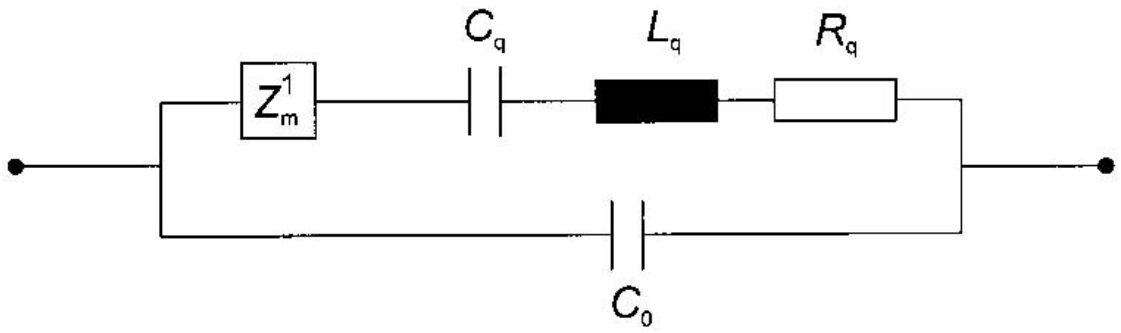

Figure 5: Modified BVD-equivalent circuit. This is a transformed three-port Mason model at near resonance and is made of distinct impedance components: C_q the capacitance, L_q the inductance, R_q the resistance, C_o the static capacitance and Z_m^1 the complex impedance. Taken from (Janshoff, Gala, & Steinem, 2000).

1.1.3. Mass Loading

Sauerbrey was the first to provide a solution to the issue of mass loading onto a quartz crystal during QCM measurement [8]. Any additional deposition of mass on the quartz crystal causes an increase in its thickness resulting in a decrease in the resonance frequency. The deposition of thin, rigid and uniform films on the quartz surface leads to a mass change per area (Δm/A) and this is related to a change in resonance frequency as illustrated here in the Sauerbrey´s model:

$$\Delta f = -\frac{2nf_o^2}{\sqrt{\rho_q \mu_q}} \cdot \frac{\Delta m}{A} = -C_f \cdot \Delta m \qquad (4)$$

With Δf being the change in resonance frequency, n the overtone harmonic number, f_o the fundamental frequency, Δm the mass change, A the piezoelectrically active surface area of quartz, ρ_q and μ_q the density and shear modulus of quartz, respectively. C_f is the integral mass sensitivity or Sauerbrey constant, which increases proportionally to the overtone number and is dependent of the fundamental frequency. C_f for a 5 MHz crystal is 0.05666 Hz/(ng/cm²).

However, the frequency changes extremely when the crystal surface in contact with a liquid oscillates. This problem was solved by Kanasawa and Gordon [21]: generating shear motion on the surface of

the quartz crystal gives rise to motion in the proximate Newtonian liquid. A plane-laminar flow is generated in the liquid by the oscillation surface, resulting in a decrease in the frequency that is proportional to the square root of the liquid density (ρ_l) *and* liquid viscosity (η_l) [1, 18], , $\left(\Delta f \propto \sqrt{\rho_l \eta_l}\right)$. Consequently, the Equation (4) ends in:

$$\Delta f = -f_o^{3/2} \sqrt{\frac{\rho_l \eta_l}{\pi \mu_q \rho_q}} \tag{5}$$

With Δf being the change in resonance frequency, f_o the fundamental frequency of the unloaded quartz, ρ_l the liquid density, η_l the liquid viscosity, μ_q the shear modulus of quartz and ρ_q the density of quartz.

The penetration depth of this sheer wave is dependent on: $\left(\pi f_0 \mu_q \rho_q\right)^{-1/2}$ and this is 250 nm for water at 20°C with 5-MHz crystal.

This Δf is a linear function of $\sqrt{\rho_l \eta_l}$ in solution with the exception of high polymer and salt solution [18].

1.1.3.1. Factors that affect QCM-sensitivity

On a typical QCM sensor the differential mass sensitivity is decreased towards the borders of the electrodes, while it is at a maximum at the center of the quartz crystal (compare Figure 6) [1]. This phenomenon is explained by the concept of energy trapping [11]. Energy trapping is the process whereby standing acoustic waves that are generated at the electrodes are confined in that region. The resonance of the quartz crystal and its corresponding resonant frequencies portray different conditions in the electrode-free region and the electrode region, owing to the extra mass of the electrodes. Observations show that there is almost a complete reflection of the lateral portions of the acoustic wave at the boundaries between the regions with and without electrodes. This acoustic wave usually travels tangential to the surface of the crystal [1]. This energy trapping, which influences the spurious modes by suppressing it and the quality factor, Q, of the resonator, by increasing it doesn't play any role in very thin (generally less than 50 nm) electrodes, since the resonant frequencies at such interfaces are very similar. Consequently, there is no confinement of the generated acoustic wave, hence, the quality factor, Q, of the resonator decreases.

The resonant frequency can also be influenced by some other parameters like the surface roughness of the quartz. Liquids can be entrapped in small cavities on hydrophilic and rough surfaces, which eventually contribute to the overall mass that is detected by the QCM. Hydrophobic cavities, on the other hand, cause air or vacuum inclusions since usually liquids don't wet them. Hence, smaller energy losses are observed on hydrophobic surfaces than on hydrophilic ones. To avoid such

frequency shifts as a result of changes in surface energies, it is necessary to use smooth surfaces when performing experiments in fluids [1].

1.1.4. Quartz Crystal Microbalance - The operating theory

Although the fundamental resonance of AT-cut quartz crystals ranges between 5 and 30 MHz, most employed quartz plates have a frequency between 4 and 10 MHz. Quartz plates with higher fundamental frequencies are very thin, and more difficult to handle [1].

When analyzing biomolecules and cells measurements are required to be done in aqueous solutions. The type of QCM setup used for this study consists of a flow system composed of a quartz that is fastened between two O-rings (Figure 7 and 15). In order to minimize damping and maximize the quality factor, it is ideal to minimize the contact of the O-ring with the resonator and to position it as far as possible outside the quartz, since the radial mass sensitivity, $s_f(r)$, is maximal at the center of the crystal at r = 0 and decays towards the edges of the quartz plate. According to a Bessel function type 1 and zero order, the square of the absolute value of this radial distribution is proportional to the radial mass sensitivity $\left(s_f(r) \propto |u(r)|^2\right)$. Empirically, the radial distribution of the shear amplitude can be related to the Gaussian function [1] (Figure 6):

$$u(r) = u_{max} exp\left(-a\frac{r^2}{R^2}\right) \quad (6)$$

where *u(r)* stands for the shear amplitude, u_{max} indicates the maximum displacement at *r = 0* and *a* the characteristic width distribution, where *a ≈ 2* for a plane-parallel 5-MHz quartz in water.

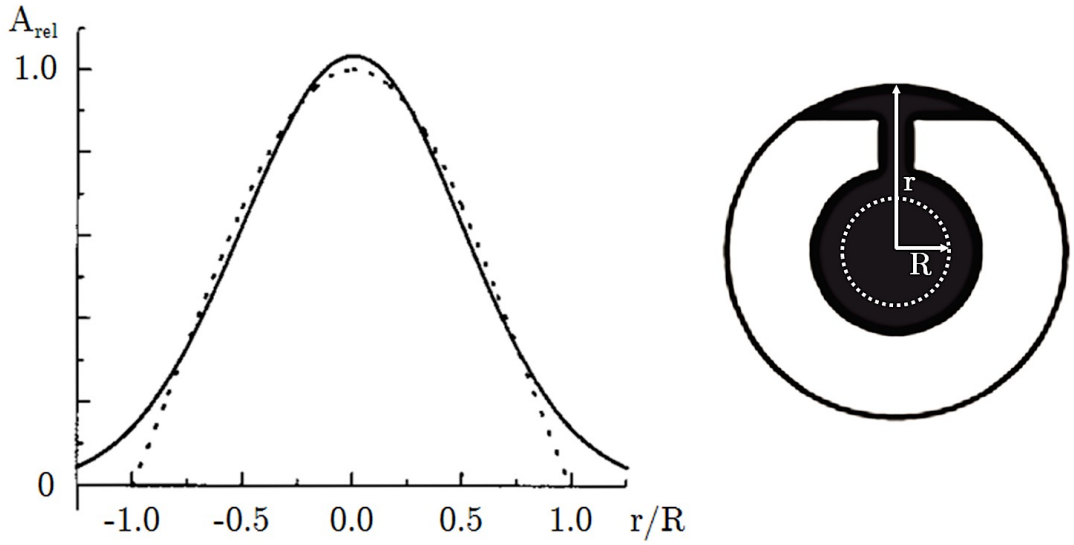

Figure 6: Oscillation amplitude: radial distribution of the relative oscillation amplitude (left panel) at the quartz surface (right panel) in accordance with a Gaussian distribution (solid line) and a Bessel distribution (dotted line). The Gaussian function comprises motion near electrode edges where r/R = 1, Bessel distribution, in contrast, decline to zero at the electrode edge [1] Taken from (Janshoff, Gala, & Steinem, 2000).

Furthermore, it is important to have the measurement chamber free from air, so as to prevent air bubbles and variation in liquid meniscus in order to exclude reflection of induced longitudinal waves at the air-liquid interface, which in turn affects the resonance frequency [1]. Analytes are added by pumping them through an inlet and outlet of the chamber cell and simultaneously, the resonance frequency can be monitored. Kinetic data as well as thermodynamic equilibrium values can also be acquired with this QCM setup.

1.1.5. Quartz Crystal Microbalance with Impedance Analyzer (QCM-IA) and Quartz Crystal Microbalance with Dissipation Monitoring (QCM-D)

Studies on bio-chemical reactions in liquid including high affinity based avidin-biotin interactions, as in the realm of this research, as well as nano-assemblies of poly-electrolyte layers are possible with the QCM-impedance analyzer (QCM-IA) and QCM with dissipation monitoring (QCM-D). In applying the impedance QCM, the Keysight E4990 impedance analyzer, whose frequency ranges from 20 Hz to 120 MHz is connected to the QCM-Flow-Cell-System (Figure 7), forming a complete QCM setup together with a graphical user interface (GUI) written in Matlab [22]. The GUI is presented either directly on the impedance analyzer operating system or on an external computer and enables the controlling of the QCM measurement [22]. The QCM impedance analyzer identifies the fundamental frequency of the quartz crystal, the harmonic resonance number and the voltage drive level. It likewise measures the frequency shift, which results in the calculation of the mass adsorption based on the Sauerbrey´s equation, as well as the resistance change of a quartz crystal, with which dissipation is determined [22]. Depending on the mass adsorption and the dissipation different parameters of the molecular interaction such as structure properties of the surface assemblies, kinetic reaction data and layer thickness can be deduced.

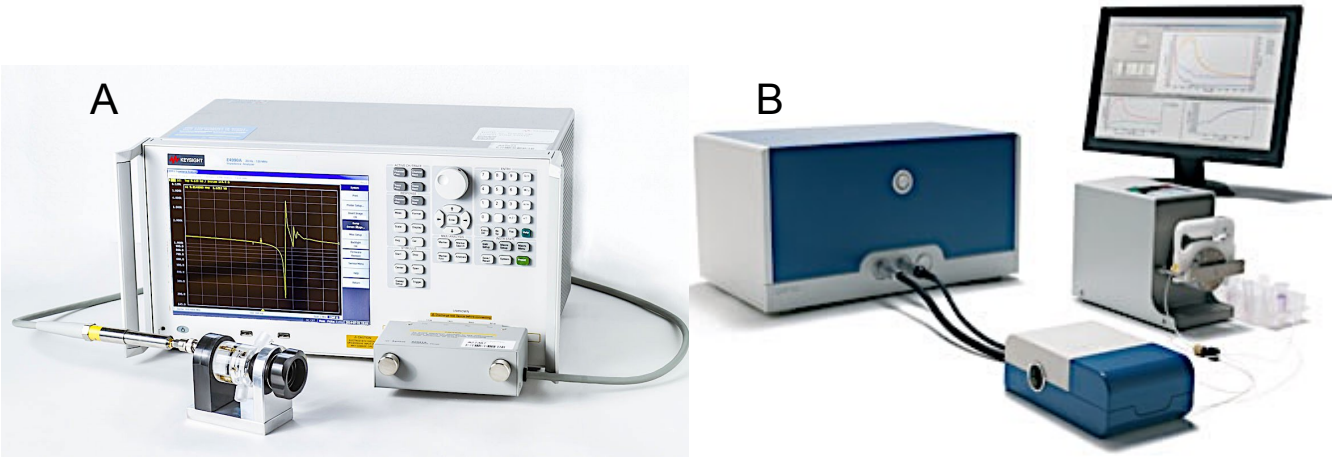

Figure 7: (A) Keysight E4990 impedance analyzer connected to QCM-Flow-Cell-System. (B) Complete system of Q-sense E1 of QCM-D.

Similar to QCM-IA, QCM-D technology permits quantitative analysis of the viscosity, shear elastic modulus and thickness of adsorbed thin layers [23]. Since the Sauerbrey relation only holds for layers, which are rigid, homogenously distributed, and thin adsorbed, soft or viscoelastic films that do not completely couple to the oscillating crystal turn out to be wrongly estimated by this relation [23]. Such a phenomenon can be detected by the dissipation signal. When the driving voltage to the crystal is turned off and the energy released from the oscillating crystal dissipates from the system, dissipation (D) is said to have occurred:

$$D = \frac{E_{lost}}{2\pi E_{stored}} \quad (6)$$

whereby E_{lost} is the energy lost in the course of one oscillation cycle and E_{stored} the total energy stored in oscillation.

Water or liquids used for analyzing can couple to the analytes that have adsorbed to the oscillating crystal. Such liquids serve as an extra dynamic mass, hence the layer is detected as viscoelastic "hydrogel". With the help of the dissipation, the differentiation between a rigid and viscoelastic thin layer can be made. Moreover, structure analysis is possible depending on the value of the dissipation, in that it can be distinguished whether the liquid-coupled-molecule is bound at a standing or lying position [23].

1.1.6. Streptavidin, Avidin and Mutant Avidin M96H

Most biosensor detection concepts are grounded on changes in viscoelastic or optical properties at the sensor interface induced by binding of biomolecules [24, 25]. An extra requirement demanded for a label-free biosensor is the resistance of the sensor surface to non-specific adsorption [2, 26]. In order to achieve this, the biosensor surface can either be coated with "protein resistant" monolayers of short or long polymer chains [27 - 29] or by forming a dense layer of bait molecules [30].

A common strategy for biomolecule immobilization to sensor surfaces is to exploit the strong affinity between biotin and the proteins streptavidin and avidin [25]. This can be accomplished by two ways:

1. biotinylated bait molecules (eg. ligand) are immobilized on a sensor surface that has been pre-functionalized with streptavidin or avidin (Figure 8A) [2], or
2. functionalizing the sensor surface with biotinylated self-assembled monolayer (SAM) and then streptavidin or avidin (Figure 8B) [2]. This serves as an interacting pocket for biotinylated bait molecules.

The approach explained in point 2 above is applied in this project.

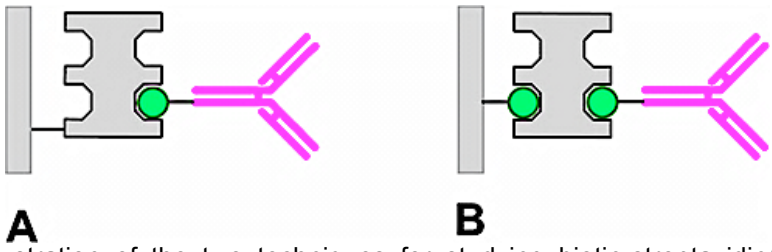

Figure 8: Schematic illustration of the two techniques for studying biotin-streptavidin/-avidin interaction. (A) Immobilization of biotinylated antibody to streptavidin/avidin-functionalized surface. (B) Immobilization of biotinylated antibody to a surface made of biotinylated-SAM and streptavidin/avidin. Taken from (Pollheimer, et al., 2013).

The proteins streptavidin, which is secreted by the bacteria streptomyces avidinii, and chicken avidin, which is extracted from egg white are functionally [31 - 33] and structurally [34, 35] analogous proteins. These 60 kDa tetrameric proteins exhibit four binding sites with extremely high and specific affinity to the 244 Da vitamin biotin, with dissociation constants of $K_d \approx 10^{-14}$–10^{-16} M, yet they possess a different isoelectric point (pI), ie. ca. ~5.5 and ca. 10 for streptavidin and avidin, respectively [25, 36, 37]. Their crystal structures are estimated to be cubic with 4.75 Å side length [31, 38]. Additionally, streptavidin and avidin portray other properties, such as high resistance to changes in pH, exposure to denaturants and temperature and due to this, they can be used under different experimental conditions [31].

M96H is an avidin mutant modified by replacing the methionine interface residues at position 96 by histidine residues [39]. This M96H has a strong biotin binding ability over a wide range of pH conditions i.e. from neutral to weekly acidic pH ranging from 4 to 10, and can easily be denatured when desired under acidic condition [2, 37]. Taking the properties of this M96H into account, it is assumed that an acidic denaturant would cause the M96H to dissociation from biotinylated SAM much easier than from streptavidin and avidin. A detailed explanation is given in section 2.1.

1.2. Introduction - Atomic Force Microscopy and Erythrocytes

1.2.1. Atomic Force Microscopy

Atomic Force Microscopy (AFM) is a member of Scanning Probe Microscopy (SPM) family whose imaging technique comprises a mechanical device, a flexible cantilever, that assesses very small forces that exist between atoms and molecules on the tip and sample surfaces when they are at close proximities (Figure 9), hence its name´s origin AFM [40]. The AFM cantilevers, which are either triangular or rectangular in shape with a sharp tip, are mostly made from silicon and/or silicon nitride wafers [41]. Since its invention in 1986 [42, 43], the AFM has turned out to be an increasingly important apparatus for studying surfaces with high resolution [43]. The fundamental concept of an AFM is based on i) the conversion of the existing attractive force into bending the cantilever to the surface, and ii) the conversion of the repulsive force into the deflection off of the surface. This deflection is detected by a laser beam, which is reflected from the back of the cantilever onto a photodiode detector. Most AFM photodiodes are made of four quadrants, the deflection brings about changes in the angle of the reflected laser beam which in turn falls on different parts of the photodiode and the calculations of these reflected spot positions result in the deflection signals: the top and bottom halves gives the vertical deflection, which measures the internal force, whilst the left and right halves evaluate the lateral twisting of the cantilever [40].

The AFM has key advantages over other high-resolution methods such as electron microscopy and X-ray diffraction: it allows imaging of fixed and live cells, nucleotides, membranes and proteins; moreover, samples do not have to be stained, coated or electron-conductors, hence, imaging with high resolution in physiological condition, in buffer or medium, which are essential for studying the structure and function of biomolecules etc. [43, 44] are possible.

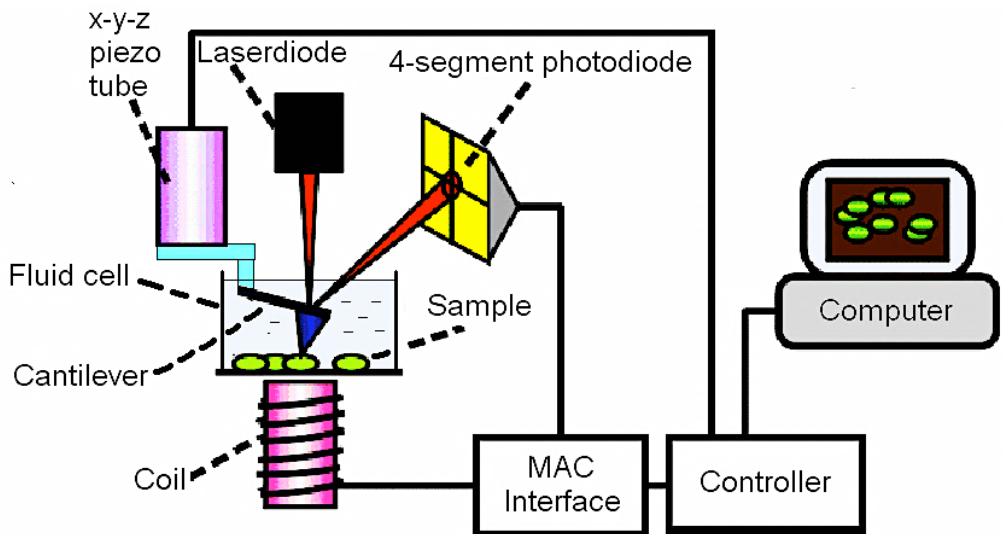

Figure 9: AFM setup. The AFM uses a cantilever with a sharp tip at its end, which is used to scan the surface of the sample. The laser reflected from the top surface of the cantilever is detected by the 4-segment photodiode, which measures the deflection of the cantilever. The piezo tube moves the cantilever in the x and y direction for scanning the sample and/or in the z direction for adjusting the distance between the tip and the sample. Taken from (Anneliese Raab).

1.2.2. Imaging Modes

There are distinct and numerous AFM imaging modes of operation available depending basically on the movement of the tip over the sample [47]. The contact mode as well as intermittent contact mode (also called the dynamic contact, tapping or AC mode) are the two most commonly used modes in AFM bio-applications. These two are also the modes used in this work.

In contact mode, the tip of the cantilever is always in contact with the surface of the sample. As the tip is raster-scanned over the sample, the detection system measures the cantilever deflection [47]. It becomes necessary to employ a feedback loop, which can help in monitoring the cantilever response and adjusting the height of the cantilever duly so that the changes in surface height will be considered, restricting the tip from pressing into the sample. Commonly the “PI” controller, hence, the proportional-integral feedback is used to control the imaging. By using the difference between the actual values and setpoint, the height position of the cantilever is altered. The fastness of the feedback in response to the change in sample height depends on the settings of the time constant of the integrator and the value for the proportional gain. In this mode, the setpoint value is the deflection of the cantilever, therefore a lower setpoint value results in a lower imaging force. The system tries to keep the force constant by contracting and extending the piezo. A topography image can be acquired by recording the voltage applied to the piezo [40].
After taking several scans with the contact mode, samples and tip may show some degradation effects, this effect is more pronounced on soft surfaces, hence contact imaging is ideal for solid surfaces.

In intermittent contact mode, an oscillating tip makes a repulsive contact with the sample surface at the bottom point of the oscillation and a monitory of the amplitude and phase of the cantilever is done near its resonance frequency [47]. Generally, the setpoint amplitude is selected and the height adjusted to correspond to this amplitude through the feedback system. The cantilever is normally driven close to the resonance frequency of the cantilever to give a reasonable amplitude for the oscillation and to also give information on the phase between the drive signal and the cantilever. In this mode, the setpoint value is the amplitude of oscillation of the cantilever at which the tip touches the sample surface, hence, a high setpoint value results in less damping by the sample and therefore a lower imaging forces. The outcome of this mode are topography, phase and amplitude images [40].
Since in the intermittent contact mode the tip is in on and off contact with the sample, the sample damage is low compared to contact mode for some samples [40].

The kind of mode used determines which characteristics the cantilever must posses. Usually, better images are given by lower forces and since in contact mode the deflection of the cantilever is determined as the tip scans over the sample, the use of soft cantilever will not only result in the same deflection but also a low force [40]. In this case, cantilevers with spring constants (k) below 0.5 N/m can be used. In summary, the deflection and the spring constant of the cantilever are directly related to the applied force [40] in accordance with Hooke´s law:

$$F = -k * d \tag{7}$$

F represents the force, *k* the cantilever spring constant and *d* the cantilever deflection. Here it is noteworthy that the deflection of the cantilever is linear to the acting force.

With respect to the intermittent contact mode, more stable in-air-images are given by stiffer cantilevers often with 200 – 400 kHz resonant frequency and spring constants of 10 N/m and above, which allow the cantilever to be free of the capillary force when it is in contact with the sample. This capillary force is however not a problem for intermittent contact mode in liquid, thus, soft cantilevers and often the contact-mode-cantilevers are used. The classical soft cantilevers in liquid normally have few kilohertz resonance frequency, however actually the cantilever is driven at the liquid cell´s resonance[40].

1.2.3. Force Spectroscopy (FS)

Apart from AFM being known for its high-resolution imaging capabilities, it is also acknowledged for high sensitive force measurements down to piconewton range in liquid environment [48]**.** This has extensively enhanced the comprehension of numerous biological and physiological processes down to the molecular level. Using the piezoelectric scanner, the base of the cantilever is moved vertically (known as scanner displacement (z)) towards the surface and retracted again [40]. The deflection of the cantilever (d) can be measured during the scanner displacement and this is generally known as the force spectroscopy (FS) [49]. In order to obtain the distance, the cantilever deflection is subtracted from the scanner displacement (z-d). The data from such experiments is converted into a force-distance curve (FDC) (Figure 10), where the cantilever deflection is converted into force using the Hooke´s law (Equation 7) [49].

Basically, the **mechanism of FS** is as follows (Figure 10): the cantilever approaches the probed surface and at some point during the approach, the attractive forces, usually capillary and Van der Waals forces, that exist between the cantilever tip and the probe overcome the cantilever spring constant and the tip jumps into contact with the surface. Upon further approach, the distance between the base and the sample becomes tighter. At this point, the deflection of the tip as well as the repulsive contact force increase linearly until reversion of the tip movement. In the course of retraction,

due to adhesion, the tip normally remains in contact with the surface causing the cantilever to deflect downwards. At some point, the force from the cantilever becomes sufficient to overcome the adhesion and the tip breaks free [40]. Information on possible adhesion can be seen in the retracting curve. Additional details about the stiffness of the surface can be derived from the slope: a hard surface yields a steeper slope while a soft surface a gentle slope.

For FS measurements in which for example the receptor-ligand interaction is probed, usually the **cantilever tip is functionalized with the ligand**. Then the FS experiment is run on the sample containing the receptor just as explained above. Nevertheless, if an interaction complex is formed between the ligand-functionalized-tip and the receptor on the sample surface, the ligand-receptor bond turns to be stretched mechanically during retracing. The loading force increases forming a parabola-like shape in the retracing curve. This parabola-like shape is formed as a result of the flexibility of the cross-linker used to attach the ligand to the tip, since such linkers do not have a single spring constant. In the end, the bond breaks at a characteristic force, the unbinding force, causing the return of the cantilever tip to its resting position, which are the jumps seen in the retrace curves. If no interaction exists between the ligand-functionalized-tip and the sample, the retraction and the tracing curves look alike.
Furthermore, the **specificity of the receptor-ligand complex** is normally proven by blocking either the ligand on the tip with complementary specific receptor (known as tip-blocking process) or the surface receptor with cognate ligands (known as surface-blocking process) [50]. By so doing, almost all specific recognition signals are expected to vanish.

A repetition of the force curves are commonly done either at diverse locations, in order to build up a map of tip-surface interaction, or repeatedly at a single well-defined position [49] so that a complete statistical understanding of the interaction can be achieved.

It is essential to calibrate the actual spring constant of the cantilevers, which can vary substantially from the stated manufacturer values, when quantitative force measurements are done. This spring constant is the force needed to bend the cantilever per unit distance and this is normally given in the unit Newton/meter (N/m) [41]. One of the common methods used for this determination is the thermal noise method, which regards the cantilever as a simple harmonic oscillator according to Butt and Hutter [41, 43, 52]. The Agilent AFM (which is the setup used in this study) has the thermal K option permitting users to calculate the spring constant of an AFM probe by taking into account the motion of the cantilever as a harmonic oscillator through implementing the equipartition theorem of fundamental thermodynamic theory [41]. The theory formulates that the kinetic energy reserved in a system at a momentum coordinate, i.e. the deflection of the cantilever from its equilibrium state, is

equivalent to one half of the thermal energy of the system [41, 53]:

$$KE_{avg} = \frac{1}{2}kBT \quad \text{.....(8)}$$

where KE_{avg} is the average thermal energy, *kB* the Boltzmann´s constant (*kB* = 1.38*10^{-23} J/K) and *T* the absolute temperature in K.

In respect of AFM probes, the deflection of a cantilever from its equilibrium position is regarded to be small, hence, it is considered to be linearly related to the forced needed to bend the cantilever as stated by Hooke´s law (Equation (7)) [41].

Generally, a simple determination of the deflection value of the cantilever and the temperature would be enough to calculate the spring constant. However, since the cantilever is not an ideal Hookean spring, a more accurate result will be achieved from the resonant peak in the Power Density Spectrum (PDS) spectra of the vibrational noise [40].

On that account, the determination is performed with the ´Spectroscopy´ feature of the AFM software, ´PicoView´ as follows: after acquiring a ´deflection vs. distance´ curve with the cantilever on a rigid surface (e.g. mica), the slope of the curve is used to calculate the sensitivity of the cantilever (nm/Volt) in the ´Advanced´ window of the ´Spectroscopy´ feature. Then a PSD plot is acquired in the ´Thermal K` window, so as to obtain the resonant frequency of the cantilever. Thereafter, the spring constant of the cantilever (N/m) is determined [41].

In order not to damage the cantilever tip, spring constant calibration of this kind is done at the end of all FS experiments.

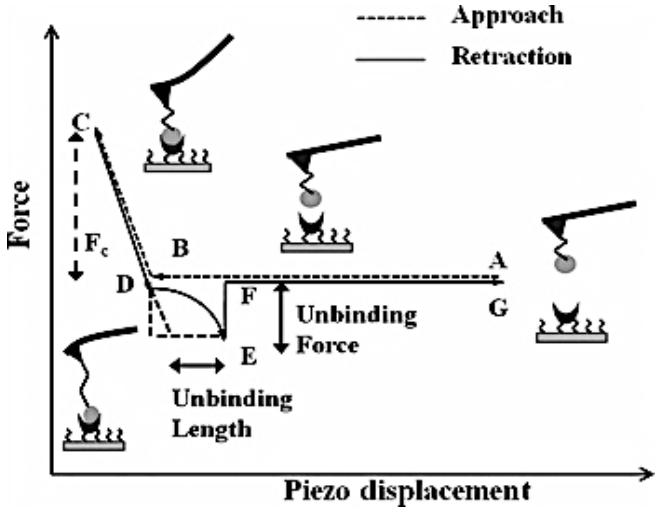

Figure 10: Schematic illustration of a typical force distance curve (FDC) of a specific ligand-receptor binding event with the piezo displacement (i.e. tip-sample distance) on the x-axis and force (or the cantilever deflection) on the y-axis. At (A) the ligand-functionalized tip approaches the receptor, at (B) the ligand contacts the receptor and the acting force increases during further approach resulting in a linear force increase until reversion of the tip movement from (C) to (D). Upon retraction, the ligand-receptor bond turns to be stretched mechanically. The loading force increased forming parabola-like shape in the retracing curve between (D) and (E). In the end, the bond breaks at a characteristic force, the unbinding force at (F), causing the return of the cantilever tip to its resting position at (G). Taken from (Bizzarri & Cannistraro, 2010).

1.2.4. Tip Chemistry

Functionalizing the cantilever tip is the norm when using FS and topography and recognition (TREC) imaging (in section 1.2.5) for in-depth insight into molecular interactions, for example between receptors and ligands. This technique requires attaching a sensor molecule (e.g. an antibody) to the tip, transforming it into a specific biosensor which can identify its cognate target molecule (e.g. an antigen) [54]. To achieve that, suitable procedures are required in which some particular points have to be considered:

a) the biomolecule to be tethered to the tip ought to be flexible enough in order to freely interact with its target molecule;
b) the force which attach the molecules ought to be stronger than the intermolecular force that is to be investigated;
c) it is ideal to attach the biomolecule at a low surface density so as to acquire a single-molecule recognition; and
d) non-specific adhesion should be avoided as much as possible [55] .

The amine-functionalization procedure is one of the known approaches used to covalently attach biomolecules to silicon tips. The amine-treated tip is reacted with a cross-linker, which equips the ligands with enough mobility and prevents it from denaturation [54]. Usually, the cross-linker is made of two functional ends, i.e., an amine reactive group on first end and vinyl sulfone or 2-pyridyldithiopropionyl groups, which binds covalently to thiols, on the second. As an alternative, aldehyde group are used to attach proteins directly via amino groups ($-NH_2$) in their lysine residues [54, 55]. It is important that the reactive group on the second end of the cross-linker is unreactive to the amino group on the tip. Therefore, the acetal group is used instead of the aldehyde group to solve this problem which occurs partially when the aldehyde group is used. Later, after the cross-linker has been attached to the tip, the acetal is then converted to an aldehyde function [54]. And this is the approach used in this study.

Typically polyethylene glycol (PEG) chains are the cross-linkers employed in this procedure. Additional advantages portrayed by this PEG are:

a) promoting the binding of the tethered biomolecule (since it can reorient itself quickly) to the complementary target molecule;
b) specific binding in FS experiment can be differentiated from non-specific tip-surface adhesion when 6-9 nm long PEG linker is used; and
c) also fast concurrent imaging of TREC is dependent of such elastic 6-9 nm long PEG linker [54].

In the tip chemistry part of this study BRAD5 antibody was used. This BRAD5 antibody functioned as a ligand and it was linked to the tip to recognize the RhD receptor on a flat erythrocyte ghost surface (detail in section 1.2.6).

1.2.5. Topography and recognition (TREC) imaging

Thanks to the invention of the simultaneous TREC imaging mode, it is possible to identify receptor sites on a surface with nanometer positional accuracy and concurrently map the topographical details [50]. This methodology enables individual receptor sites in the recognition image to be assigned to structures from the topographical image. In this way, varieties of proteins or other biomolecules can be specifically recognized and mapped on cells, membranes or other subcellular structures [44].

The use of a sensing ligand-functionalized AFM tip is the precondition for imaging of this kind as explained in section 1.2.4. In TREC, AC mode is employed, whereby the cantilever is oscillated close to its resonance frequency with constant amplitude (section 1.2.2). The electronic circuit in the PicoTREC box split the oscillation signal into upper and lower parts (Figure 11). The upper part of the amplitude which is determined by the molecular recognition yields the recognition image and in contrast, the lower part which is being used for driving the AFM feedback loop produces the topography image.

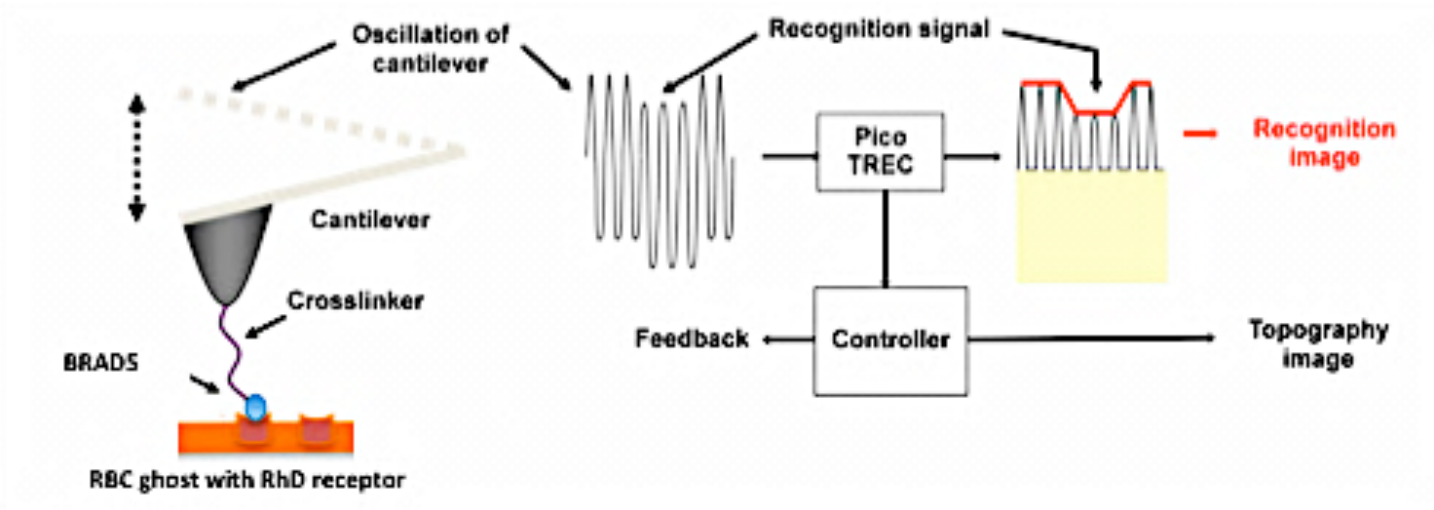

Figure 11: Schematic demonstration of the principle of TREC imaging on RhD-receptor with cantilever tip functionalized with BRAD5. The signal resulting from the oscillation of the cantilever is split into two parts in the TREC box: the lower and the upper part yielding the topography and recognition image respectively. Modification from (Ahiable, 2013) with the permission of Dr. Rong Zhu.

1.2.6. The Red Blood Cells (RBC) or the Erythrocytes (ERY)

The Red Blood Cells (RBC), also known as erythrocytes (ERY) (Figure 12) are the transporters of oxygen in the body and they develop from bone marrow stem cells [3]. Also, these cells are the most common type of blood cells in the human. Due to the immense content of hemoglobin, which is an iron-containing protein that binds oxygen and is responsible for the cell´s red color, the RBCs tend to be anucleated and lose their organelles during maturation in mammals [3, 4]. Approximately, 270 million hemoglobin molecules per cell, of which each has four heme groups, ensure oxygen transport [3]. The natural life-span of the RBCs in the circulatory system prior their selectively removal by macrophages in the reticuloendothelia system (RES) is 100 – 120 days [3, 56]. The shape of the erythrocyte is circular from the top view but biconcave from the side view [3, 4]. The normal human RBCs usually are 7 - 8 µm in diameter [3, 4]. According to Dean [5], the surface consists of a lipid bilayer and also of a lot of membrane receptors. One of the most complex blood group classifications known in humans is the Rh blood group. Actually, in the field of transfusion medicine it is the next in importance to the ABO blood group. About 50 Rh antigens are known so far [5]. As part of a protein complex in the RBC membrane, these Rh antigens are exclusively expressed in cells of the erythroid line, thus only in RBCs. The highly immunogenic function of these antigens is the main cause of hemolytic disease of the newborn (HDN) and hemolytic transfusion reaction (HTR) and this disease can be prevented by administration of antibodies against such antigens [5]. Among others, the most significant Rh antigens are D, C, E, c and e. The majority of the human race, precisely 85% Caucasians, 92% Blacks, and 99% Asians, are RhD positive [5]. This D antigen has a variation of 35 amino acids from the C/c and E/e antigens, and exactly this difference is the reason behind its dominate immune response [57]. Immunoglobulin G (IgG) makes up greater part of the Rh antibodies and the minority is immunoglobulin M (IgM) [5]. For this research, the BRAD5 was used. The BRAD5 is a human monoclonal IgG1 anti-RhD antibody produced from a stable Epstein-Barr virus-transformed B-lymphoblastoid cell lines [55]. The mechanism reveals that upon the interaction between RBC-bound IgG and IgG Fc receptors (FcyR) on the effector cells, the anti-D-coated RBCs are eliminated from the circulation by mononuclear phagocytic cells in the spleen [58].

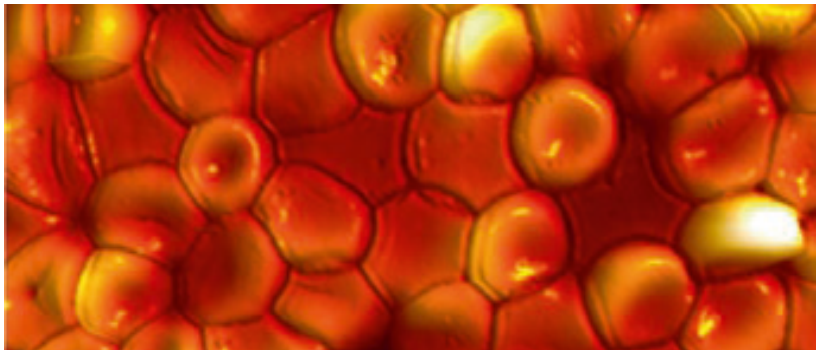

Figure 12: AFM image illustrating erythrocytes on poly-L-lysine coated glass. Taken from (Ebner, Schillers, & Hinterdorfer, 2011).

2. Aims

2.1. Project aim for Regeneration in QCM

Biotin-streptavidin or -avidin biotechnique is employed in several application fields like DNA hybridization [59, 60], screening [61, 62], and protein interactions [63]. Due to the broad implementation of this methodology, it has become appealing for nearly all surface based sensing systems, as in the case of QCM in this study. A drawback in this biotin-streptavidin or -avidin technique is the need for complete regeneration down to the functionalized gold-coated-quartz electrodes after each measurement. In other words, it is desired to cleave the streptavidin or avidin that binds to the biotin so that further immediate measurement with the same gold electrode can be done.

The motive behind this regeneration is as follows:

a. It saves time, since the quartz crystals need to be cleaned under harsh conditions before each functionalization and measurement step. The cleaning and functionalization procedures usually take a whole day.
b. It saves cost: as the most urgent requirement for in situ exchange of bait molecules is experienced in occurrence where the removal of the prey molecule from the biotinylated bait is impossible without denaturing the latter [2]. In such a case, it is necessary to dispose the whole quartz crystal after each single measurement.
c. The deviation between different sensors, which is a problem of some product lines, is eradicated [2].
d. Human intervention for crystal exchange and concomitant interruption of the work flow is eliminated [2].

Due to the above motivation, the aim of this project was to establish a protocol in which the streptavidin-, avidin- and M96H-bridge that link the adsorption of biotinylated-bait-prey complex to a biotinylated-SAM quartz surface (Figure 13B) can be regenerated rigorously (Figure 13C) to allow further analysis.

The preliminary step to take for the accomplishment of this purpose is to firstly functionalize the gold coated quartz crystal with biotinylated SAM composed of biotin-PEG_8-thiol linker, mixed with either hydroxyl-PEG_6-thiol or methoxy-PEG_6-thiol (Figure 14) at different ratio. By this means, non-specific interaction can be eliminated. Then, bind avidin, streptavidin and M96H via the high affinity interaction between them and biotin online. And finally, regenerate the biotinylated SAM surface with two different solutions: 8 M Guanidine-hydrochloride (GuHCl) at pH 1.5 and Regeneration Solution X (RSX). Please note that the RSX is patented, hence, its actual composition is restrained. It is expected that the acidicity of the denaturant will cause a protonation of the histidine in the subunit position of M96H and

this will promote the binding of the denaturant to the subunit and subsequently causing a faster dissociation of M96H than streptavidin and avidin. This assumption is to be verified in this study.
Subsequently, the application of the successful regeneration method was to be investigated with Human Rhinovirus (HRV) and its biotinylated antibody 8F5.

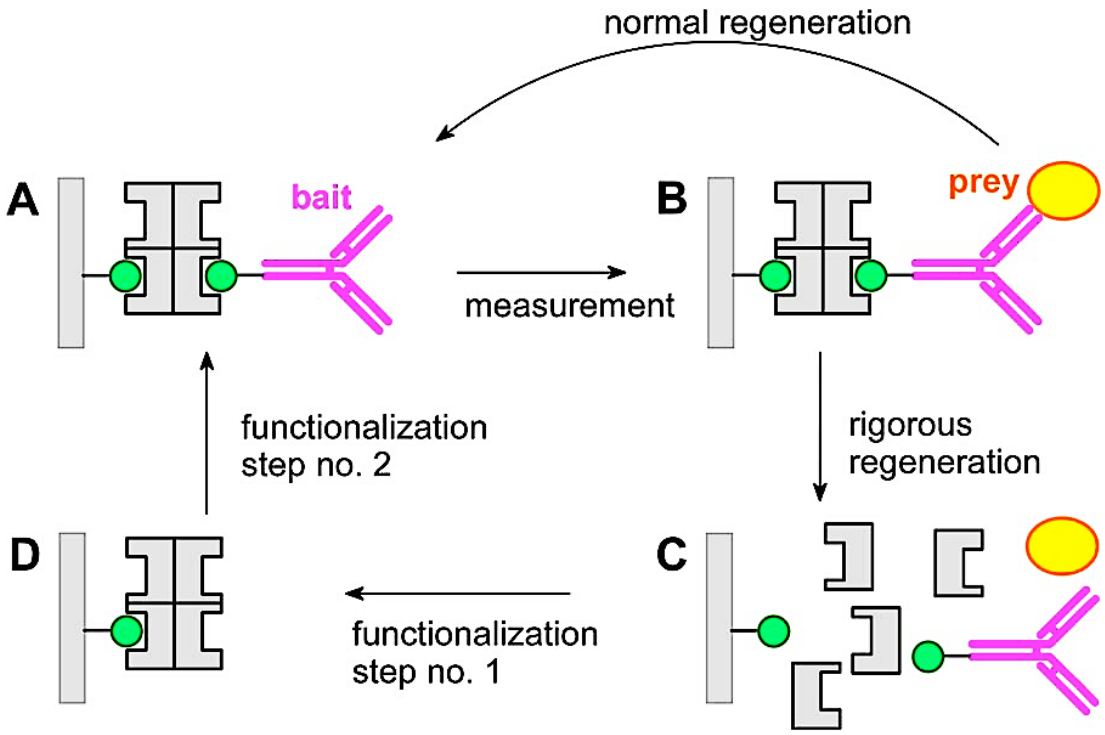

Figure 13: Illustration of normal and rigorous regeneration with a denaturant. (A) Biotinylated bait (or antibody) binding on a biotinylated SAM with either streptavidin, avidin or M96H bridging in between undergoes a measurement where a prey (or ligand) binds to the bait. The prey is either removed by normal regeneration in which the biotinylated bait and the bridge remain intact (A) or by rigorous regeneration in which the bridge is dissociated (C), upon which a new round of functionalization step with streptavidin, avidin or M96H (D) was possible. Taken from (Pollheimer, et al., 2013).

2.2. Project aim for ERY and AFM

Understanding the interaction of RhD antigens on the RBCs with its specific antibody D as well as their distribution on the RBCs is a vital area of investigation that could be of great contribution to the medical field. The ultimate and primary experimental aim of this project was to provide a protocol for preparing flat RBC ghosts. In this context, RBC ghosts refer to RBCs that are depleted of hemoglobin and have lost either most or all of their internal proteins [64]. The RBC ghosts would then make it possible to investigate their surface RhD receptors by applying AFM, hence, the next goal.
The general approach to isolating cellular membranes was to attach the cell on a functionalized surface and thereafter remove the cell body [50, 65, 66]. The flat RBC ghosts were, therefore, to be

achieved by attaching RBC membranes on a functionalized glass cover slip, then flushing out hemoglobin as well as residues of cytoskeletal proteins and subsequently fixing back the membranes to each other. The advantages of such technique were diverse:

a) a stiff membrane would be obtained because instead of on a soft cytosol, the ERYs would lie on a hard support;
b) since there would not be any underlying structures, for example cytoskeleton, a flat membrane would be acquired. These flat and stiff membranes would permit a high resolution AFM imaging [50].

And finally, to specifically investigate the RhD receptors on the flat ghost, the cantilever tip was to be functionalized with the antibody BRAD5. Then measurements revealing interaction forces were to be carried out on the RBCs, as well as TREC mapping, which would result in visualization, identification and quantification of the RhD receptors.

3. Experimental

3.1. Chemicals and equipment

3.1.1. Chemicals for functionalization of QCM sensor with biotinylated SAM.

1. Biotin-polyethelene glycol $(PEG)_8$-thiol (Polypure, Norway)
2. Hydroxyl- polyethelene glycol $(PEG)_6$-thiol (Polypure, Norway)
3. Methoxy- polyethelene glycol $(PEG)_6$-thiol (Polypure, Norway)
4. Ethanol (VWR, Fontenay-sous-Boris, France)
5. Hydrogen Peroxide (VWR, Fontenay-sous-Boris, France)
6. Ammonium solution min. 25% (VWR International, Fontenay-sous-Boris, France)
7. Gas Nitrogen
8. Water, Milli-Q water (mQH_2O), purified and deionized to a resistivity of 18.2 MΩ·cm with Milli-Q system (MilliPore,France)
9. Sodium dodecyl sulfate (SDS)

3.1.2. Equipment for functionalization of QCM sensor with biotinylated SAM.

1. Rotary evaporator
2. Small glass bottles
3. Quartz crystal holder (JKU, Institute of Biophysics, Austria)
4. Quartz crystal incubating chamber (JKU, Institute of Biophysics, Austria)
5. Quartz crystal: AT-cut quartz crystals (ICM, USA), sputter-coated with 100 nm thick gold layer on 10 nm chromium adhesive layer, with a diameter of 13.7 mm and a fundamental resonance frequency of 10 MHz
6. QCM-D sensor crystal: AT-cut quartz (Q-Sense, Sweden), sputter-coated with 100 nm thick gold layer on 50 nm chromium adhesive layer, with a diameter of 14 mm and a fundamental resonance frequency of 5 MHz were used.
7. Chemical hood
8. Tweezers
9. Ultrasonic bath (VWR International, Fontenay-sous-Boris, France)

3.1.3. Chemicals for QCM Measurements and Regeneration

1. Avidin, chicken egg white (amresco, Solon, Ohio)
2. Streptavidin (amresco, Solon, Ohio)
3. Avidin mutant M96H was constructed for bacterial expression in E. coli by introducing mutation M96H to OmpA chicken avidin in pET101/D (Hytönen, 2004) (Pollheimer, et al., 2013)

4. Phosphate buffered saline (PBS): 5 mM Na_2HPO_4, 150 mM NaCl, pH 7.3.
5. Guanidine Hydrochloride (GuHCl)
6. Antibody 8F5 (Vienna Biocenter (VBC), Austria)
7. Human Rhinovirus (Vienna Biocenter (VBC), Austria)
8. Succinimidyl-6-(biotinamido)hexanoate (NHS-LC-Biotin), (ThermoFischer Scientific, USA)
9. Dimethyl sulfoxide (DMSO)

3.1.4. Equipment for QCM Measurements and Regeneration

1. Vortex
2. Eppendorf tubes
3. Chemical hood
4. Liquid chamber (Institute of Biophysics, Linz, Austria)
5. Automatic programmable syringe pump (NE-1000, New Era Pump Systems Inc., USA)
6. Peristaltic pump(Ismatec Reglo Digital M2-2/12 from Q-sense, Sweden)
7. Keysight E4990 impedance analyzer (Keysight, Malaysia)
8. QCM-D: Q-sense E1 from Q-sense, Sweden [23, 67]:
    a. Measurement Chamber Platform QCP 101: QCP 101 is a temperature controlled compact design which can hold one sensor in one flow module. The samples are injected via an inlet and outlet by using a peristaltic pump included in the system.
    b. Peristaltic pump, Ismatec Reglo Digital M2-2/12: To introduce the sample to the chamber a constant liquid flow rate is provided by this automatic Peristaltic pump from Q-sense.
    c. Electronics Unit QE 401: This is the core of the system, which enables high sensitivity, multi-channel, multi-frequency, ranging from 1 to 70 MHz with up to the 13th overtone, 65 MHz for a 5 MHz crystal, and temperature-controlled measurements, from18 to 45°C. The Electronics Unit serves as the link between the Measurement Chamber and the PC.
    d. Software QSoft 401 and Q-Tools 2.0: QSoft 401 is used for the acquisition of data. For each sensor the responses of the two parameters, f and D, are plotted on the PC-screen in real time. QTools is applied for data analyzation and presentation of results such as creating different plots or conducting mathematical modelling of measurement results extracting mass, thickness, viscoelastic properties, kinetic constants and identifying adsorption phases. The data can also be imported/exported to Excel, BMP, JPG, WMF files for further processing.

3.1.5. Chemicals for preparation of flat ERY ghost

1. Phosphate buffered saline (PBS): 5 mM Na_2HPO_4, 150 mM NaCl, pH 7.4.
2. Ethylene glycol tetra-acetic (EGTA) (Sigma, Deisenhofen,Germany).

3. Very low salt buffer (vlsb): 0.3 mM Na_2HPO_4/NaH_2PO_4, 0.2 mM EGTA, pH 7.4).
4. Isotonic PBS with 0.2 mM EGTA
5. Poly-I-lysine (PLL) (Sigma-Aldrich, Steinheim, Germany).
6. Glutaraldehyde – Solution 25% (AppliChem, Darmstadt, Germany).
7. Ultrasonic bath (VWR International, Fontenay-sous-Boris, France)
8. Acetone (VWR International, Fontenay-sous-Boris, France)

3.1.6. Equipment for preparation of flat ERY ghost

1. Microcentrifuge 5417R (Eppendorf, Hamburg, Germany).
2. Glass cover slips (Thermo Scientific, Braunschweig, Germany)

3.1.7. Chemicals for tip Chemistry

1. Ethanolamine hydrochloride (Sigma–Aldrich, Austria).
2. Ethyleneglycol-bis(Succimidyl-succinate) = EGS (Sigma–Aldrich, Austria).
3. PBS: pH 7.3, 140 mmol NaCl, 2.7 mmol KCl, 10 mmol Na_2HPO_4, 1.8 mmol KH_2PO_4
4. Citric acid 1% solution
5. NaOH, 100 mM
6. Chloroform
7. Diethyl ether
8. Isopropanol
9. Sodium cyanoborohydride, ($NaCNBH_3$)
10. BRAD5 antibody (NHS Blood and Transplant, Norway)
11. Triethylamine (TEA)
12. 1 M ethanolamine (pH 8.0) was prepared by dissolving 975 mg ethanolamine hydrochloride in water at a final volume of 10 mL and adjusting the pH to 8.0 with 20% NaOH

3.1.8. Equipment for tip Chemistry

1. Molecular sieve 0.4 nm (Merck, Germany).
2. Desiccator 5 L with O-ring

3.1.9. Chemicals and equipment for imaging flat ERY Ghost

1. PicoPlus AFM equipped with MACMode controller (Agilent, Santa Clara, USA).
2. MSCT SiN_3 cantilever k = 0.01 N/m (Veeco, Santa Barbara, USA).
3. AFM fluid cell, ~22 mm diameter.

4. PBS: 5 mM Na_2HPO_4, 150 mM NaCl, pH 7.4.
5. Purified RBCs ghost

3.1.10. Chemicals and equipment for FS of flat ERY ghost

1. Aminopropyl-triethoxysilane (APTES).
2. Triethylamine (TEA).
3. Acetal-polyethylene glycol (PEG)-NSH cross-linker
4. Specific target molecule, BRAD5 antibody
5. MSCT Si_3N_4 cantilever k = 0.01 N/m (Veeco, Santa Barbara, USA).
6. AFM setup equipped with a topography and recognition imaging (TREC) box (Agilent, Santa Clara USA).

3.1.11. Chemical and equipment for TREC imaging of flat ERY ghost

1. Magnetically coated AFM cantilever (Keysight, USA), spring constant ~0.1 N/m.
2. Aminopropyl-triethoxysilane (APTES).
3. Triethylamine (TEA).
4. Acetal-polyethylene glycol (PEG)-NSH cross-linker
5. BRAD5 antibody (NHS Blood and Transplant, Norway)
6. AFM setup equipped with a topography and recognition imaging (TREC) box (Agilent, Santa Clara USA)

3.2. Methods: QCM and QCM-D Measurements

3.2.1. Portioning biotin-PEG_8-thiol with hydroxyl/methoxy-PEG_6-thiol

Prior to starting the QCM experiments, SAM components at different ratios of biotin-PEG_8-thiol : hydroxyl/methoxy-PEG_6-thiol were prepared. The portioning was done by preparing a stock solution in ethanol of 0.5 µM biotin-PEG_8-thiol (788 g/mol), hydroxyl-PEG_6-thiol (386.5 g/mol) and methoxy-PEG_6-thiol (356.5 g/mol). Then they were proportioned as shown in Table 1 into 2 ml glass bottles, and after they had been mixed well, the ethanol was evaporated by using rotary evaporator. At the end, the bottles were sealed and stored in a -20°C freezer.

Additionally, aliquots of pure hydroxyl-PEG_6-thiol and methoxy-PEG_6-thiol were prepared using the same procedure. Whenever functionalization with any of these biotinylated linkers was desired, the right portion would be thawed, dissolved in 300 µl ethanol and then used for the incubation. In cases where the ratios 1:500 and 1:1000 were needed, an appropriate dilution of 1:250 as well as the pure matrix thiol portions were done to get the required ratio.

Table 1: Portioning of biotin-PEG_8-thiol to the matrix thiol (hydroxyl/methoxy-PEG_6-thiol)

Ratio of Biotin-PEG_8-Thiol : Hydroxyl/Methoxy-PEG_6-Thiol (0.5 µM)	**Biotin-PEG_8-Thiol : Hydroxyl -PEG_6-Thiol**	**Biotin-PEG_8-Thiol : Methoxy-PEG_6-Thiol**
1:5	208 µl : 1040 ml	208 µl : 1040 ml
1:20	65 µl : 1.31 ml	65 µl : 1.31 ml
1:50	27 µl : 1.35 ml	27 µl : 1.35 ml
1:100	13.5 µ :1.35 ml	13.5 µ :1.35 ml
1:250	5.5 µl : 1.75 ml	5.5 µl : 1.75 ml

3.2.2. Cleaning protocol for the measuring chambers

The cleaning of the QCM liquid chamber (Figure 15B) was done as followed:

1. Every part of the liquid chamber including the inlet, outlet and tubes was sprayed thoroughly with 10% SDS solution in mQH_2O .
2. Completely rinsed with mQH_2O.
3. Dried under a stream of nitrogen gas.
4. Inserted a freshly functionalized quartz sensor and went ahead with the QCM measurement.

This cleaning procedure was done prior every measurement.

The cleaning of the QCM-D flow module (Electronics Unit QE 401) (Figure 15A) was done as followed:

1. The different parts of the flow module was dismantled.
2. The metallic parts were separated from the plastic parts and place into separate big beaker.

3. About 10% of SDS solution in mQH_2O was added to cover up all the parts.
4. Then immersed in sonicator bath for 20 min.
5. All parts were thoroughly rinsed with distilled water, subsequently with mQH_2O and then dried with nitrogen gas.
6. The parts were then remounted together.

The extensive cleaning procedure above was done once a while. For normal cleaning after each measurement the procedure below was followed:

1. The flow module was thoroughly rinsed with mQH_2O and the quartz sensor was removed.
2. The parts of the flow module interior that were visible were dried with nitrogen.
3. Freshly functionalized quartz sensor was inserted and this was followed by the QCM-D measurement.

3.2.3. Cleaning and Functionalization of Quartz Crystal with biotin-PEG_8-thiol linker mixed with hydroxyl/methoxy-PEG_6-thiol at different ratio

In order to couple the quartz crystal with biotin-PEG_8-thiol : hydroxyl/methoxy-PEG_6-thiol, the cleaning process was done in the chemical hood and the coupling procedure was performed as followed:

1. The chip-holder and the working tweezers were placed in a beaker and rinsed thrice with mQH_2O.
2. Freshly prepared basic piranha solution, which consisted of mQH_2O: H_2O_2: ammonium with the ratio 5:1:1, was added and place in a pre-heated mQH_2O of 75°C. This was allowed to boil for 15-20 min.
3. The beaker including its contents was transferred into another bigger beaker of mQH_2O at room temperature (RT) to cool for about 4 min.
4. The chip-holder was rinsed 5 times with mQH_2O.
5. Steps 1 to 4 were also carried out on the incubating-holder, which would be used for the incubation.
6. The quartz crystal was transferred into the chip-holder and rinsed trice with mQH_2O.
7. Step 2 to 4 were repeated twice, but finally rinsed 10 times with mQH_2O.
8. The quartz crystal was rinsed 4 times in ethanol. At the fourth round, the chip was left in the ethanol for 5 min.
   Note: The quartz crystal was kept in liquid throughout the cleaning process.
9. Firstly, the incubating-holder was dried with gas nitrogen and next the quartz crystal and then they were placed in the holder.
10. The desired ratio of the linker biotin-PEG_8-thiol : hydroxyl/methoxy-PEG_6-thiol was dissolved in 300 µl ethanol. Prior to the dissolution, the linker had been stored in the -20 °C freezer and allowed to thaw on a drying silica gel during the cleaning steps.

11. The dissolved linker was added to the incubating-chamber, closed with the chamber lid and sealed with parafilm. This was incubated for at least 12 hours (usually overnight).
12. On the next day, the chip-holder was placed in a beaker of ethanol and sonificated for 5 min.
13. The ethanol was discarded and another fresh ethanol was added. Then the quartz functionalized quartz crystal was placed in the holder and sonificated for 5 min.
14. The functionalized quartz crystal (Figure 14) was dried with gas nitrogen and placed in a cleaned chamber as illustrated in section 3.2.2 above.
15. The next step was the QCM-measurement as detailed below in section 3.2.4 or 3.2.7.

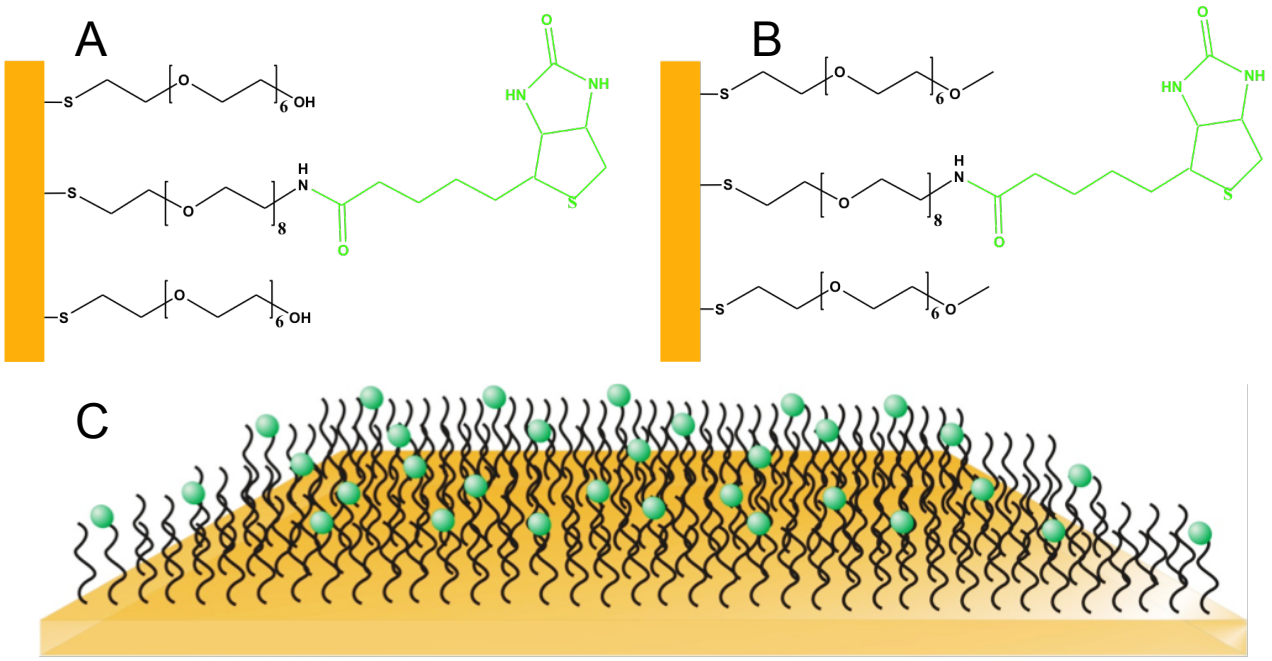

Figure 14: Illustration of a functionalized gold coated quartz crystal. (A) Chemical exhibition of biotin-PEG_8-thiol : hydroxyl-PEG_6-thiol (B) Chemical exhibition of biotin-PEG_8-thiol : methoxy-PEG_6-thiol. (C) Schematic illustration of biotin-PEG_8-thiol to the matrix thiol. gold color represents quartz surface, black PEG-thiol linkers and green the biotin.

3.2.4. QCM Measurement of 0.5 µM streptavidin, avidin or M96H on functionalized biotin-PEG_8-thiol : hydroxyl/methoxy-PEG_6-thiol quartz crystal and regeneration with 8 M GuHCl at pH 1.5 or regeneration solution X (RSX)

Firstly, the functionalized quartz crystal was clamped between the two x-rings of the chamber, either electronics unit QE 401 or liquid chamber, by putting the two complementary parts together (Figure 15). The chamber was then mounted in its holder. With the help of the pump, either automatic syringe pump (for QCM-IA) or peristaltic pump (for QCM-D), the chamber was filled up with PBS buffer (pH 7.3) at 250 µl/min and then the flow rate was switched to 50 µl/min. It was very important to make

sure that air bubbles were neither in the inlet-tube nor in the liquid cell.

Next, if measuring with QCM-D, the software QSoft 401 was run by setting the temperature to 25°C, then finding the resonance and subsequently starting the data acquisition. Alternatively, when using QCM-IA for the measurement, the connection from the liquid chamber over the impedance analyzer to the computer was established with the QUI and thereafter the data were acquired.

The real-time measurement was then monitored on the computer. After the PBS was allowed to flow until equilibration was reached, the protein of interest, which was 0.5 µM of either streptavidin, avidin or M96H in pH 7.3 PBS, was inserted from the eppendorf tube over the inlet-tube into the chamber for 7 to 10 min until saturation was reached. The saturation revealed a dense coverage of the protein on the layer of biotinylated SAM. Usually, before switching from one solution to the other in QCM-IA setup, the data acquisition, as well as the pump were paused and then resumed immediately after the switch, contrary, only the pump was paused during switching between solutions in QCM-D measurement. Subsequently, PBS was again run so that loosely adsorbed protein could be washed away. This step was then followed by a 20 to 30 min regeneration step, by running 8 M GuHCl in pH 1.5 PBS or RSX through the cell so as to dissociate the adsorbed protein from the biotin. Afterwards, a washing step was done with PBS at a high flow rate of 450 or 500 µl/min for 5 min, so that all denaturant solutions could be completely washed out of the chamber. Then the flow rate was reduced to the original rate of 50 µl/min until the system equilibrated. The whole process starting from the addition of either streptavidin, avidin or M96H was repeated as often as desired, normally three times. At the end of the measurement, the data acquisition was stopped and that was followed by running at least 2 ml of mQH_2O through the chamber. Then air was sucked through the chamber to get rid of as much liquid as possible and finally the chamber was dismantled.

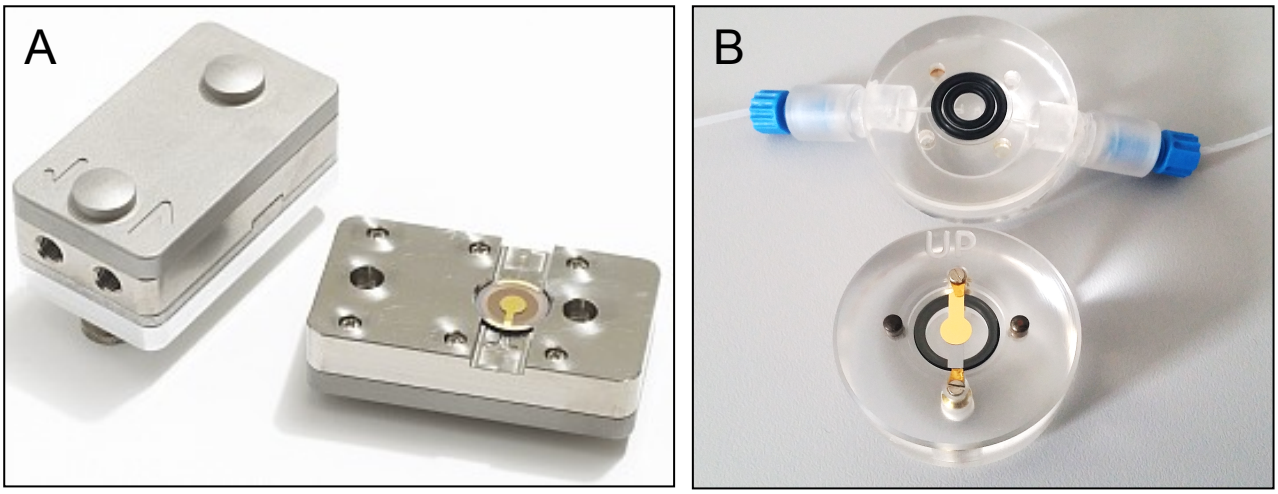

Figure 15: Electronics Unit QE 401 for QCM-D (A) and liquid chamber with the liquid flow-cell (B) showing the correct way to insert the quartz crystals in such a way that both electrodes are in contact with the electric ends.

3.2.4.1. Data analysis

At the end of every measurements, the acquired QCM-IA data were exported into text files while QCM-D data were exported into excel file. The data were further analyzed with Microsoft Excel: Mac 2011 or Origin 6.0.lnk. The determination of the delta frequency shift for each protein was done by calculating the difference between the frequency of PBS after it had equilibrated just before and after the protein adsorption. Frequency shifts achieved from measurements carried out with QCM-IA at the 3rd harmony were always normalized by dividing them by 3. Regarding QCM-D measurements, frequency shifts had been already normalized automatically by the software. Also, the data were obtained at the fundamental frequency and at several overtones. However, since the variation among the overtone signals was significantly small, only results from the 3rd overtone are shown.
Please, note that all frequency shifts values are presented in the absolute form.

3.2.5. Inspection of non-specific adsorption

In order to control whether non-specific adsorptions were eliminated during the QCM-IA and QCM-D measurements, 0.5 µM of streptavidin, avidin and M96H were run on a quartz sensor that had been coupled with pure matrix of PEG_6-thiol (hydroxyl/methoxy-PEG_6-thiol) employing similar measuring processes as mentioned in section 3.2.4. above. A measurement which resulted in no change in frequency shift upon the running of the proteins would imply a complete ruling out of non-specific adsorption.
Data processing and evaluation were executed as explained in section 3.2.4.1.

3.2.6. Biotinylation of antibody 8F5

The target was to prepare a biotinylation of 10 biotins per 8F5 antibody. Hence, the biotinylation of the antibody of 2.2 mg/ml, which was equivalent to 14.67 µM, was performed as follows:

1. Exactly 0.91 mg NHS-LC-biotin, with molecular weight 454.54 Da, was dissolved in 0.2 ml of DMSO resulting in a 10 mM solution.
2. Then 6 µl of the10 mM NHS-LC-biotin solution was added to 400 µl of 14.67 µM antibody 8F5 in an eppendorf tube, which corresponded to 5.86 nmol.
3. After mixing them shortly with a vortex, the solutions were allowed to react for 1 hour at RT, while a short mixing was done in between every 20 min.
4. Afterwards, the product was subjected to dialysis against PBS (pH 7.3) at RT overnight to purify any free NHS-LC-biotin form the biotinylated antibodies.
5. The purified biotinylated-8F5 solution was stored in the fridge and was later on used for section 3.2.7. below.

3.2.7. Application of reversible immobilization of M96H, HRV and 8F5 antibody on biotinylated SAM using QCM-IA setup

Firstly, the functionalized quartz crystal sensor was mounted in the liquid chamber in such a way that the electrodes were connected to the poles as shown in Figure 15B and with the help of the syringe pump the chamber was filled up with PBS (pH 7.3) at 250 µl/min and then the flow rate was switched to 50 µl/min. Next, a connection between the impedance analyzer and the computer was established and the software for the measurement was run with QUI. The QCM real-time measurement was then started and monitored on the computer. The PBS was allowed to flow until equilibration was reached. Then 0.5 µM of M96H in pH 7.3 PBS was inserted from an eppendorf tube over the inlet-tube into the chamber till saturation was reached in about 5 – 10 min. The saturation revealed a dense coverage of the protein on the layer of biotinylated SAM. Whenever switching from one solution to the other, the data acquisition as well as the pump flow were paused and then resumed immediately after the switch. Subsequently, PBS was again run so that loosely adsorbed protein could be washed away. After equilibration was reached with the PBS, the biotinylated-8F5 was injected, followed by PBS and then the HRV.

Succeeding running PBS of pH 7.3, 8 M GuHCl in pH 1.5 PBS solution was run through the cell chamber for 30 min so as to dissociate the M96H from the biotin. Thereafter, a washing step was done with PBS pH 7.3 at a high flow rate of 450 to 500 µl/min for 5 min, so that all GuHCl could be completely washed out of the chamber. After the washing step, the flow rate of the PBS pH 7.3 was reduced to 50 µl/min and the running was continued until equilibration was reached. Then again, M96H was injected. From this frequency shifts, a determination of the amount of M96H that had dissociated from the biotin was possible. Once more, measurement with biotinylated-8F5, followed by HRV was run and was completed by another regeneration step, as well as a final injection of M96H. Thereafter, PBS was run and the acquisition of data was stopped. As followed, 2 ml of mQH_2O was run through the chamber. Then air was sucked through it to get rid of as much liquids as possible and finally the chamber was dismantled.

Data processing and evaluation was executed as explained in section 3.2.4.1.

3.3. Methods: RBCs and AFM investigation

3.3.1. Preparation of flat ERY ghosts

The preparation of flat ERY ghosts was carried out as follows:

1. The glass cover slips were placed in a cover-slips-holder in a beaker of acetone and ultra-sonicated in water bath for 5 min.
2. Then the acetone was poured out and a second round of washing in acetone was repeated as in step 1. Part of the acetone was poured out in order to get rid of any dirt that might had accumulated on the surface of the acetone. The cover slips were kept in the remaining acetone.
3. Next, the glass cover slips were dried one after the other with a stream of nitrogen gas, placed in a petri dish and coated with 150 - 300 µl of 0.01% PLL in H_2O for 30 – 90 min.
4. While waiting for the completion of step 3, the RBCs were purified. First, 4 drops of venous blood, which had been collected by a donor from the hospital, was diluted in 1000 µl of isotonic PBS (pH 7.4) containing 0.2 mM EGTA and centrifuged at 3800 rpm for 4 min. Afterwards, the supernatant was discarded, the pellets were suspended in 1000 µl of isotonic PBS and this purification procedure was repeated thrice. Then 3 µl of the RBC-pellets were dissolved in 1800 µl PBS (pH 7.4) to get a ratio of 1:600.
   Note: The RBC-pellets were not allowed to dry during this step.
5. The PLL-coated glass cover slips in step 3 were washed twice with mQH_2O, dried with nitrogen gas and each was placed in a small petri dish.
   Note: The succeeding steps 6 to 9 were done in a cold room
6. Between 400 and 500 µl of RBC-suspension was transferred onto the PLL-coated glass cover slips and cold-shocked for 15 min by placing them on ice-blocks in a closed cold box. Likewise, the very low salt buffer (vlsb) was placed on the ice-blocks for it to have the same temperature as the samples.
7. By a strong spray of vlsb in a zig-zag motion from one end of the cover slip to the other end (Figure 16), a shear stress was exerted on the immobilized RBCs. By doing so, the membranes were opened and all the proteins within the RBCs were washed out. The remnants of the washing-vlsb were sucked up with a clean tissue at one end of the petri-dish.
8. Immediately, 1000 µl of 1 vol% of 25%-glutaraldehyde–solution in PBS (pH 7.4) was added to the RBC samples and incubated for 30-45 min.
9. The samples were washed thrice with 2000 µl of PBS with 5 min of incubation in between the PBS exchange.

The prepared ghosts were either used immediately for AFM investigation or stored at 4°C and used the following day.

Most of the times, it was also desired to have samples, which could be stored at a dried state so that they could be used even after some months. Hence, after the step 9 above, the samples were washed ten times with mQH_2O with 5 min of incubation within the mQH_2O exchange. After that, the samples were allowed to dry at RT overnight and finally each sample was stored at RT in a petri dish, optionally under argon, and sealed with parafilm. Whenever a sample was needed for AFM investigation, these dried ghost samples could be rehydrated with PBS for about 30 min and then be used.

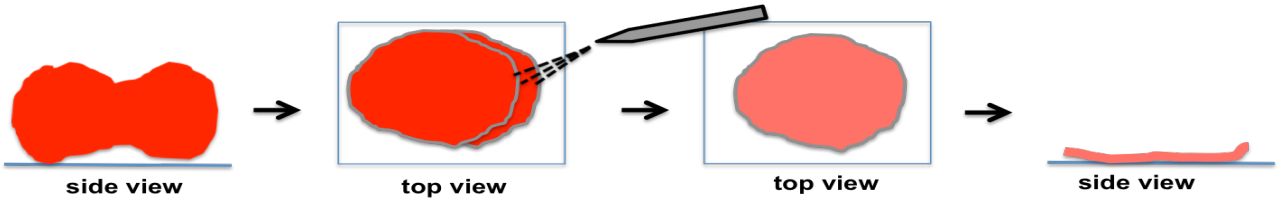

Figure 16: Schematic overview of shear opening procedure of red blood cells. Erythrocytes are exposed to fluid flow-imposed shear stress and as a result, the cells are opened, exposing their cytoplasmic side of the membrane.

3.3.2. AFM imaging in contact mode

For imaging of ghosts by AFM the contact mode was used. Prior to imaging, PBS was allowed to attain RT. The cantilever (MSCT, Bruker) was fixed onto the scan head and this was then inserted into the AFM. Thereafter, with the help of the camera, the laser point was adjusted to the tip of cantilever C and aligned. The flat RBC ghost sample dish was mounted on the AFM sample plate, followed by selecting the right scanner and setting the “Contact Mode” in the PicoView menu. The setpoint value was set higher than the deflection oscilloscope for about 0.5 and the cantilever was approached to the sample. The size of the image, speed, angle, points and I and P gains were entered and the imaging was started and saved. The servo gains were adjusted as high as possible without oscillation in the feedback signal. The images were measured at the resolution of 512 sample lines and with a scanning speed in the range of 1 -2 lines/s depending on the area to be imaged.

At the end, the images were analyzed with the Gwyddion 2.41 software.

3.3.3. Tip chemistry for coupling BRAD5 antibodies

APTES coating by vapor phase deposition is the optimum method to amino-functionalize cantilevers. In this process, a non-dense monomolecular silane layer with suited physical and chemical behavior was formed on the AFM tip [50].

Among the many developed hetero- and homo-bifunctional cross-linkers, the acetal-PEG-NHS linker was coupled to the AFM tips (Figure 17) according to Ebner et al. [47] and Gruber H.J. [51] as follows:

1. The MAClevers (Agilent) or MSCT cantilevers (Bruker) were washed 3 x 5 min in chloroform and dried with a gentle stream of nitrogen gas.
2. Again they were washed 3 x 5 min with ethanol and dried with a gentle stream of nitrogen gas.
3. A 5-l desiccator was filled with argon. Then a vial with 10 µl TEA and another of 30 µl freshly distilled APTES were placed inside.
4. The cleaned cantilevers were laid in the desiccator, flushed with argon for 60 s and left to react for 2 h.
5. The vials were removed from the desiccator and the desiccator was flushed with argon for 5 - 10 min. Then the APTES-coated tips were stored for at least 2 days under argon and the functionalization was continued.
6. An amount of 1 mg of acetal-PEG-NHS was dissolved in 0.5 ml chloroform, the solution was transferred into a reaction chamber, 30 µl of TEA was add and mixed.
7. The cantilevers were placed in the reaction chamber straight away, covered and allowed to incubate for 2 h.
8. The cantilevers were washed 3 x 10 min with chloroform and dried with nitrogen gas.
9. The cantilevers were dipped in 1% citric acid (in mQH_2O) for 10 min, rinsed 3 x 5 min in mQH_2O and dried with nitrogen gas.
10. A fresh preparation of a 1 M solution of $NaCNBH_3$ with 20 mM NaOH was done by using 13 mg $NaCNBH_3$, 20 µl of 100 mM NaOH and180 µl mQH_2O.
11. The cantilevers were laid on parafilm in a polystyrene petri dish and 100 µl of human IgG1 anti-RhD antibody BRAD5 solution in PBS buffer was added onto the cantilevers.
12. Then 2 µl of the 1 M $NaCNBH_3$ stock solution was added and after careful mixture the reaction was covered with lid and allowed to react for 1 h.
13. Thereafter, 5 µl of ethanolamine was added, mixed cautiously, covered with lid and allowed to react for 10 min.
14. Using PBS, the cantilevers were washed 3 x 5 min.
15. And finally, one of the cantilevers was mounted in an AFM setup and the rest were stored under PBS in a 24 well plate, which had been underlaid with parafilm at 4°C and were used within 1-2 weeks.

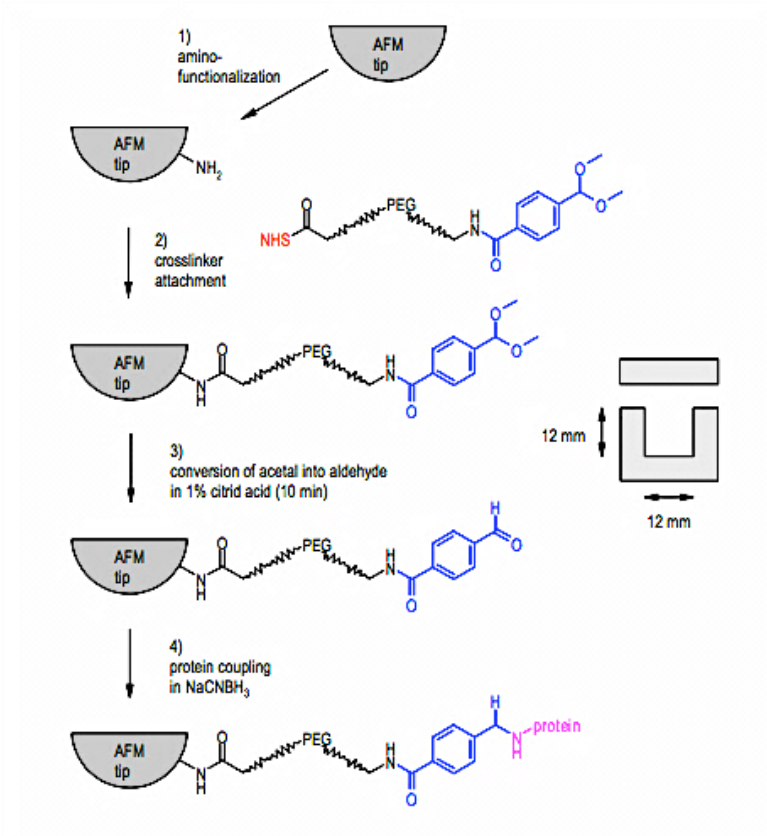

Figure 17: Tip chemistry of AFM cantilever and incubation chamber. AFM tip is amino-functionalized, coupled with acetal-PEG-NHS, followed by the conversion of acetal into aldehyde and subsequently tethered with protein (i.e. BRAD5 antibody in this case) via the amine residue of a lysine of the protein. Taken from (Gruber, 2015).

3.3.4. Force Distance Curve (FDC) Measurement on Cells

Prior to FDC measurements of the RhD receptors on the flat RBC ghosts, the PBS was allowed to attain RT. The sample was mounted on the AFM sample plate. Thereafter, the cantilever tip that had been functionalized with BRAD5 antibody was mounted on a cantilever holder on the top of the scanner and inserted into the AFM. Care was taken to always keep the functionalized cantilever tip at a wet condition in order to preserve the activation of the tip. With the help of the camera, the laser point was adjusted to the tip of the desired cantilever (MSCT, Bruker) and aligned. Generally measurements were started with cantilever C (k~0.01 N/m) then B (k~0.02 N/m) and finally with D (k~0.03 N/m). The force distance curves were measured continuously with fixed scanning range of 3 µm, cycle time of 1s, and force limit of 0.5 V for cantilevers B and C and 0.3 V for cantilever D. The tip was approached manually step by step by clicking “close” button for approaching 1 µm per step until the force distance curve showed the contact point between the tip and the RBC ghost surface. The scanning range was shifted in z direction, so that the contact force between the tip and the ghost

surface was as low as possible. In search for a good spot, the force distance curves were measured a couple of times at one position, then the measurements would be stopped and the tip would be withdrawn for about 50 µm, moved to a different position by using x- and y-translational micro-screws and another round of force measurement would be done. When a good spot was found, hundreds of force cycles were recorded at that position and the tip was moved within the same window of about 5x5 μm^2 area by increments until thousands of force curves were accumulated.

The force distance curves were analyzed with MATLABR2009b and Kspec, which was a custom written Matlab routine.

3.3.4.1. Specificity control

Subsequently, the specific interaction between the RhD receptors on the flat RBC ghosts and the BRAD5 antibody was controlled by employing surface blocking. This was achieved by adding 140 µl of 0.25 mg/l BRAD5 (in PBS) to the above RBC ghost sample, which was in a sample plate of about 400 µl of PBS. This was incubated for 110 min at RT. Thereafter, force distance curve measurements were carried out on the blocked surface with the BRAD5-functionalized-tip by applying the same procedure mentioned in the section above.

The principle behind this surface block is that the free BRAD5 antibodies could form a complex with the RhD receptors. Owing to the complex formed between BRAD5 and RhD receptors, any further interaction between the BRAD5-functionalized-tip and the RhD receptors would be prevented, resulting in a positive specificity control.

3.3.4.2. Measurement of spring constant of cantilever

In order to determine the accurate spring constant of the cantilever, which can vary substantially from stated manufacturer values, mica was placed on the AFM sample plate and approached in contact mode. After that, the function ´Spectroscopy´ was selected and the “Rate”, “Start”, and “End” parameters were entered. Subsequently, a force curve was recorded. On the recorded force curve, 2 points were marked on the slope and using the ´ruler´ and ´deflection sensitivity´ functions, the sensitivity of the cantilever (nm/Volt) was calculated in the ´Advanced` window of the `Spectroscopy` feature. Thereafter, a PSD plot was acquired in the `Thermal K´ window and the resonance frequency of the cantilever was obtained. Finally, the spring constant of the cantilever (N/m) was determined.

3.3.5. Simultaneous TREC imaging on ghosts

The recognition imaging of the flat RBC ghosts (Figure 11) were performed in PBS buffer at RT. Prior the TREC imaging a contact mode imaging with MSCT cantilever was carried out as explained in 3.3.2. so as to verify the success of the ghost preparation. Then the MSCT cantilever was changed to a BRAD5-functionalized MAClever and it was automatically approached onto the RBC ghost. This approaching step was crucial, since the functionalized molecules on the tip could be destroyed upon hard contact. Consequently, the velocity used for approaching was set as low as possible. After the tip had touched the surface, the amplitude-distance curve was measured continuously and the amplitude set point was adjusted so that the set point was just a little bit lower than the free amplitude (practically, about 0.5 V lower than the free amplitude). Then, the amplitude-distance curve measurement was stopped and the imaging was started. The servo gains were adjusted as high as possible without oscillation in the feedback signal. The images were measured with a scanning speed of 3 µm/s.

4. Results and discussion

4.1. QCM and QCM-D measurements

In the realm of this project, the formation of the SAM, which consisted of the mixture of biotin-PEG_8-thiol with either hydroxy-PEG_6-thiol or methoxy-PEG_6-thiol was successful (Figure 14). This achievement made the investigation of reusable avidin based anti-absorptive gold functionalization for biosensing QCM measurements possible and the results beneath confirm that.

4.1.1. AFM measurements on QCM quartz crystal

An investigation of the topography of the quartz crystal was made. This was accomplished by using contact and tapping mode AFM and the gold coated crystal of 10 MHz was imaged at two different stages:

1. after the crystal had been cleaned under the harsh condition and functionalized with biotin-PEG_8-thiol and methoxyl-PEG_6-thiol with the ratio 1:5 as indicated in section 3.2.3. an area of 500 by 500 nm^2 was scratched by applying high indentation force (Figure 18a);
2. immediately after the first adsorption of 0.5 µM avidin to the functionalized crystal (like at point 1) was determined with the QCM-IA (Figure 18c); as explained in section 3.2.4. the same AFM imaging process as in point 1 was repeated on the crystal (Figure 18b).

Observation of the images reveal that scratching of a 500x500 nm² area did not yield observable changes in both contact and tapping mode topography images of the biotin-PEG_8-thiol layer, since no scratched area was visible (Figure 18a). The scratching however resulted in an area with removed avidin molecules only in the tapping mode image and this is highlighted white in Figure 18b.

It is likely that during scratching in contact mode, the cantilever tip only brushes through the biotin-PEG_8-thiol / methoxyl-PEG_6-thiol linkers, therefore making it difficult to remove avidin molecules. In the tapping mode, on the other hand, since the tip was moving up and down it was able to easily cleave off avidin molecules as it moved upwards.

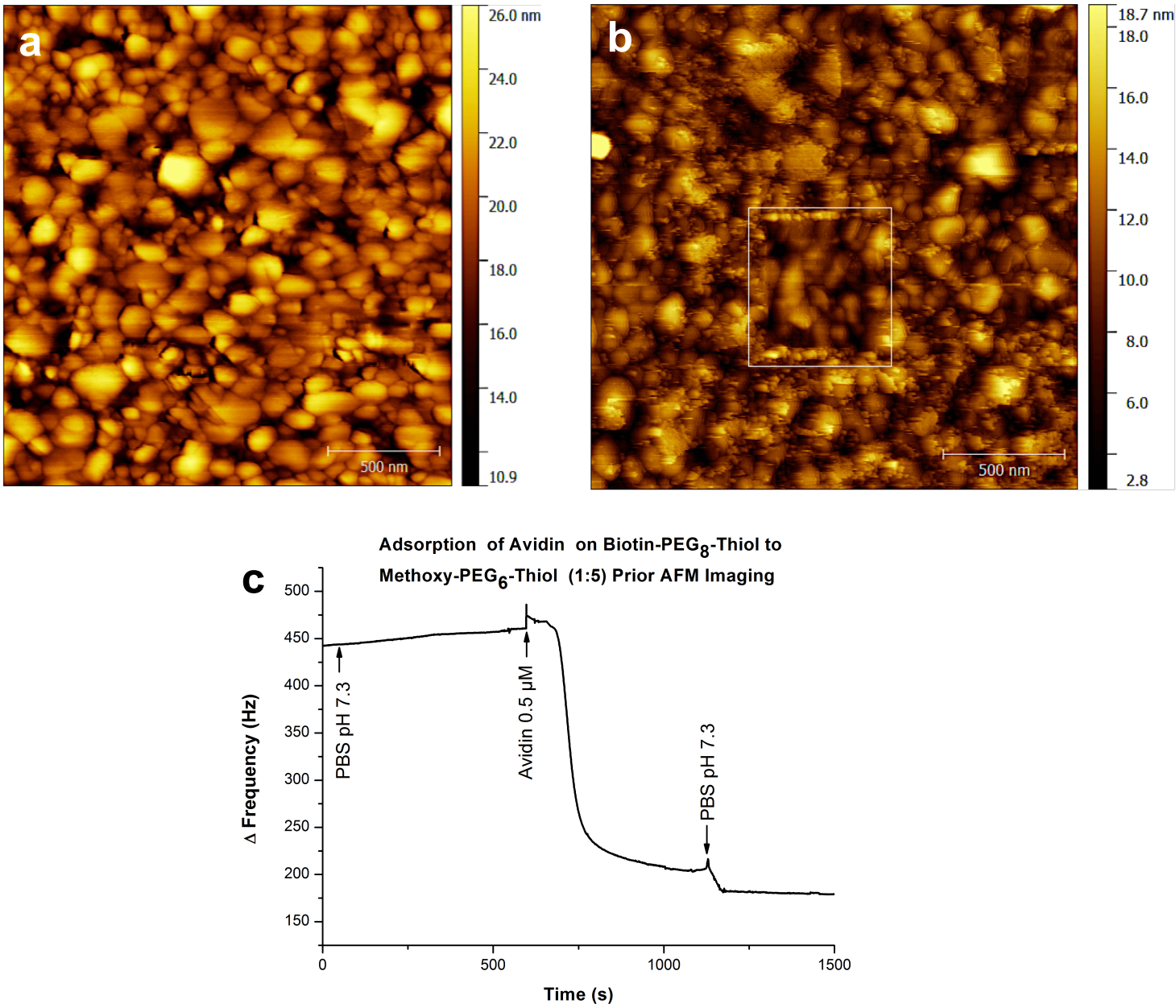

Figure 18: Tapping mode AFM images of biotin-PEG_8-thiol and methoxyl-PEG_6-thiol functionalized quartz sensor before (left panel) and after (right panel) adsorption of avidin. The bottom panel shows the QCM measurement of the avidin adsorption to the biotin-PEG_8-thiol / methoxyl-PEG_6-thiol (1:5) linker. 500 by 500 nm² areas were scratched off in both AFM images, however, only the adsorbed avidin was successfully removed (marked within the white square) and not the linkers.

4.1.2. Regeneration of biotin-PEG_8-thiol / hydroxyl-PEG_6-thiol linker with RSX

In QCM measurements, where the biotin-streptavidin or biotin-avidin biotechnique is applied, it has become necessary to totally regenerate the biotinylated layer linking the gold-coated-quartz electrode and the avidin mutant M96H for further immediate biotin-avidin investigations, so as to save time, cost and have other benefits (see section 2.1). Hence, the investigation of the avidin mutant M96H to a linker composed of biotin-PEG_8-thiol and hydroxyl-PEG_6-thiol functionalized quartz sensor including its

subsequent regeneration was carried out on the QCM-IA setup using the 1st harmony (Table 2 and Graph 1). The absolute Δ frequency shifts upon the adsorption of M96H onto biotin were 75.73 Hz, 75.09 Hz and 66.91 Hz for the ratios 1:5, 1:100 and 1:250, respectively. From these values, it can be concluded that a minimum ration of 1:100 was needed to get a dense surface coverage of M96H. After the very stable interaction between the biotin and M96H had been interrupted with the RSX, a respective surface recovery of 99.95 ± 1.34 %, 92.26 ± 7.87 % and 100.87 ± 4.07 % was achieved. Hence, one can certainly deduce from these results that the dissociation of M96H from the biotinylated linker was possible with the application of the regeneration solution RSX. Besides, when M96H was run on a quartz sensor, which had been functionalized with only a hydroxyl-PEG_6-thiol linker, no adsorption of M96H was observed. This observation was expected, because the linker was responsible for specific interaction. Thus, without biotin, there was no alternative means by which M96H would have been adsorbed to the sensor.

Table 2: Reversible adsorption of 0.5 µM M96H to different ratios of biotin-PEG_8-thiol and methoxyl-PEG_6-thiol functionalized quartz sensor using RSX.

			Ratio of Biotin-PEG_8-Thiol to Hydroxyl-PEG_6-Thiol		
		Hydroxyl-PEG_6-Thiol	**1 to 5**	**1 to 100**	**1 to 250**
M96H	Δ Freq. (Hz)	0	75.73	75.09	66.91
	Recovery with RSX (Hz)	-	75.69 ± 1.01	69.28 ± 5.91	67.49 ± 2.72
	Recovery with RSX (%)	-	99.95 ± 1.34	92.26 ± 7.87	100.87 ± 4.07

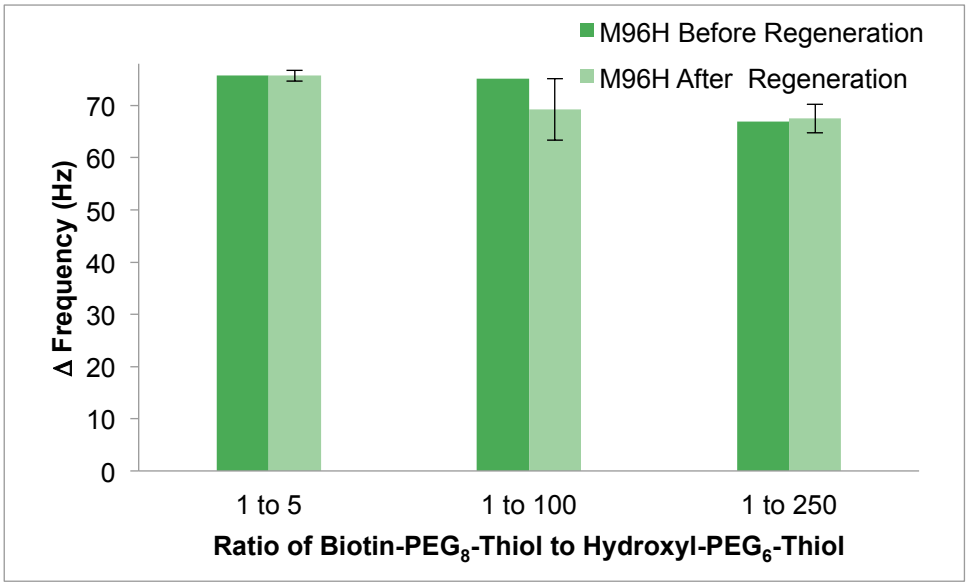

Graph 1: Delta frequency shift of 0.5 µM M96H on a biotinylated SAM of gold coated quartz surface before and after regeneration with 8 M GuHCl acidic solution.

4.1.3. Regeneration of biotinylated linker, biotin-PEG_8-thiol and hydroxyl/methoxyl-PEG_6-thiol, with GuHCl

As mentioned above in section 4.1.2. the motive behind the regeneration was to reuse the biotin-functionalized gold-coated-quartz sensor for subsequent biotin-streptavidin/-avidin/-M96H analysis. The following are the results achieved from the QCM measurements where the biotinylated linkers, biotin-PEG_8-thiol/methoxyl-PEG_6-thiol and biotin-PEG_8-thiol/hydroxyl-PEG_6-thiol, were regenerated with GuHCl.

It is important to indicate that the 3rd harmony was used for the upcoming measurements, since the sensitivity of the setup, as well as the results were expected to be improved by doing so. Nevertheless, the results had been eventually normalized from the 3rd harmony to the fundamental tone. In addition, two different setups, QCM-IA (marked gray in tables 3 and 5) and QCM-D were used for the successful completion of the measurements with chemically modified SAM, biotin-PEG_8-thiol and hydroxyl-PEG_6-thiol. Due to this, the absolute Δ frequency shifts varied from one setup to the other: data from QCM-D were about 32% smaller than the data from QCM-IA. Despite the variation, the interactions were reproducible and the correlation between the shifts was attainable. More so, the regenerations from both setups were comparable percentagewise. As a result, the recovered surface after regeneration is shown as a percentage so that the correlation can be easily seen.

The Δ frequency shifts achieved as a result of the first adsorption of the probed proteins (0.5 µM of streptavidin, avidin and M96H) on the quartz crystal, which had been chemically modified with biotin-PEG_8-thiol and matrix thiol (hydroxyl/methoxyl-PEG_6-thiol) at different ratios, and their subsequent recovered shifts in percentage after regeneration with 8 M GuHCl solution at pH 1.5, are presented in the tables 3, 5 & 6 and their corresponding graphs 2, 3, 4 & 5.

It is worth noting that a minimum ratio of 1:100 was needed to get a dense surface coverage of the avidin and streptavidin, which resulted in Δ frequency shifts of 75 to 80 Hz when working with QCM-IA and 22 to 25 Hz when working with QCM-D (summarized in Table 4). This is in the range with QCM-D frequency shift presented by Nilebäck et al. where they immobilized streptavidin on SAM made of oligo(ethylene glycol) (OEG) with –OH or biotin terminals and had frequency shift of 22 ± 3 Hz [25]. Also, M96H has about 80 Hz on QCM-IA measurement with 1st harmony and around 100 Hz with 3rd harmony (Table 4).

As evident in the cases of streptavidin and avidin, the succeeding recoveries of biotinylated SAM were incomplete. This was due to the high stability of the proteins and bonding strength, which became even stronger when two or more streptavidin- or avidin-binding-pockets were occupied by adjacent biotin molecules. The measurements show that the higher the ratio of biotin-PEG_8-thiol to the matrix thiol, (which implied an increase in the number of streptavidin and avidin molecules, that were bound

to two adjacent biotin residues) the higher the fraction of streptavidin and avidin not being removed by 8 M GuHCl at pH 1.5. Considering that, a higher recovery with the ratio 1:500 and 1:1000 in the cases of streptavidin and wild-type avidin should be expected. This however is not always the case here and an explanation for this phenomenon could be based on the preparation of the linkers: the 1:500 and the 1:1000 were prepared by diluting the 1:250 with pure hydroxyl-PEG_6-thiol. On account of that, the probability of two adjacent biotin residues binding to a streptavidin and avidin molecule is higher than if such linkers were prepared like the others in section 3.2.1.

A closer observation of the overall regeneration presented in table 3, 4 and 5 revealed variations depending on the kind of thiol matrix immobilized on the gold surface. In table 3, where the biotin-PEG_8-thiol/hydroxyl-PEG_6-thiol linkers with the ratios 1:5, 1:100 and 1:250 were used, 17.58±3.38%, 38.55±7.43% and 52.17±7.97% of avidin recovery as well as 25.25±2.18%, 53.65±9.61% and 80.81±7.75% of streptavidin recovery were detected respectively after the regeneration steps. Whilst in table 5, the regeneration of biotin-PEG_8-thiol/methoxyl-PEG_6-thiol linkers of the ratios 1:5, 1:100, 1:250 and 1:500 resulted in avidin recovery of 13.59±3.79%, 22.64±5.57%, 38.59±6.93% and 58.56±13.51% respectively and streptavidin recovery of 15.75±49%, 23.41±2.34&, 35.41±8.13% and 57.17±12.60% respectively. From these values it is concluded that the regeneration of biotin-PEG_8-thiol/hydroxyl-PEG_6-thiol functionalized quartz sensor for both streptavidin and avidin worked 7 to 30% better than regeneration of biotin-PEG_8-thiol/methoxyl-PEG_6-thiol. It may be presumed that hydrogen bonding and steric effects positively influenced the increase in dissociation of streptavidin and avidin from the biotin-PEG_8-thiol/hydroxyl-PEG_6-thiol linkers.
Moreover, a deduction from the above results show that regeneration of biotin-PEG_8-thiol/hydroxyl-PEG_6-thiol linkers with GuHCl worked from a range of 8 to 29% better with streptavidin than with avidin, when the ratios 1:500 and 1:1000 were excluded (Table 3 and Graph 3). The charges of the proteins were likely to play a role in this dissociation behavior, causing the neutrally charge streptavidin to dissociates better than the positively charged avidin from such SAM.
Generally, the adsorption of streptavidin and avidin to biotin-PEG_8-thiol/methoxyl-PEG_6-thiol functionalized quartz sensor as well as their subsequent regenerations could be seen as similar, due to the negligible differences in their values (Table 5 and Graph 4).

Finally, specificity control was performed with the QCM-IA setup for 0.5 µM of avidin and streptavidin on quartz sensors functionalized with hydroxyl-PEG_6-thiol only (Table 3). The observed shifts -1.97 Hz for avidin and +2.3 for streptavidin were owed to drifts which can be ignored. Hence, the adsorption of avidin to streptavidin to the biotin-PEG_8-thiol/hydroxyl-PEG_6-thiol functionalized sensor was certainly specific.

Further, during the specific control that was carried out on QCM-D setup with 0.5 µM avidin, streptavidin and M96H on methoxyl-PEG_6-thiol coupled sensor, there seemed to be a slight frequency shift but in the opposite direction (Table 5 and Graph 17 in appendix). Those shifts however, eventually returned to the base line during the injection of PBS. This implied that whatever that might had caused the shift had been gotten rid of in the course of washing with PBS. The resulting shift of 0 Hz at the end therefore proved the specificity of avidin, streptavidin and M96H to biotin on biotin-PEG_8-thiol/methoxyl-PEG_6-thiol functionalized quartz sensor.

Table 3: Reversible adsorption of 0.5 µM avidin and streptavidin to different ratios of biotin-PEG_8-thiol and hydrooxyl-PEG_6-thiol functionalized quartz sensor using 8 M GuHCl at pH 1.5. The data marked gray are from QCM-IA setup and the unmarked ones are from QCM-D setup. The absolute ∆ frequency shifts varied from one setup to the other. Despite the variation, the interactions were reproducible and the correlation between the shifts was attainable.

			Ratio of Biotin-PEG_8-Thiol to Hydroxyl-PEG_6-Thiol				
		Hydroxyl-PEG_6-Thiol	1 to 5	1 to 100	1 to 250	1 to 500	1 to 1000
Avidin	∆ Freq. (Hz)	(minus)1.97	23,7	80.53	67.96	33.14	24.33
	Recovery after regeneration (%)		17.58 ± 3.38	38.55 ± 7.43	52.17 ± 7.97	78.56 ± 5.17	60.28 ± 10.95
Streptavidin	∆ Freq. (Hz)	(plus) 2.3	23.5	24.27	14.57	34.33	-
	Recovery after regeneration (%)		25.25 ± 2.18	53.65 ± 9.61	80.81 ± 7.75	69.79 ± 7.50	-

Table 4: Absolute ∆ frequency shift of dense coverage of 0,5 µM streptavidin, avidin and M96H on biotinylated SAM. The data marked gray are from QCM-IA setup and the unmarked ones are from QCM-D setup. The absolute ∆ frequency shifts varied from one setup to the other. Despite the variation, the interactions were reproducible and the correlation between the shifts was attainable.

Ratio: From 1:5 to 1:100	**∆ Frequency Shift of Dense Coverage**				
	Streptavidin	Avidin	Avidin	M96H	M96H
Biotin-PEG_8-Thiol / Hydoxyl-PEG_6-Thiol	23.89 ± 0.54	23.7± 0.8	78 ± 2.58	79.13 ± 4.99	-
Biotin-PEG_8-Thiol / Methoxyl-PEG_6-Thiol	24.1 ± 2.25	22,87 ± 2.27	-	22.2 ± 0.64	98.35 ± 6.72

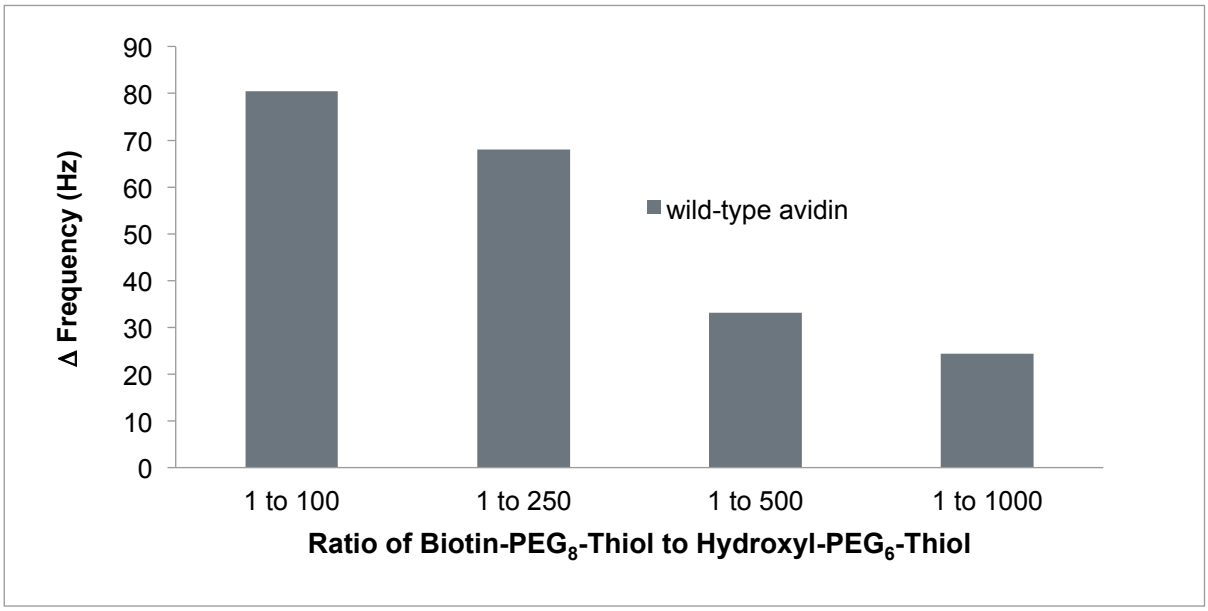

Graph 2: Absolute delta frequency shift of of 0.5 µM avidin to different ratios of biotin-PEG_8-thiol and hydrooxyl-PEG_6-thiol functionalized quartz sensor using QCM-impedance-analyzer.

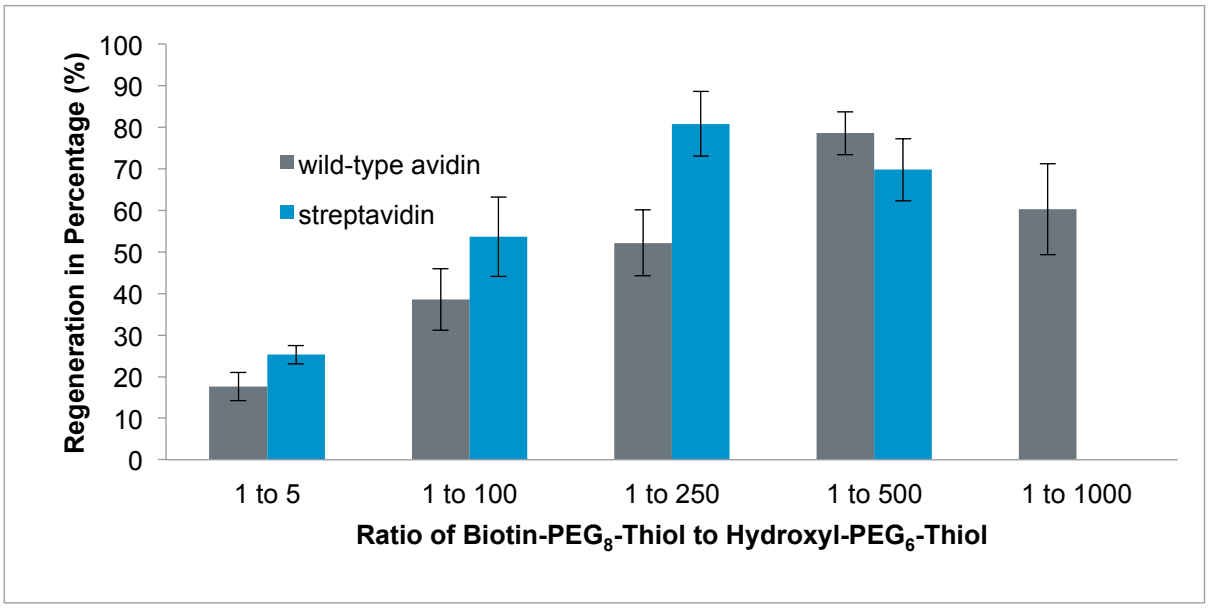

Graph 3: Percentage regeneration of 0.5 µM from different ratios of biotin-PEG_8-thiol and hydrooxyl-PEG_6-thiol functionalized quartz sensor using 8 M GuHCl at pH 1.5

Table 5: Reversible adsorption of 0.5 µM avidin and streptavidin to different ratios of biotin-PEG_8-thiol and methoxyl-PEG_6-thiol functionalized quartz sensor using 8 M GuHCl at pH 1.5. Data acquired with QCM-D. Delta frequency shifts are given in absolute value.

			Ratio of Biotin-PEG_8-Thiol to Methoxyl-PEG_6-Thiol				
		Methoxyl-PEG_6-Thiol	1 to 5	1 to 100	1 to 250	1 to 500	1 to 1000
Wild-type avidin	Δ freq. (Hz)	0.1	25.4	22.2	19.3	11.1	-
	Recovery after regeneration (%)		13.59 ± 3.79	22.64 ± 5.57	38.59 ± 6.93	58.56 ± 13.51	-
Streptavidin	Δ freq. (Hz)	0	25.4	21.5	19.3	11.2	6.2
	Recovery after regeneration (%)		15.75 ± 4.9	23.41 ± 2.34	35.41 ± 8.13	57.17 ± 12.60	66.4 ± 14.03

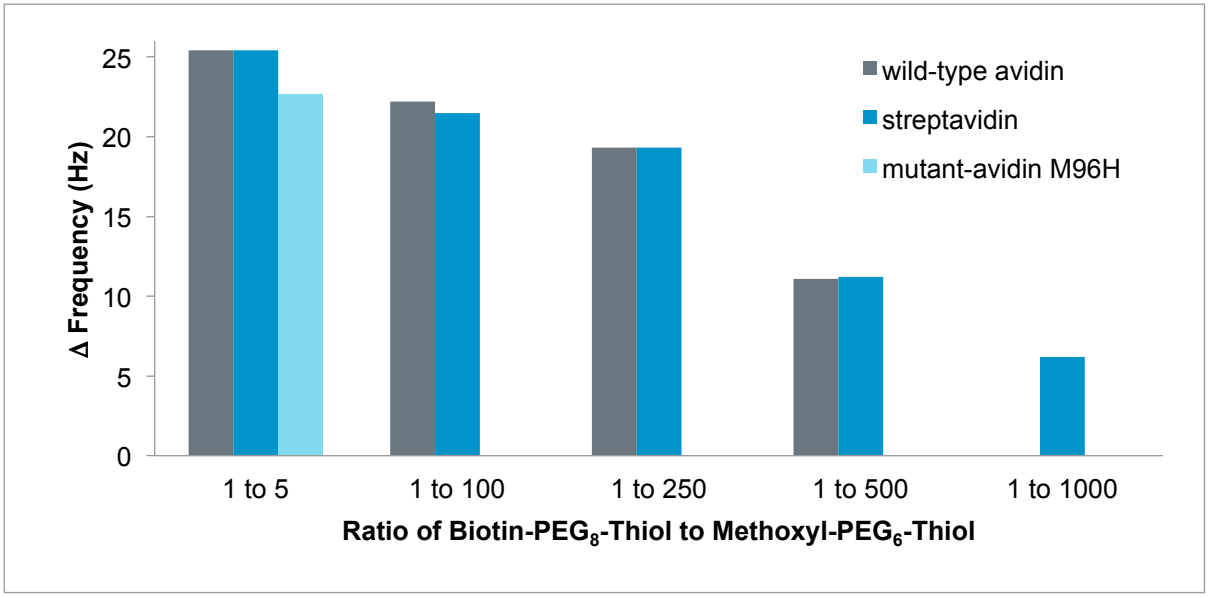

Graph 4: Absolute delta frequency shift of 0.5 µM avidin, streptavidin and M96H to different ratios of biotin-PEG_8-thiol and methoxyl-PEG_6-thiol functionalized quartz sensor.

In spite of the incomplete dissociation discovered with respect to streptavidin and avidin in Table 3 & 5 and Graph 3 & 4 above, the avidin mutant M96H could be almost completely dissociated by 8 M GuHCl at pH 1.5. Inasmuch as the highest ratio of SAM was used, 98,62 ± 0,8 % and 94,14 ± 1,78 % of the biotin-M96H interaction was reversible (Table 6 and Graph 5). This favorable outcome may be justified as demonstrated in Figure 19: since the methionine position 96 that was located in the subunit-subunit interface had been replaced with histidine [37], it is proposed that the 8 M GuHCl (in pH 1.5 of PBS) on the one hand causes protonation of the histidine residue, which on the other hand induces the dissociation and denaturation of the subunits.

Table 6: Reversible adsorption of 0.5 µM M96H to 1:5 ratio of biotin-PEG_8-thiol/methoxyl-PEG_6-thiol functionalized quartz sensor using 8 M GuHCl at pH 1.5. The data marked gray are from QCM-IA setup and the unmarked ones are from QCM-D setup. Delta frequency shifts are given in absolute value.

		Methoxyl-PEG_6-Thiol	Ratio of Biotin-PEG_8-Thiol to Methoxyl-PEG_6-Thiol (1:5)	
M96H	Δ Freq. (Hz)	0.3	21.75	103.1
	Recovery after regeneration (%)	-	98.62 ± 0.8	94.14 ± 1.78

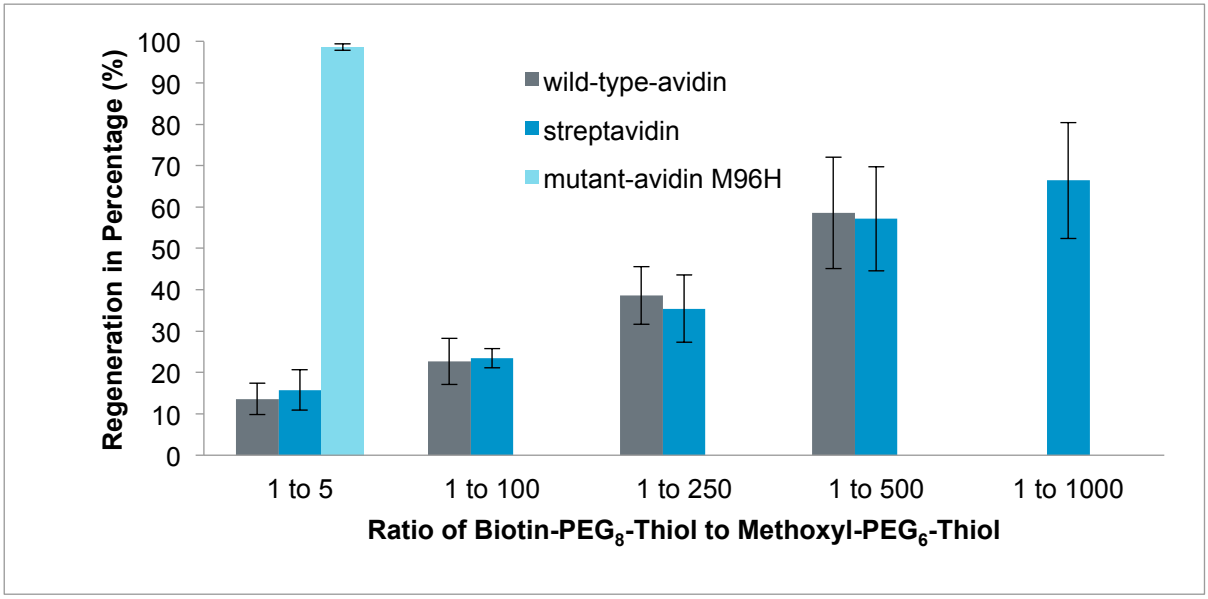

Graph 5: Percentage of regeneration of 0.5 µM avidin, streptavidin and M96H to different ratios of biotin-PEG_8-thiol and methoxyl-PEG_6-thiol functionalized quartz sensor using 8 M GuHCl at pH 1.5.

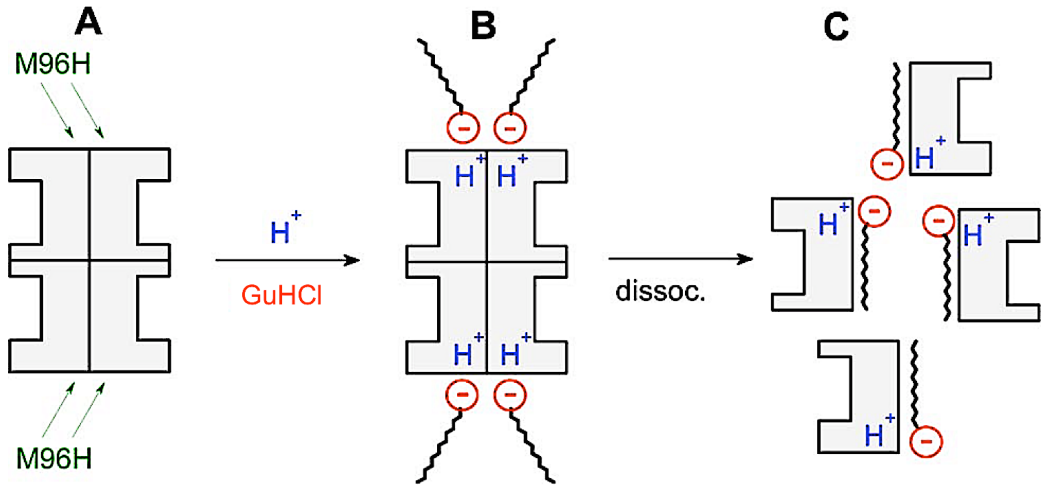

Figure 19: Postulation of the interaction between acidic GuHCl and M96H. The methionine position 96 that has been replaced with histidine is located at the subunit-subunit interface [37] (A). It is proposed that acidic GuHCl activates the histidine residue to undergo protonation (B) which induce the dissociation and denaturation of the subunits (C). Taken from (Pollheimer, et al., 2013) with modification.

4.1.4. Application of reversible immobilization of M96H

Following the successful regenerating experiment, in which almost 100% of the M96H-biotin interaction was reversible, an application of this technique was investigated. This was done by immobilizing biotinylated-8F5 antibody, an antibody specific to the HRV, to the M96H, followed by the adsorption of HRV. Subsequently, a regeneration was done and then the whole interaction steps starting from M96H were repeated. This is shown in Table 7 and split in Graph 6 & 7. It is very obvious to notice the slow kinetic of the HRV. Likewise, it is important to take the energy dissipation (i.e. the resistance) into consideration. And as can be seen, the dissipation shift correlated with the size of the HRV. In the first round of regeneration, 43.39% of the biotinylated SAM of 1:50 biotin-PEG_8-thiol/methoxyl-PEG_6-thiol was recovered, whilst 31.29% was regained in the second stage. Since the 8F5 was multiple biotinylated (i.e. 10 times), the generation of complex cross-linkers could not be ruled out and this in turn could have negatively affected the regeneration process resulting in a decrease in the expected surface recovery. Interestingly, the second absolute frequency shift of the biotinylated-8F5 was 45.65 Hz higher than the first one. This phenomenon is very justifiable: it was assumed that during the second round of immobilization, the biotinylated-8F5 did not only bind to the M96H, but also to the first set of biotininylated-8F5 which had not dissociated during the previous regeneration step. All in all, I will therefore recommend that the amount of the cross-linkers should be reduced to maybe 1:250 so that the regeneration step could be more successful.

Table 7: QCM measurement on a biotin-PEG_8-thiol/methoxyl-PEG_6-thiol (1:50) functionalized quartz sensor with 0.5 µM M96H, biotinylated-8F5 antibody, HRV and their regeneration with 8 M GuHCl at pH 1.5. Data acquired with QCM-IA setup. Delta frequency shifts are given in absolute value.

Protein	Δ Frequency Shift (Hz)
1st M96H	90.67
NHS-LC-biotin-8F5	51.33
HRV (Human Rhinovirus)	69
2nd M96H	39.34 (= 43.39% Regeneration)
NHS-LC-biotin-8F5	96.98
HRV	22.9
3rd M96H	28.37 (= 31.29% Regeneration)

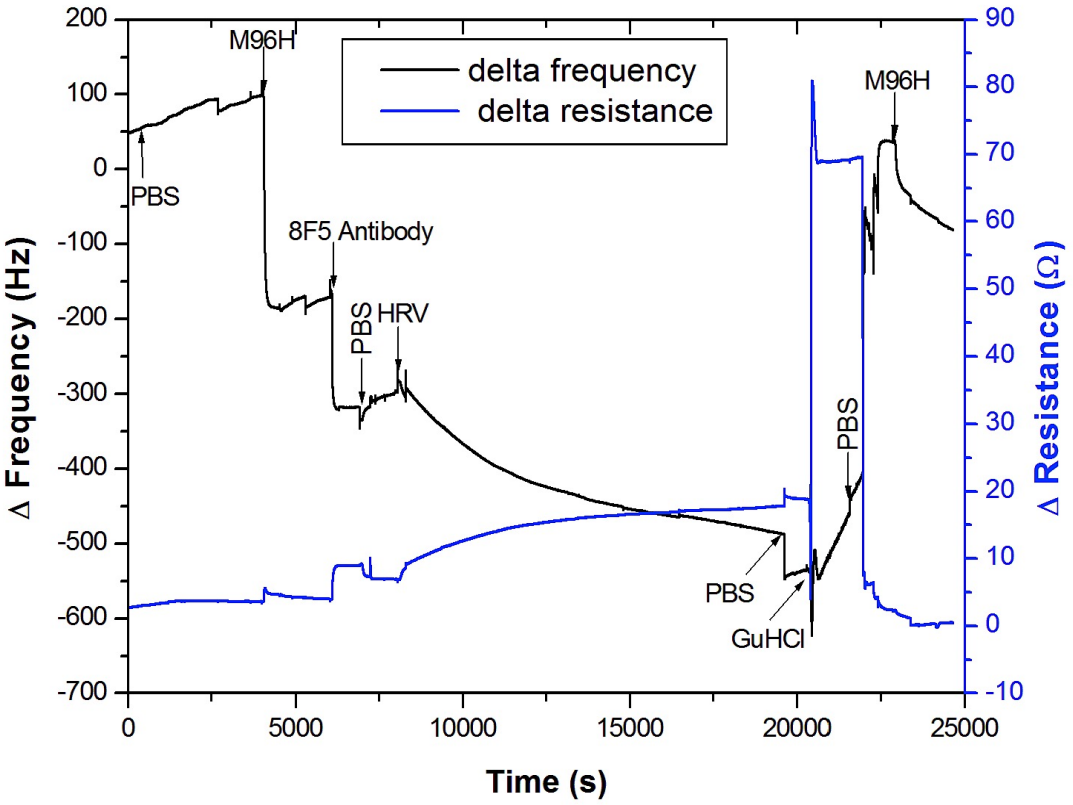

Graph 6: QCM measurement on a biotin-PEG_8-thiol/methoxyl-PEG_6-thiol (1:50) functionalized quartz sensor with 0.5 µM M96H, NHS-LC-biotin-8F5 antibody, HRV and their regeneration with 8 M GuHCl at pH 1.5

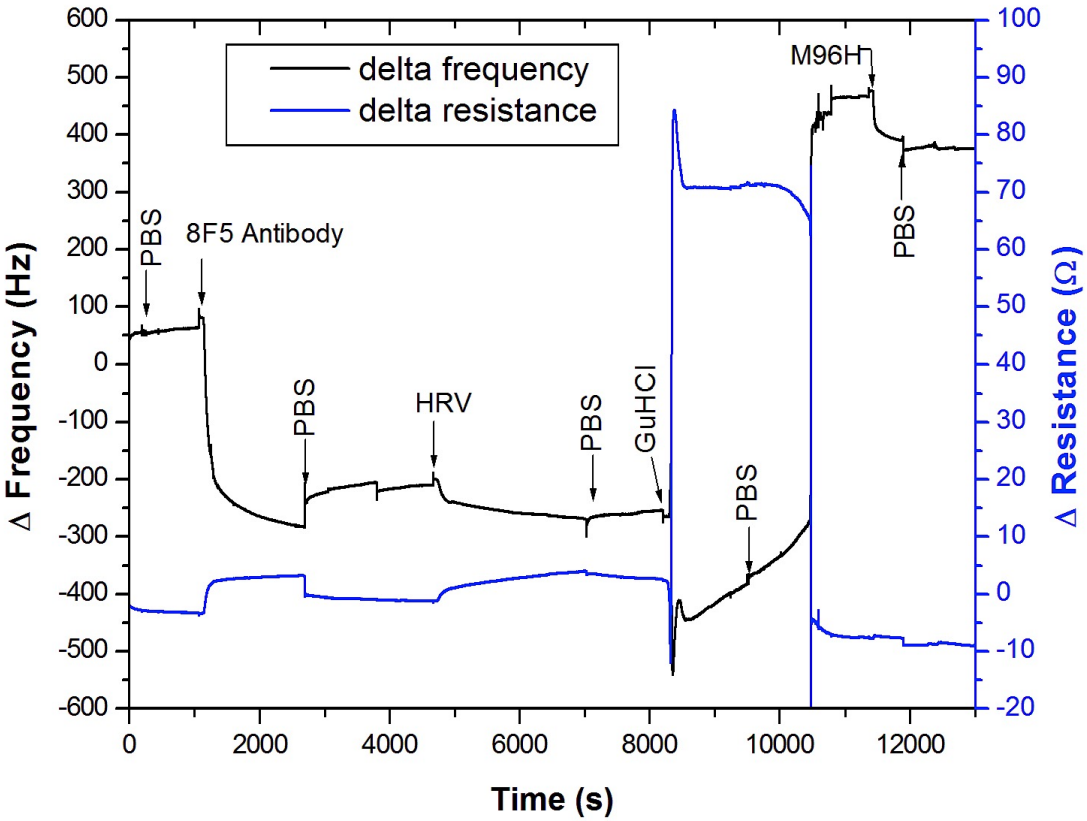

Graph 7: Continuation of Graph 6: QCM measurement on a biotin-PEG_8-thiol/methoxyl-PEG_6-thiol (1:50) functionalized quartz sensor with 0.5 µM M96H, NHS-LC-biotin-8F5 antibody, HRV and their regeneration with 8 M GuHCl at pH 1.5.

4.2. AFM investigations on flat RBC ghosts.

In order to gain a better insight into the distribution and mechanism of RhD receptors on the ERYs, this thesis also aims at investigating flat ERY ghosts by employing AFM. This research involves flat ERY ghosts preparation, topography imaging, tip-chemistry, FS measurement and TREC measurement. The results that were obtained are shown and discussed below.

4.2.1. Contact mode AFM measurement on flat RBC ghosts

After a preparation of ERY membranes, contact mode imaging was performed to verify the success of the preparation. From the 3D topography images in Figure 20 and its corresponding 2D in Figure 21, the structural details of the flattened ERY ghost can be observed: they have no curvature like the normal ERYs, but are circular and flat in shape with diameters ranging from 10-12 µm (Figure 22). Observations revealed that rehydrated dried-ghosts are usually smaller in height than freshly prepared ghosts as can be seen in the zoom-in images and their cross section in Figure 22. Fresh ghost are usually 40 to 50 nm in height while the rehydrated dried ones are 25 to 30. These structural details of course vary just a little from the normal ERYs, such as 7-8 µm of diameter [3, 4]. This is due to the fact that ghosts were free from cytoskeletal proteins, yielding instead of curvatures, a flat circular shape which resulted in wider diameters. Besides, the drying process caused most inter-membrane liquids to dry out, which explains the reduction in height compared to the freshly prepared ghosts. Additionally, the small openings seen in some of the ghosts imply that the ghosts are indeed made of two membranes. The few higher structures are folds of the ERY membranes that could not perfectly fixed back to their original positions. Furthermore, one can notice that the ERY ghosts are stably attached to the PLL-coated glass, indicating the practicability of force measurements on these membranes.

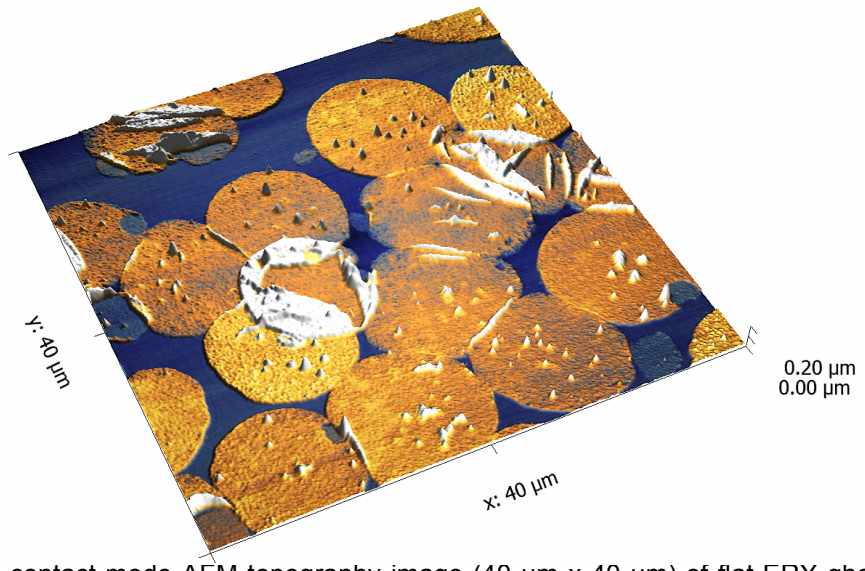

Figure 20: A 3D contact mode AFM topography image (40 µm x 40 µm) of flat ERY ghosts, acquired in PBS buffer. The white high structures are folds resulting from some membranes that have not fixed back to their original positions. And the gray-like small openings or holes located at the edges of some ghosts reveal openings of the membranes or tearing of some part of the upper membranes.

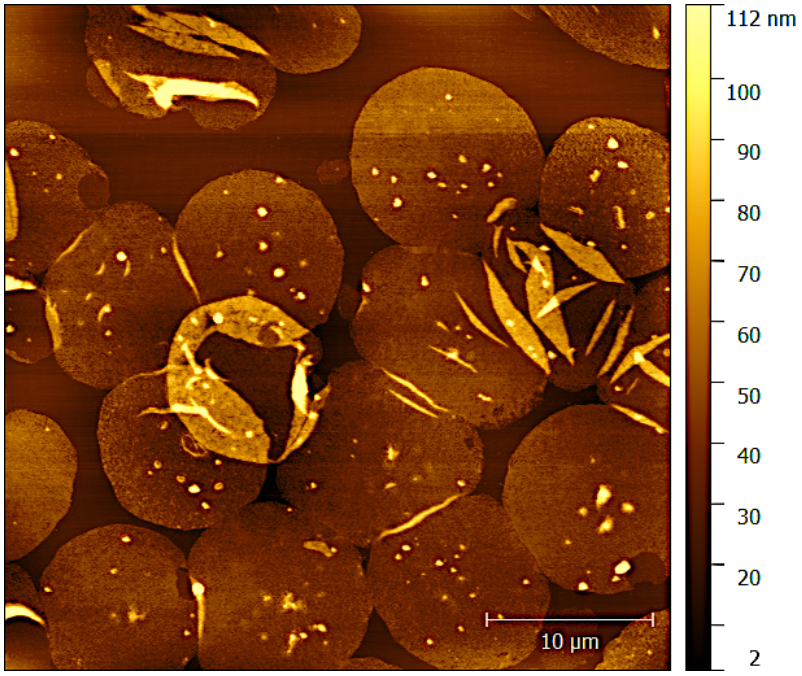

Figure 21: AFM contact mode topography image of rehydrated dried-ghost. This is a 2D 40 µm x 40 µm AFM topography image of flat ERY ghosts attached to PLL-coated glass coverslip. The white high structures are folds resulting from some membranes that could not fixed back to their original positions. And the small openings or holes located at the edges of some ghosts reveal openings of the membranes or tearing of some part of the upper membranes.

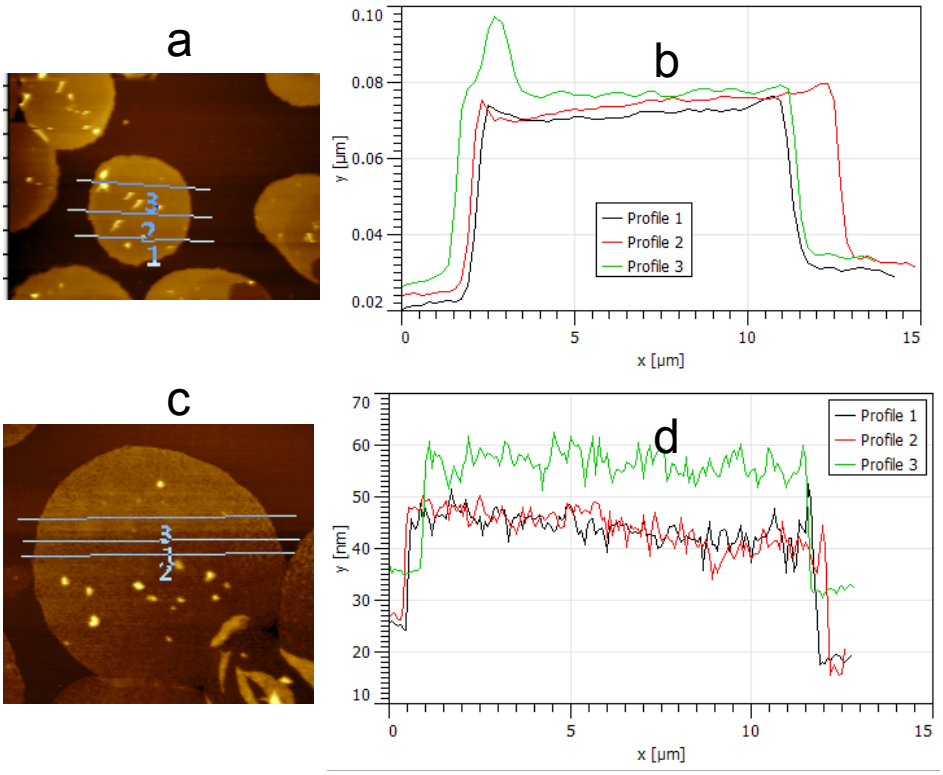

Figure 22: AFM contact mode topography images of a) zoom-in on a single fresh ghost with b) its corresponding cross sections and c) zoom-in on a single rehydrated dried-ghost with d) its corresponding cross sections.

4.2.2. FS measurements on flat RBC ghosts

High sensitivity force measurements were acquired on flattened ERY ghost membranes with BRAD5-antibody-functionalized AFM tips as described in section 3.3.4.

As shown in Graph 8, force distance curves were obtained by approaching a BRAD5-functionalized tip to the surface of flat ERY ghost, followed by retraction. As a result, the interaction between the BRAD5-functionalized AFM tip and the RhD receptors on the ERY ghost surface was checked. While approaching, the tip first contacted the cell and the acting force increased during further approach resulting in a linear force increase until reversion of the tip movement. Upon a succeeding retraction, the cantilever relaxed. If a bond occurred between the BRAD5 on the AFM tip and a RhD- receptor on the ERY membrane, this BRAD5-RhD-receptor bond would turn to be stretched mechanically during retracing (Graph 8). The loading force increased, forming parabola-like shape in the retracing curve as a result of the changing spring constant of the PEG-cross-linker used to functionalize the tip. In the end, the bond broke at a characteristic force, the unbinding force, causing the return of the cantilever tip to its resting position, which are the jumps seen in the black retrace curves. If there was no binding between the BRAD5 on the tip and the RhD-receptor on the cell membrane, the retraction and the tracing curves look alike (insert of Graph 8).

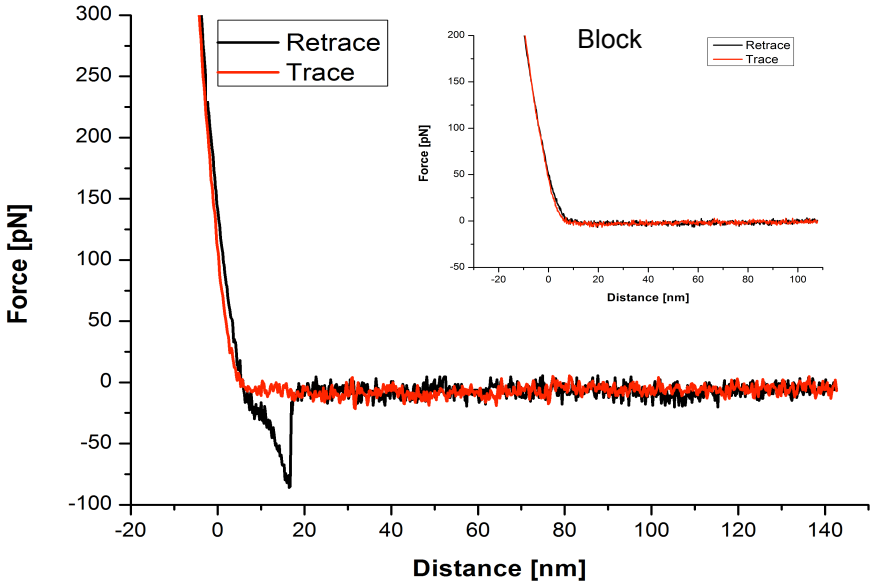

Graph 8: Force-distance curve of a single RhD-BRAD5 antibody unbinding event of 86 pN unbinding force and 16 nm unbinding length. The cantilever tip was functionalized with BRAD5 via an acetal-PEG-NHS cross-linker. The inserted curve is the force distance cycle of no binding event after blocking the binding with free BRAD5 antibody.

Subsequently, the unbinding force between BRAD5 antibody and RhD-receptor was determined before and after surface block of the RhD-receptor by repeated measurements of the force-distance curves for 2300 to 3000 times. Then the probability density function (PDF) of the unbinding force was

constructed. The PDF was constructed in the following way: for each curve with a binding event, a Gaussian curve was drawn with the measured unbinding force as mean value and the standard deviation of the noise in the force distance curve as the standard deviation of the Gaussian curve. All the Gaussian curves corresponding to each unbinding event were added together and normalized yielding the experimental PDF of the unbinding force (Graph 9). The experimental PDF was further fitted by the Gaussian function. The unbinding force with the highest probability was then determined from the position of the maximum in the Gaussian distribution.

For measurements of 2363 force distance curves before blocking, the unbinding force with the highest probability determined was 86.4 pN at 16.6 nm unbinding length and a total of 34.8% binding probability (Graph 9 and 10) . After blocking the RhD-receptors for 110 min, 3031 foce distance curves were recorded with a total binding probability of 10.1 % and unbinding force along with unbinding length with the highest probability of 82.3 pN and 12.1 nm (Graph 9 and 10). The force distance curves evaluated here were measured continuously with fixed scanning range of 3 µm, cycle time of 1s, and force limit of 0.3 V.

The distribution of the unbinding force vs. unbinding length in Graph 11 including the results above confirms the specificity of the interaction between BRAD5 antibody and RhD-receptors, in the sense that the distribution behaviour of the unbinding force before blocking was almost the same as after blocking. The high binding probability of 34.8% before blocking and a drop to 10.1% after blocking is in agreement with the fact that there are high amount of surface receptors of RhD on ERY. However, nearly 100% blocking of the receptors is usually not possible with surface blocking. An alternative choice of blocking in order to overcome this phenomenom is the tip blocking, in which the functionalized AFM tip could be prevented from interacting with RhD-receptors. In such a case, binding probability would have droped to almost 0%.

Furthermore, the most probable unbinding forces before (which is 86.4 pN) and after blocking (which is 82.3 pN) are similar in amount, hence, attesting also to the specificity of this force determination.

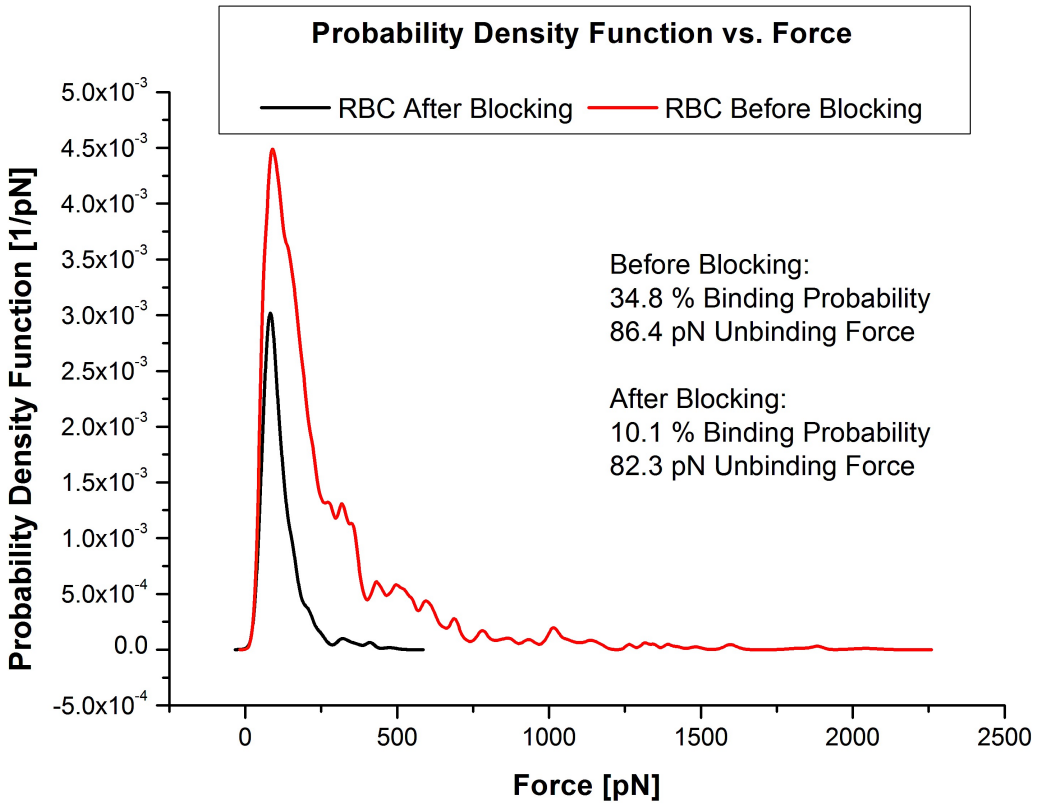

Graph 9: Probability density function vs. force graph of BRAD5 antibody-RhD-receptors complex before (red) and after (black) blocking. The block is shown relative to the specific interaction.

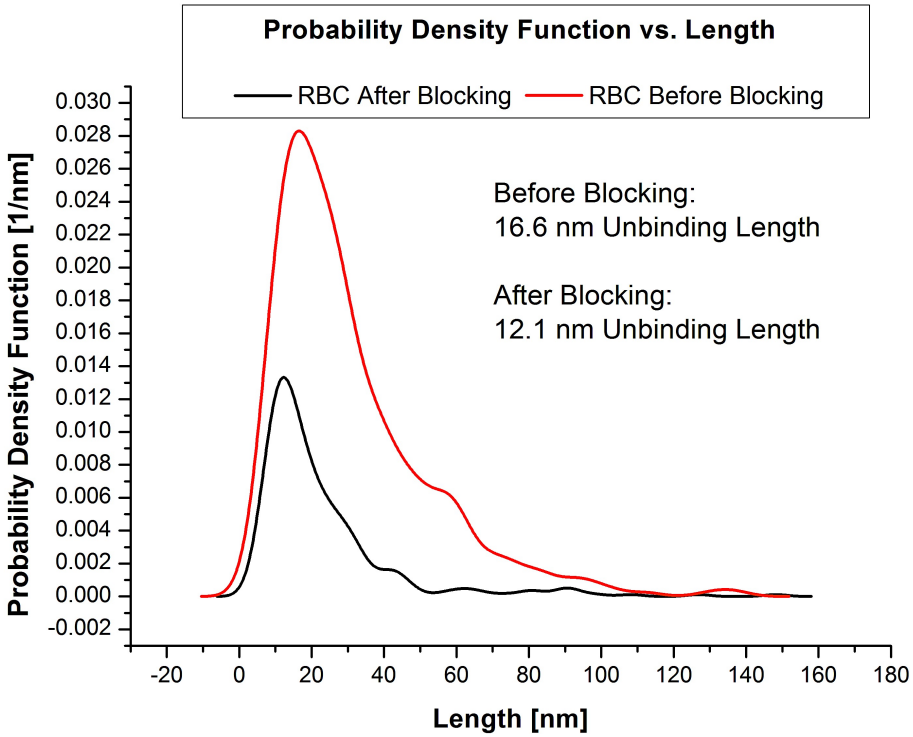

Graph 10: Probability density function vs. length graph of BRAD5 antibody-RhD-receptors complex before (red) and after (black) blocking.

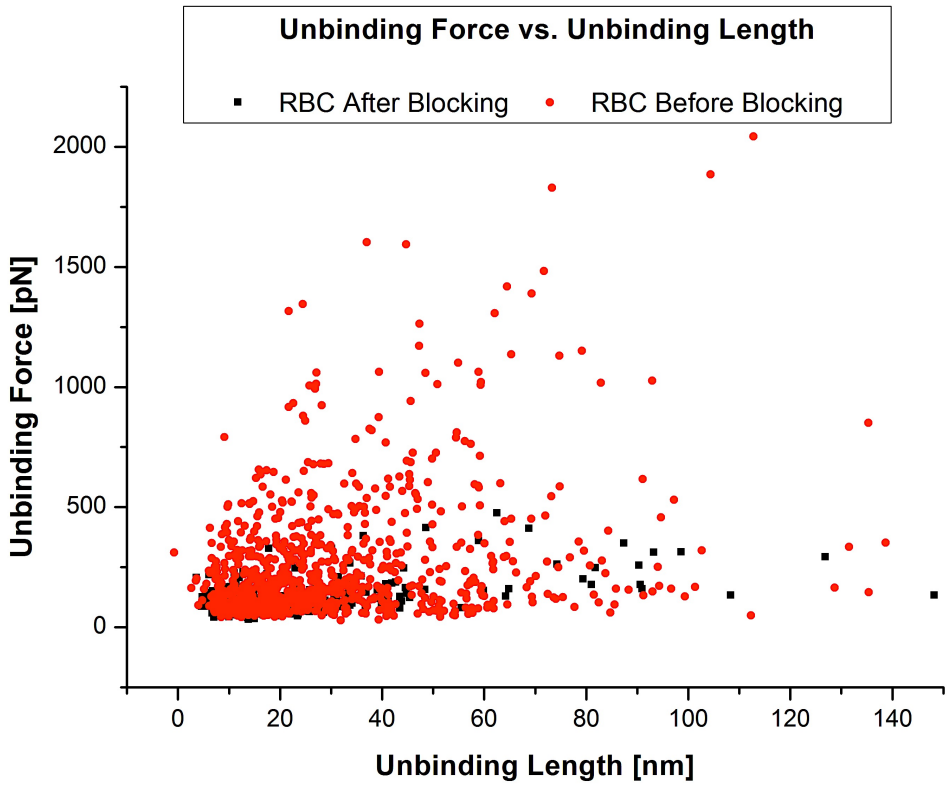

Graph 11: Distribution of unbinding force vs. unbinding length graph of BRAD5 antibody-RhD-receptors complex before (red) and after (black) blocking.

4.2.3. TREC Measurements on flat ERY ghosts

TREC imaging mode in AFM yields fine structural details with nanometer positional precision of topography and at the same time reveals recognition events on the probed surface. In respect of this, simultaneous TREC imaging was carried out on flattened ERY ghost membranes with AFM tip, which had been functionalized with BRAD5 antibody as described in section 3.3.5. (Figure 23). The dark spots marked in recognition image (Figure 23B), which are missing in the topography image (Figure 23A) could be the recognition positions of RhD receptors. Even so, since this is just a preliminary TREC experiment, one could not certainly conclude on the distribution behavior of the RhD receptors on the ERY surface. Therefore, in the near future, further examination of such TREC images will be done so as to confirm whether the receptors are mostly located at the edges or center of the ERY.

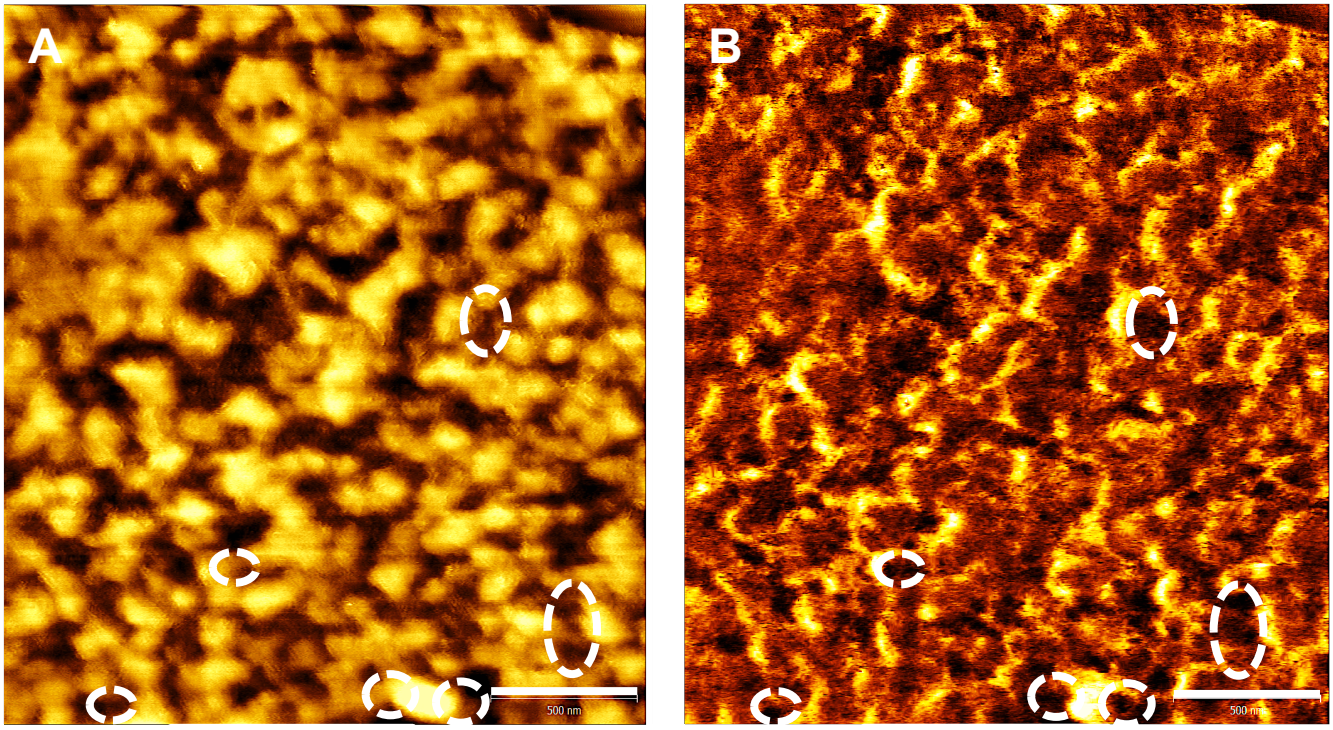

Figure 23: Topography and recognition images of isolated RBC membranes. (a) Topography image and b) recognition image of flat RBC membrane. Dark spots in the recognition images (b) exhibit the positions of specific interaction that exist between the BRAD5-functionalized tip and the RhD receptors. The positions in (a) and (b) correspond to each other. Scale bar is 500 nm.

5. Conclusions

Putting the main target of the first part of this thesis, i.e. the providing of a protocol for re-usable QCM sensor that will enable biotinylated bait molecules to be immobilized to the sensor surface followed by the binding of a prey molecule to the bait, in focus, I have succeeded in preparing biotinylated QCM-IA and QCM-D sensors by coupling SAMs of biotin-PEG_8-thiol mixed with hydroxyl/methoxy-PEG_6-thiol at different ratios. Upon investigating streptavidin, avidin and avidin mutant M96H, which were to serve as bridge between the biotinylated sensor and bait, the goal was successfully achieved with M96H. Even though very resistant to pH change (from 10 to 4), M96H could be denaturized by 8 M GuHCl at pH 1.5 as well as by RSX, resulting in a successful complementarity to a similar SPR study [2], in which SDS (0.25%) and citric acid (2.5%) was used for the denaturation. The regenerations of biotinylated SAMs in the cases of streptavidin and avidin were rather not complete: results proved that a higher biotin/matrix thiol ratio correlates with a higher fraction of bivalently bound streptavidin and avidin molecules, hence corresponding to a higher fraction of streptavidin and avidin not being removed by 8 M GuHCl at pH 1.5.

Additionally, the PEG linkers with biotin and -OH/-OCH_3 terminals did not only allow specific adsorption of streptavidin, avidin and M96H to the sensor, but also yielded fast and highly reproducible measurements.

Moreover, the preliminary application of the re-usable biotinylated-QCM sensor with biotinylated 8F5 antibody and human rhinovirus, bridged by M96H, was partially successful. Cross-linking of the biotinylated-8F5 antibody was assumed to be the factor that hindered the total reversibility of this step.

QCM seems not to be so much explored compared to other label-free and online biosensors, such as SPR. A vital basis of expansion in this area is the generation of biotinylated and reusable SAM sensors, as accomplished here with QCM-IA and QCM-D, which facilitate extremely sensitive and specific protein analysis. QCM, however, can offer some advantages over SPR because it is far less expensive.

Furthermore, the aim of the second part of this thesis on flat ERY ghosts investigation with AFM has likewise been attained. Flat ERY ghosts were successfully prepared by flushing out hemoglobin and all other internal proteins form within the cell and fixing the membranes to each other. Contact mode AFM imaging provided an overview of the topography of the ERY ghosts. Due to its high sensitivity, the AFM could detect the interaction force of a single molecular RhD-BRAD5 unbinding event at 86.4 pN unbinding force and 16.6 nm unbinding length. The unbinding probability of 34.8% had reduced to 10.1% after surface blocking, producing evidence for specificity as the unbinding force of 82.3 pN of blocked receptors was similar to not-blocked ones.

Thanks to TREC being an exceptional technique with the ability to recognize single binding event on cells with nanometer accuracy, it offered me the chance to image the distribution of the specific binding events of BRAD5-RhD on the ERY ghost surface. This eventually revealed domains of RhD receptors with the size of tens of nanometers, indicating the existence of RhD on the ERY membrane.

6. Appendix

This chapter covers some of the results that were not shown in the chapter 4 of results and discussion so as to have a broad overview on how they look like.

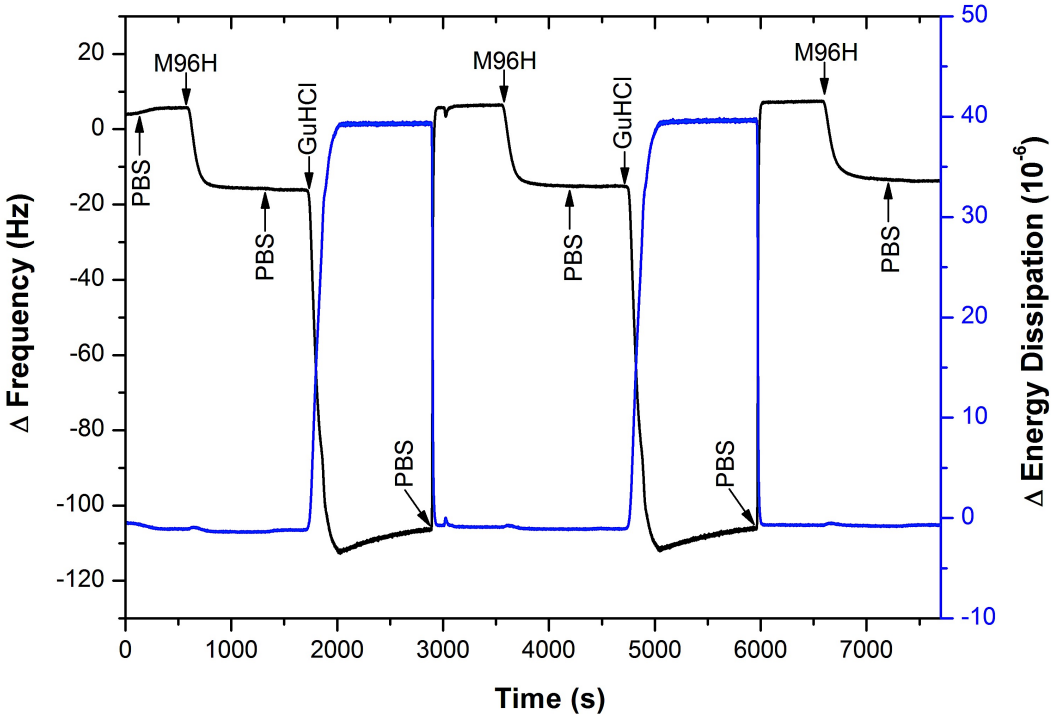

Graph 12: Regeneration of 0.5 µM M96H from a 1:5 ratio of biotin-PEG_8-thiol and methoxyl-PEG_6-thiol functionalized quartz sensor using 8 M GuHCl at pH 1.5.

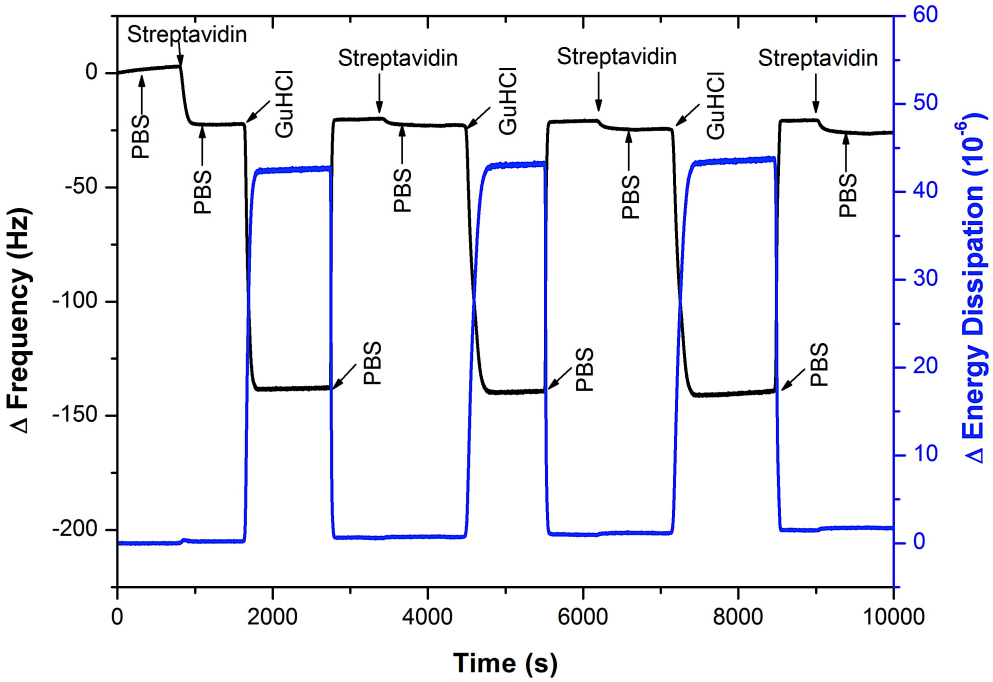

Graph 13: Regeneration of 0.5 µM Streptavidin from a 1:5 ratio of biotin-PEG_8-thiol to methoxyl-PEG_6-thiol functionalized quartz sensor using 8 M GuHCl at pH 1.5.

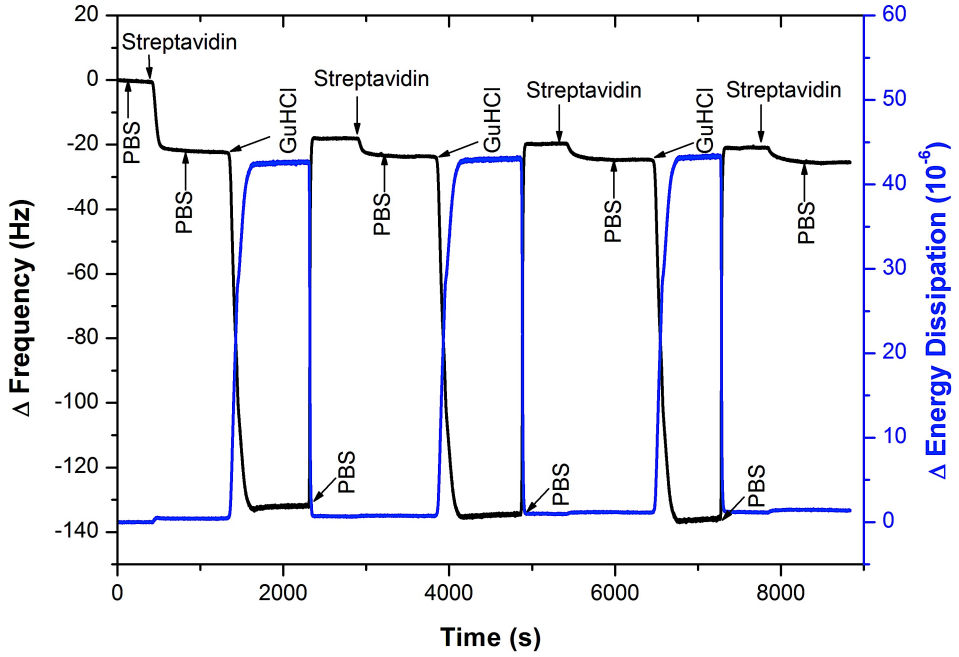

Graph 14: Regeneration of 0.5 µM Streptavidin from a 1:100 ratio of biotin-PEG_8-thiol to methoxyl-PEG_6-thiol functionalized quartz sensor using 8 M GuHCl at pH 1.5.

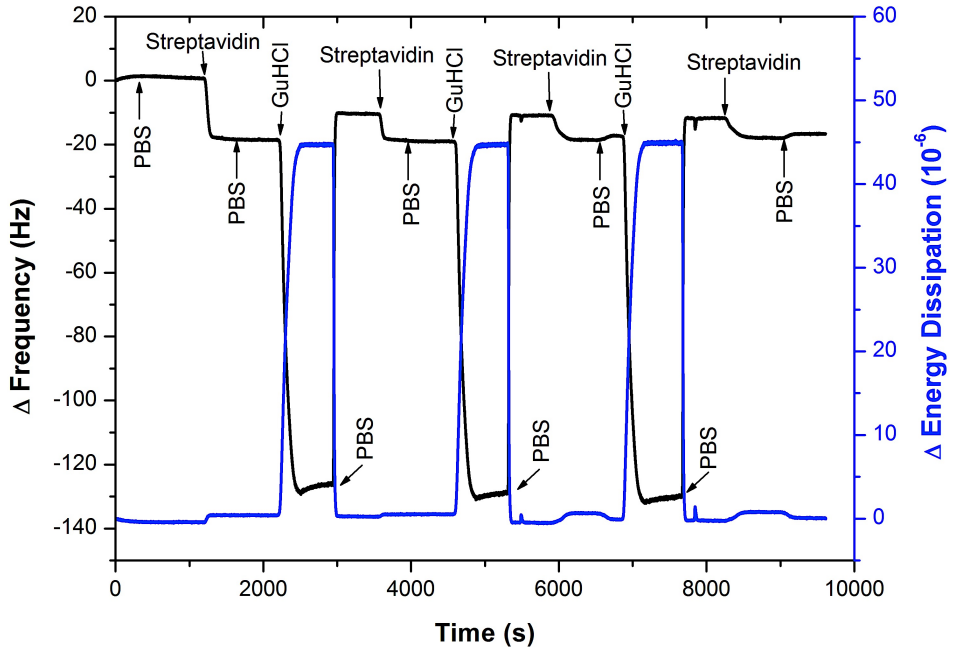

Graph 15: Regeneration of 0.5 µM Streptavidin from a 1:250 ratio of biotin-PEG8-thiol to methoxyl-PEG6-thiol functionalized quartz sensor using 8 M GuHCl at pH 1.5.

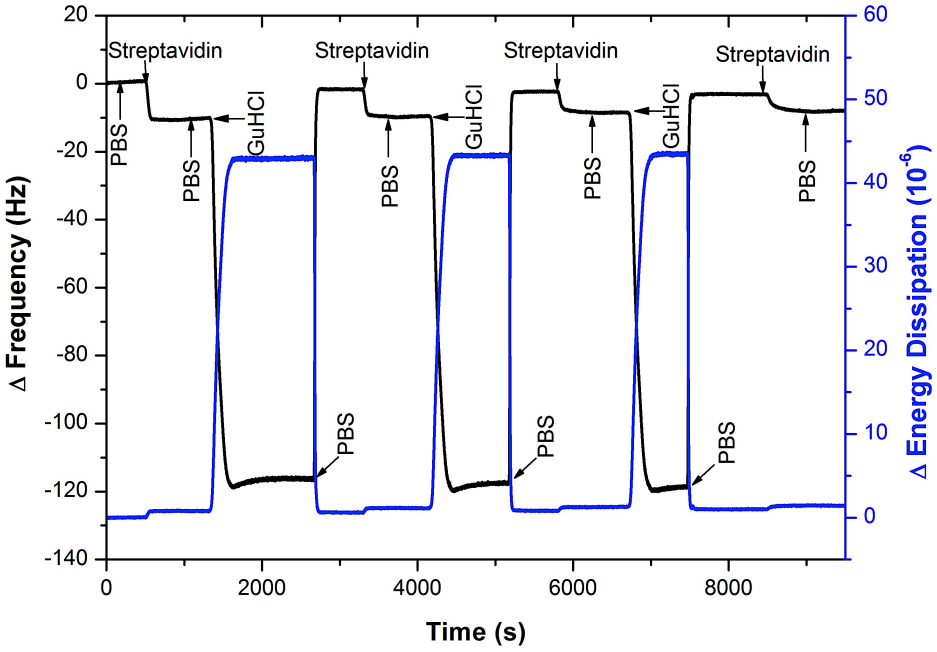

Graph 16: Regeneration of 0.5 µM streptavidin from a 1:5 ratio of biotin-PEG_8-thiol to methoxyl-PEG_6-thiol functionalized quartz sensor using 8 M GuHCl at pH 1.5.

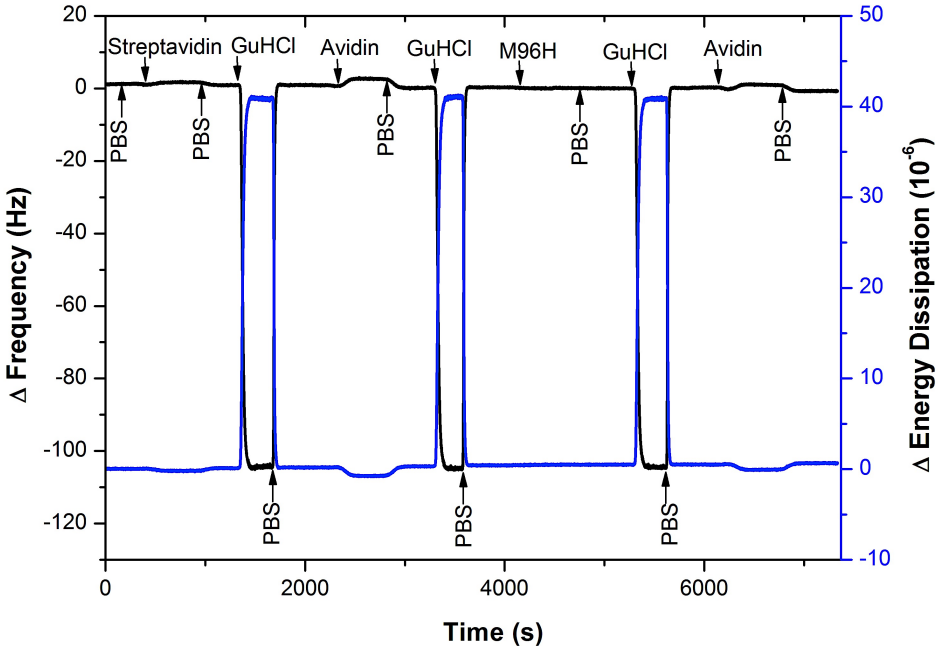

Graph 17: Specificity control of 0.5 µM streptavidin, avidin and M96H on methoxyl-PEG_6-thiol functionalized quartz sensor and regeneration with 8 M GuHCl at pH 1.5.

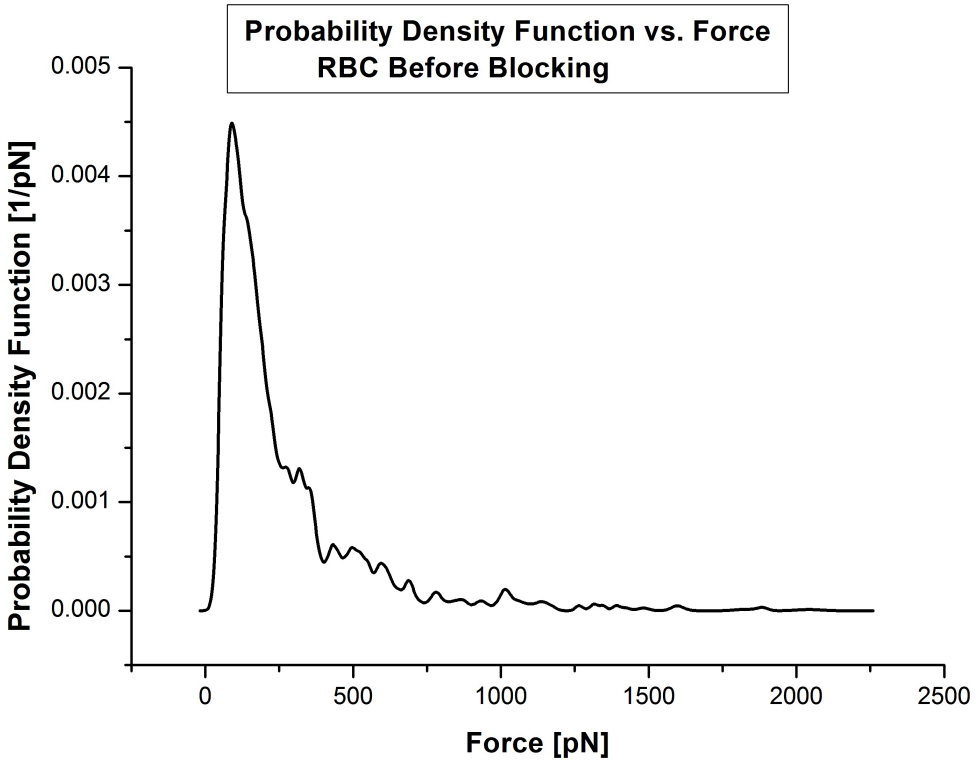

Graph 18: Probability density function vs. force graph of BRAD5 antibody-RhD-receptors complex before blocking.

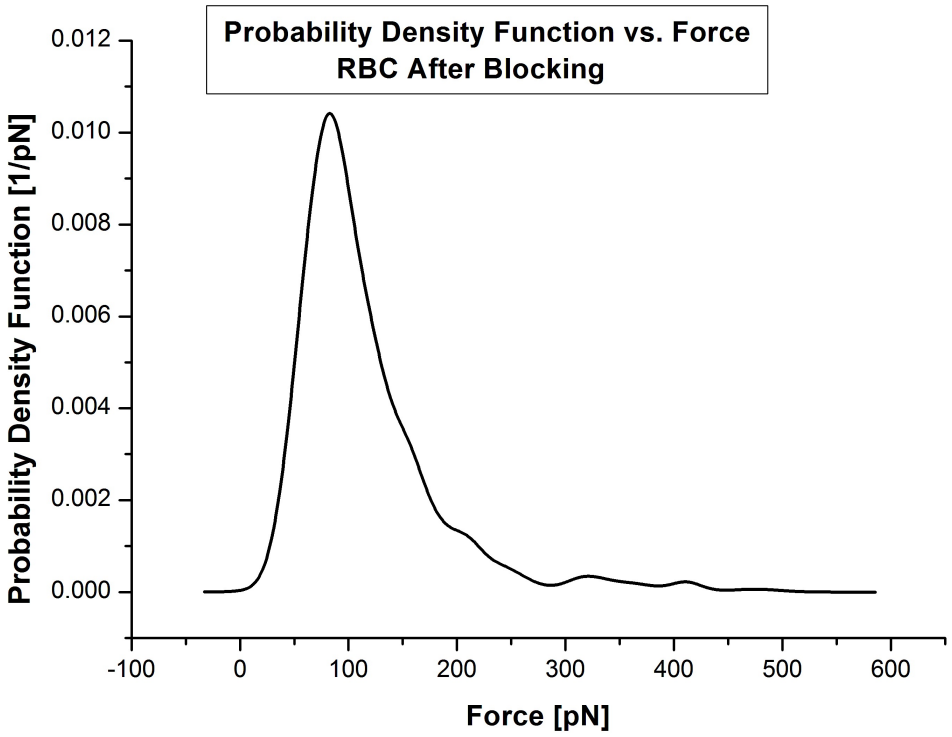

Graph 19: Probability density function vs. force graph of BRAD5 antibody-RhD-receptors complex after blocking.

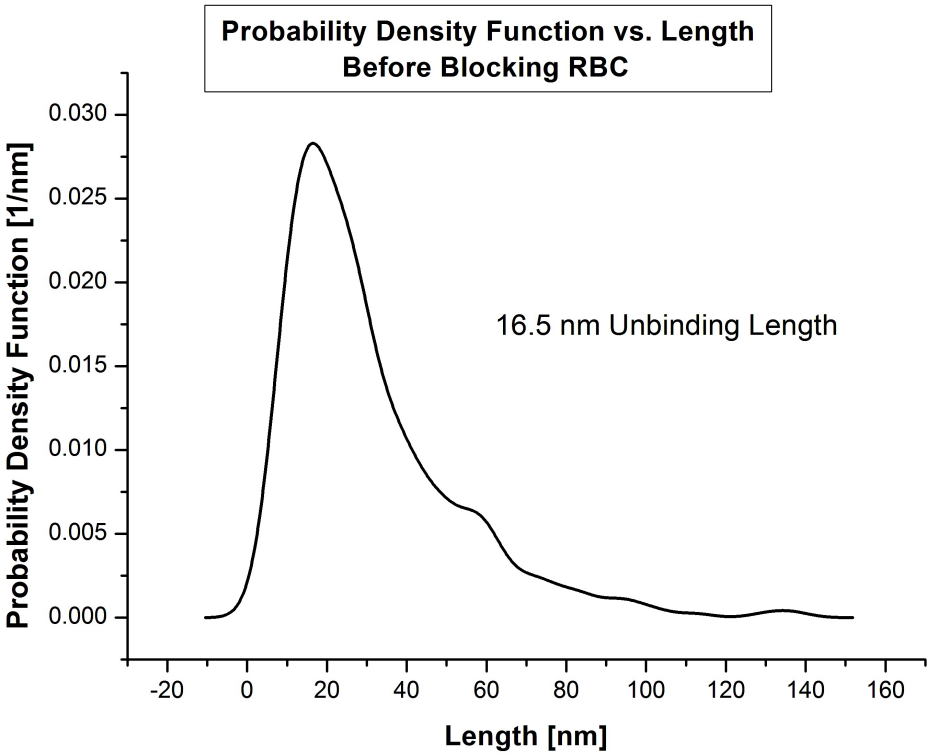

Graph 20: Probability density function vs. length graph of BRAD5 antibody-RhD-receptors complex before blocking.

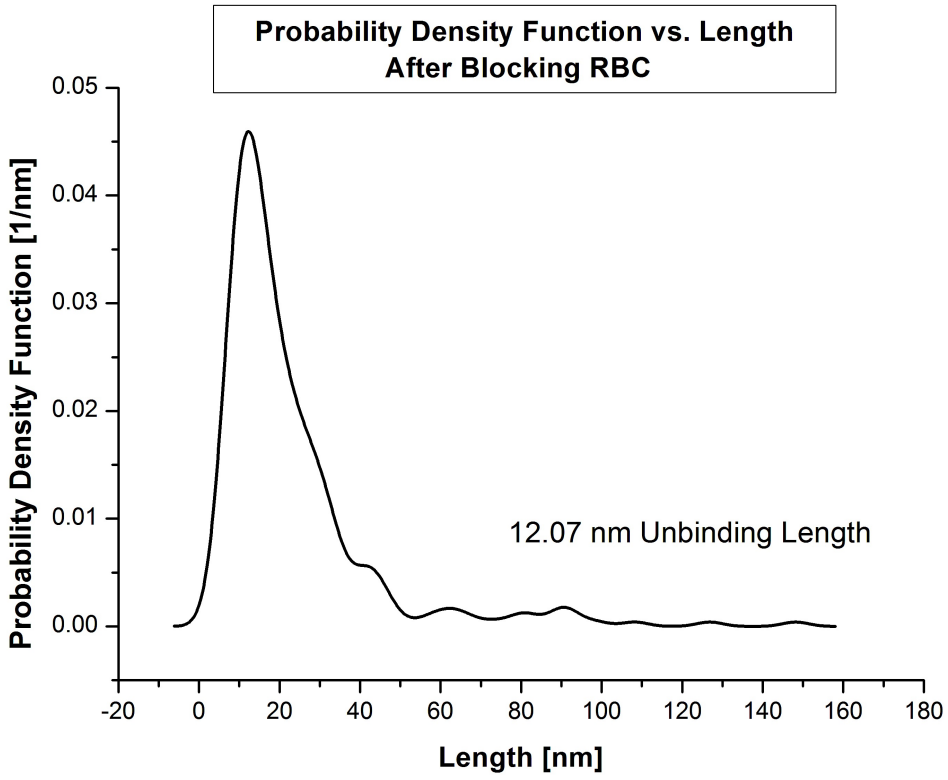

Graph 21: Probability density function vs. length graph of BRAD5 antibody-RhD-receptors complex after blocking

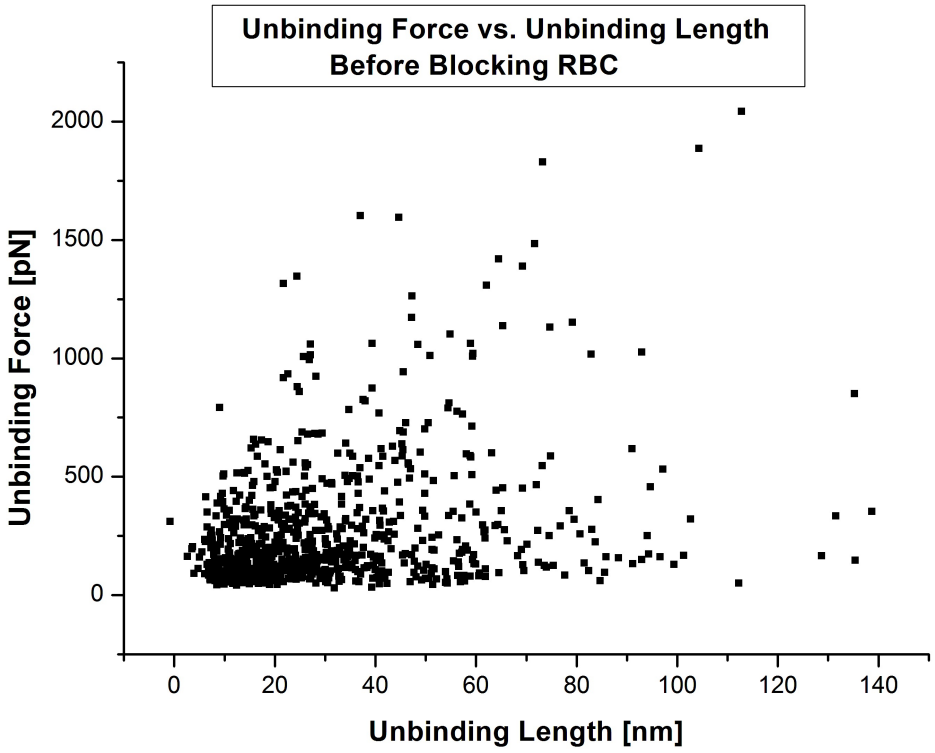

Graph 22: Distribution of unbinding force vs. unbinding length graph of BRAD5 antibody-RhD-receptors complex before blocking

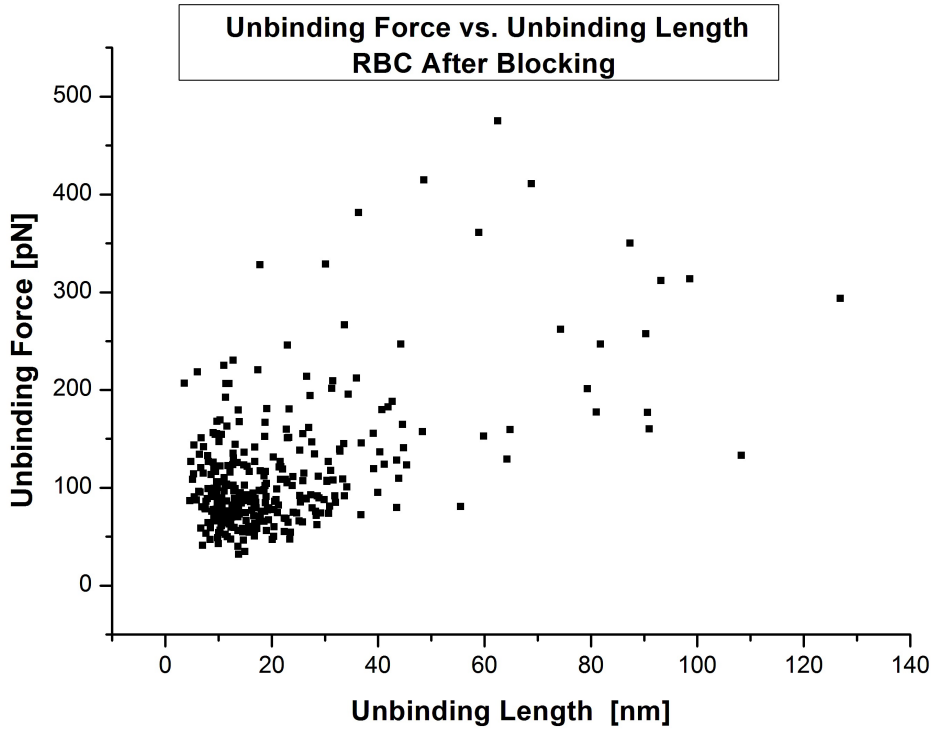

Graph 23: Distribution of unbinding force vs. unbinding length graph of BRAD5 antibody-RhD-receptors complex after blocking

7. Bibliography

1. Janshoff, A., Gala, H.-J., & Steinem, C. (2000). Piezoelectric Mass-Sensing Devices as Biosensors-An Alternative to Optical Biosensors? *Angewandte Chemie Int. Ed. , 39*, 4004-4032

2. Pollheimer, P., Taskinen, B., Scherfler, A., Gusenkov, S., Creus, M., Wiesauer, P., et al. (2013). Reversible Biofunctionalization of Surfaces with a Switchable Mutant of Avidin. *Bioconj. Chem , 24*, 1656−1668.

3. Pierige, S., Serafini, S., Rossi, L., & Magnani, M. (2008). Cell-Based Drug Delivery. Adv Drug Deliv Rev , 60 (2), 286-295.

4. Doohan, J. P. (1999, October 11). Biological Science Santa Barbara City Collage. Retrieved Febuary 22, 2016, from http://www.biosbcc.net/doohan/sample/htm/Blood%20cells.htm

5. Dean, L. (2005). Blood Groups and Red Cell Antigens. Bethesda, MD: NCBI.

6. Wildling, L., Unterauer, B., Zhu, R., Rupprecht, A., Haselgrübler, T., Rankl, C., et al. (2011). Linking of Sensor Molecules with Amino Groups to Amino-Functionalized AFM Tips. *Bioconjugate Chem.* (22), 1239–1248.

7. Buttry, D. A., & Ward, M. D. (1992). Measurement of Interfacial Processes at Electrode Surfaces with the Electrochemical Quartz Crystal Microbalance. Chem. Rev. , 92 (6), 1355-1379.

8. Sauerbrey, G. (1959). Verwendung von Schwingquarzen zur Wägung dünner Schichten und zur Mikrowägung. *Z. Phys* , 155, 206-222

9. Nomura, T., & Okuhara, M. (1982). Frequency Shifts of Piezoelectric Quartz Crystals Immersed in Organic Liquids. Anal. Chem. Acta , 142, 281-284.

10. ICM, M. I. (1998-2006). Retrieved April 2016, from http://www.icmfg.com/quartzmicrobalance.html

11. Rosenbaum, J. F. (1988). Bulk Acoustic Wave Theory and Device. Boston: Artech-house.

12. Carrera, E., Brischetto, S., & Nali, P. (2011). Plates and Shells for Smart Structures: Classical and Advanced Theories for Modelling and Analysis. Chichester: A John Wiley & Sons Ltd

13. Currie, J., & Currie, P. (1880). Développement, par compression, de l'électricité polaire dans les cristaux hémiédres a faces inclinées. C.R. Acad. Sci. Paris , 91, 294-295.

14. Ballantine, D. S., White, R. M., Martin, S. J., Ricco, A. J., Zellers, E. T., Freye, G. C., et al. (1997). Acoustic Wave Sensors. San Diego: Academic press.

15. Kurz, G., & Mathis, W. (1994). Oszillatoren. Heidelberg: Hüthig

16. Bottom, V. E., B., A., & S., M. (1982). Introduction to Quartz Crystal Unit Design. New York: van Nostrand Reinhold.

17. Jones, T. A., Kleitz, M., Lundström, I., & Göpel, W. (1995). *Micro- and Nano-sensor Technology/Trends in Sensor Markets.* Weinheim: VCH.

18. O'Sullivan, C., & Guilbault, G. (1999). Commercial Quartz Crystal Microbalances – Theory and Applications. *Biosensors & Bioelectronics , 14*, 663–670.

19. Goka, S., Okabe, K., Watanabe, Y., & Sekimoto, H. (2000). Multimode Quartz Crystal Microbalance. *Jpn. J. Appl. Phys. , 39*, 3073.

20. Mason, W. P. (1965). *Physical Acoustics* (Vol. 2A). New York: Academic Press.

21. Kanasawa, K., & Gordon, J. (1985). A Liquid Phase Piezoelectric Detector. *Anal. Chem. , 57*, 1771–1775.

22. Kasper, M., Traxler, L., Salopek, J., Grabmayr, H., Ebner, A., & Kienberger, F. (2016). Broadband 120 MHz Impedance Quartz Crystal Microbalance (QCM) with Calibrated Resistance and Quantitative Dissipation for Biosensing Measurements at Higher Harmonic Frequencies. *Biosensors , 6* (2), 23.

23. *Biolin Scientific, Progress Together*. (2016). Retrieved 03 10, 2016, from Biolin Scientific: http://www.biolinscientific.com/q-sense/technologies/

24. Cooper, M. A. (2003). Label-free Screening of Bio-molecular Interactions. *Anal. Bioanal. Chem. , 377* (5), 834-842.

25. Nilebäck, E., Feuz, L., Uddenberg, H., Valiokas, R., & Svedhem, S. (2011). Characterization and Application of a Surface Modification Designed for QCM-D Studies of Biotinylated Biomolecules. *Bios. Bioelec. , 28*, 407– 413.

26. Cooper, M. A. (2009). Sensor surfaces and receptor deposition. In M. A. Cooper, *Label-free biosensors: Techniques and applications* (1st Edition ed., p. 110−142). Cambridge: Cambridge University Press.
27. Cha, T., Guo, A., Jun, Y., Pei, D., & Zhu, X.-Y. (2004). Immobilization of Oriented Protein Molecules on Poly(Ethylene Glycol)-Coated Si(111). *Proteomics 4* , 10965−10976.

28. Lofas, S., & Johnsson, B. (1990). A Novel Hydrogel Matrix on Gold Surfaces in Surface Plasmon Resonance Sensors for Fast and Efficient Covalent Immobilization of Ligands. *J. Chem. Soc., Chem. Commun.* , 1526−1528.

29. Prime, K. L., & Whitesides, G. M. (1993). Adsorption of Proteins onto Surfaces Containing End-attached Oligo(Ethylene Oxide): A Model System Using Self-assembled Monolayers. *J. Am. Chem. Soc , 115*, 10714−10721.

30. Su, X., Chew, F. T., & Li, S. F. (2000). Piezoelectric Quartz Crystal Based Label-free Analysis for Allergy Disease. *Biosens. Bioelectron. , 15*, 629−639.

31. Laitinen, O. H., Hytonen, V. P., Nordlund, H. R., & Kulomaa, M. S. (2006). Genetically Engineered Avidins and Streptavidins . *Cell. Mol. Life Sci , 63* (24), 2992–3017
32. Green, N. M. (1975). Avidin. *Adv. Prot. Chem. , 29*, 85–133.

33. Green, N. M. (1990). Avidin and Streptavidin. *Methods Enzymol. , 184*, 51–67.

34. Weber, P. C., Ohlendorf, D. H., Wendoloski, J. J., & Salemme, F. R. (1989). Structural Origins of High-affinity Biotin Binding to Streptavidin. *Science , 243*, 85–88.

35. Livnah, O., Bayer, E. A., Wilchek, M., & Sussman, J. L. (1993). Three-Dimensional Structures of Avidin and the Avidin- Biotin Complex. *Proc. Natl. Acad. Sci. USA , 90*, 5076– 5080.

36. Vermette, P., Gengenbach, T., Divisekera, U., Kambouris, P. A., Griesser, H. J., & Meagher, L. (2003). Immobilization and Surface Characterization of NeutrAvidin Biotin-binding Protein on Different hydrogel Interlayers. *J. Colloid Interface Sci. , 259* (1), 13–26.

37. Wilchek, M., & Bayer, E. A. (1988). The Avidin-Biotin Complex in Bioanalytical Applications. *Anal. Biochem. , 171* (1), 1-32.

38. Hendrickson, W. A., Pähler, A., Smith, J. L., Satow, Y., Merritt, E. A., & Phizackerley, R. P. (1989). Crystal Structure of Core Streptavidin Determined from Multiwavelength Anomalous Diffraction of Synchrotron Radiation. Proc. Natl. Acad. Sci. U. S. A. , 86 (7), 2190–2194.

39. Nordlund, H. R. (2003). Introduction of Histidine Residues into Avidin Subunit Interfaces Allows pH-Dependent Regulation of Quaternary Structure and Biotin Binding. *FEBS Letters , 555* (3), 449–454.

40. Science, N. f. (2012). *NanoWizard® AFM Handbook.* JPK Instruments AG.

41. Johnson, W. (2008). *Agilent Technology.* Retrieved May 23, 2016, from http://cp.literature.agilent.com/litweb/pdf/5990-3293EN.pdf

42. Binning , G., Quate , C. F., & Gerber , C. (1986). Atomic force microscope. *Phys Rev Lett , 56*, 930-933.

43. Hutter , J. L., & Bechhoefer , J. (1993). Calibration of Atomic-Force Microscope Tips. *Rev Sci Instrum , 64*, 1868-1873.

44. Keinberger, F., Ebner, A., Gruber, H. J., & Hinterdorfer, P. (2006). Molecular Recognition Imaging and Force Spectroscopy of Single Biomolecules. *Acc Chem Res , 39*, 29-36.

45. Ahiable, J. E. (2013, March). Investigation of CHOk1 Cell Expressing Human Serotonin Transporter (SERT) Fused with Yellow Fluorescent Protein and the Interaction between SERT and Citalopram by Using Atomic Force Microscope . *Bachelor Thesis*.

46. Frederix, P., Akiyama, T., Staufer, U., Gerber, C., Fotiadis, D., Muller, D., et al. (2003). Atomic Force Bio-Analytics . *Curr Opin Chem Biol , 7*, 641-647.

47. Dufrêne, Y., & Hinterdorfer, P. (2008). Recent Progress in AFM Molecular Recognition Studies. *Pflugers Arch - Eur J Physiol , 256*, 237-245.

48. Sotres, J., Lostao, A., Wildling, L., Ebner, A., Gomez-Moreno, C., Gruber, H., et al. (2008). Unbinding Molecular Recognition Force Mapsof Localized Single Receptor Moleculesby Atomic Force Microscopy. *ChemPhysChem , 9*, 590-599.

49. Gross, L., Mohn, F., Moll, N., Liljeroth, P., & Meyer, G. (2009). The Chemical Structure of a Molecule Resolved by Atomic Force Microscopy . *Science , 325* (5944), 1110-1114.

50. Ebner, A., Schillers, H., & Hinterdorfer, P. (2011). Normal and Pathological Erythrocytes Studied by Atomic Force Microscopy. In *Atomic Force Microscopy in Biomedical Research* (Vol. 736, pp. 223-241). Humana Press.

51. Bizzarri , A. R., & Cannistraro, S. (2010). The Application of Atomic Force Spectroscopy to the Study of Biological Complexes Undergoing a Biorecognition Process. *Chem. Soc. Rev. , 39*, 734-749.

52. Butt, H., & Jaschke, M. (1995). Calculation of Thermal Noise in Atomic Force Microscopy. *Nanotechnology , 6*, 1-7.

53. Cook, S., Schaffer, T., Chynoweth, K., Wigton, M., Simmonds, R., & Lang, K. (2006). Practical Implementation of Dynamic Methods for Measuring Atomic Force Microscope Cantilever Spring Constants. *Nanotechnology , 17*, 2135.

54. Gruber, H. J. (2015). *JKU, Institute of Biophysics.* Retrieved 07 21, 2015, from http://www.jku.at/biophysics/content

55. Gross, L., Mohn, F., Moll, N., Liljeroth, P., & Meyer, G. (2009). The Chemical Structure of a Molecule Resolved by Atomic Force Microscopy . *Science , 325* (5944), 1110-1114.

56. Beutler, E., Lichtman, M. A., Coller, B. S., & Kipps, T. J. (1995). *Williams Hematology (Fith Edition).* New York: Mc-Graw-Hill, Inc.

57. Westhoff, C. M. (2004). The Rh Blood Group System in Review: a New Face for the Next Decade. *Transfusion , 44*, 1663-1673.

58. Kumpel, B. M., Goodrick, M. J., Pamphilon, D. H., Fraser, I. D., Poole, G. D., Morse, C., et al. (1995). Human Rh D Monoclonal Antibodies (BRAD-3 and BRAD-5) Cause Accelerated Clearance of Rh D+ Red Blood Cells and Suppression of Rh D Immunization in Rh D- Volunteers. *Blood , 86* (5), 1701-170.

59. Aung, K. H. (2008). DNA Assembly on Streptavidin Modified Surface: A Study Using Quartz Crystal Microbalance with Dissipation or Resistance Measurements. *Sens. Actuator B: Chem. , 131* (2), 371–378.

60. Höök, F. R. (2001). Characterization of PNA and DNA Immobilization and Subsequent Hybridization with DNA Using Acoustic-Shear-Wave Attenuation Measurements. *Langmuir , 17* (26), 8305–8312.

61. Huang, R. H. (2001). Simultaneous Detection of Multiple Cytokines from Conditioned Media and Patient's Sera by an Antibody-Based Protein Array System. *Anal. Biochem. , 294* (1), 55–62.

62. Prieto-Simon, B. C. (2008). Novel Highly-Performing Immunosensor-Based Strategy for Ochratoxin A Detection in Wine Samples. *Biosens. Bioelectron. , 23* (7), 995–1002.

63. Lee, G., Chrisey, A., & Colton, J. (1994). Direct Measurement of the Force between Complementary Strands of DNA. *Science , 266*, 771-773.

64. *Farlex Partner Medical Dictionary.* (2012). Retrieved May 9, 2016, from http://medical-dictionary.thefreedictionary.com/Haematology+Erythrocyte+Ghost

65. Nikova, D., Lange, T., Oberleithner, H., Schillers, H., Ebner, A., & Hinterdorfer, P. (2006). Atomic Force Microscopy in Nanomedicine. In *Applied Scanning Probe Methods III* (pp. 1-26). Berlin: Springer.

66. Oberleithner, H., Schillers, H., Schneider, S., & Henderson, R. (2001). Nanoarchitecture of Plasma Membrane Visualized with Atomic Force Microscopy. In *Ion Channel Localization Methods and Protocols methods in Phamacology and Toxicology* (pp. 405-424). Totowa, NJ: Humana Press.

67. LOT-QuantumDesign-GmbH. (2016). *LOT-QuantumDesign.* Retrieved 03 18, 2016, from LOT-QuantumDesign: http://83.169.23.21/de/en/home/qsense/qsensee1/